



UvA-DARE (Digital Academic Repository)

Statistical properties of resonances in chaotic elastic cavities: time reversal invariance and feedback

Antoniuk, O.

Publication date

2011

Document Version

Final published version

[Link to publication](#)

Citation for published version (APA):

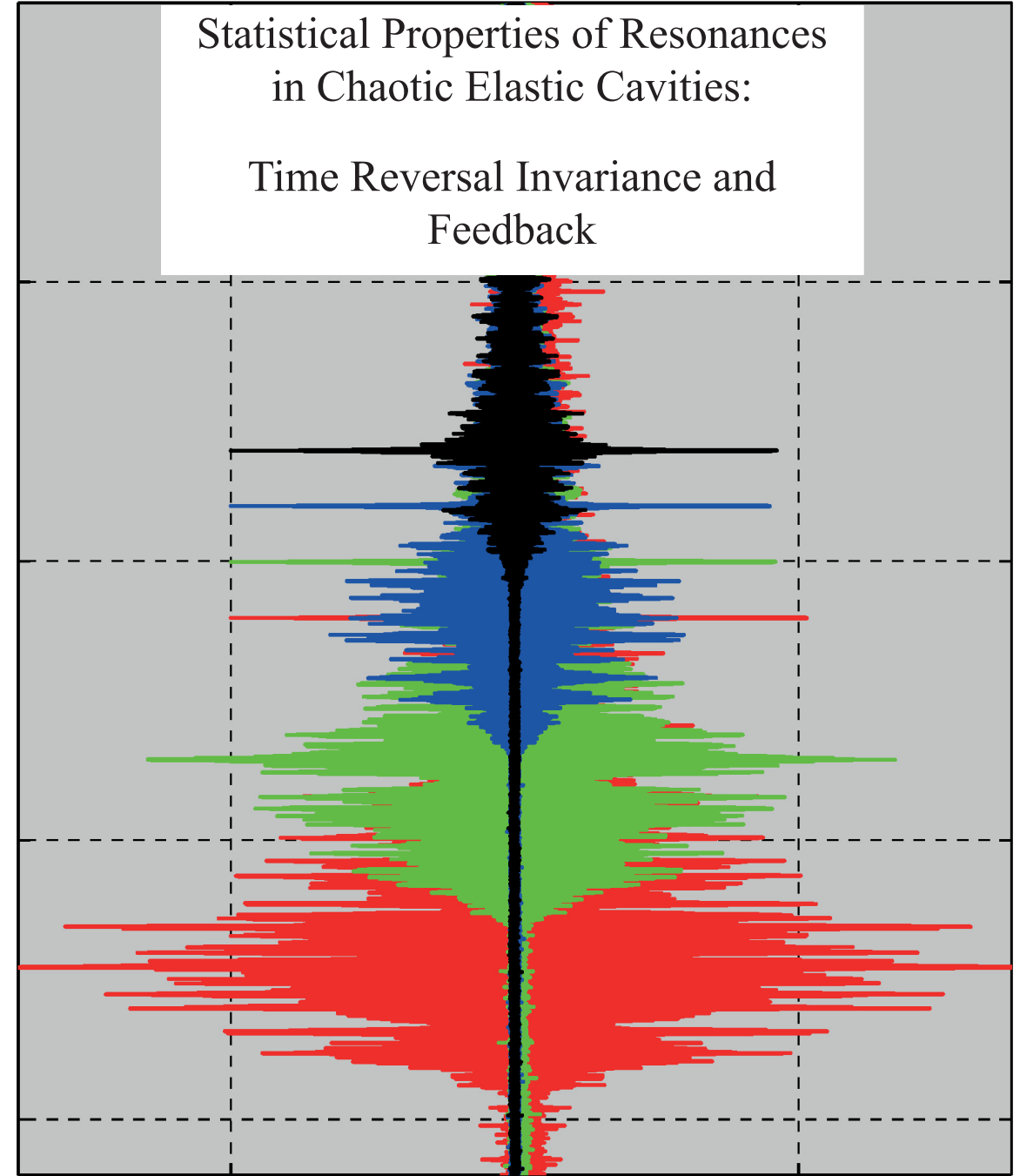
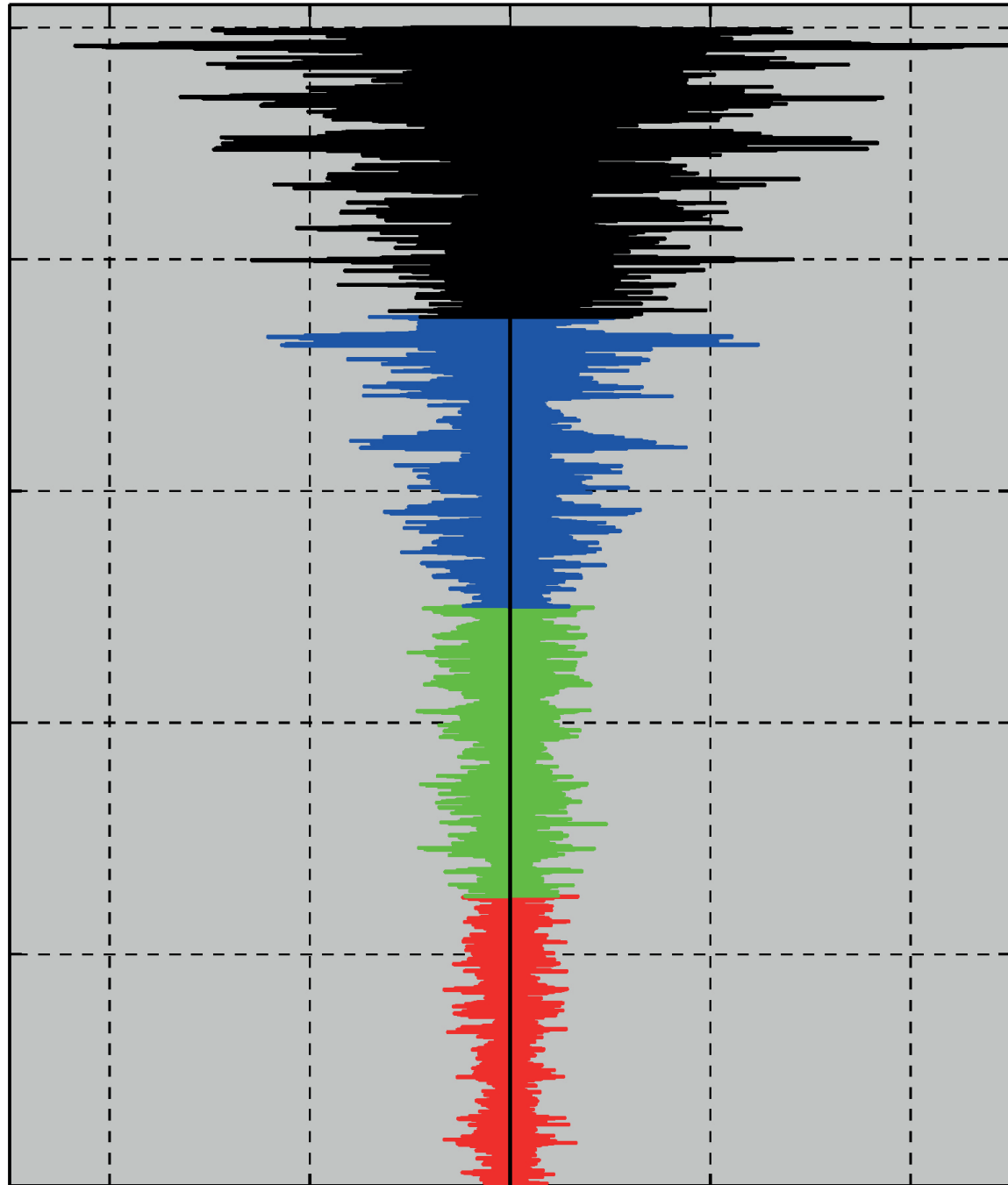
Antoniuk, O. (2011). *Statistical properties of resonances in chaotic elastic cavities: time reversal invariance and feedback*. [Thesis, fully internal, Universiteit van Amsterdam].

General rights

It is not permitted to download or to forward/distribute the text or part of it without the consent of the author(s) and/or copyright holder(s), other than for strictly personal, individual use, unless the work is under an open content license (like Creative Commons).

Disclaimer/Complaints regulations

If you believe that digital publication of certain material infringes any of your rights or (privacy) interests, please let the Library know, stating your reasons. In case of a legitimate complaint, the Library will make the material inaccessible and/or remove it from the website. Please Ask the Library: <https://uba.uva.nl/en/contact>, or a letter to: Library of the University of Amsterdam, Secretariat, Singel 425, 1012 WP Amsterdam, The Netherlands. You will be contacted as soon as possible.



Statistical Properties of Resonances in Chaotic Elastic Cavities



Statistical Properties of Resonances in
Chaotic Elastic Cavities:
Time Reversal Invariance and
Feedback

Statistical Properties of Resonances in
Chaotic Elastic Cavities:
Time Reversal Invariance and Feedback

ACADEMISCH PROEFSCHRIFT

ter verkrijging van de graad van doctor
aan de Universiteit van Amsterdam,
op gezag van de Rector Magnificus
prof. dr. D. C. van den Boom,
ten overstaan van een door het college voor promoties
ingestelde commissie,
in het openbaar te verdedigen in de Agnietenkapel
op donderdag 29 september 2011, om 12.00 uur

door

Oleg Antoniuk

geboren te Kyiv, Oekraïne

Promotiecommissie:

Promotor: Prof. dr. G. H. Wegdam

Copromotor: Dr. R. Sprik

Overige leden: Prof. dr. T. Guhr

Prof. dr. A. Lagendijk

Prof. dr. C. A. J. Klaassen

Prof. dr. M. S. Golden

Prof. dr. D. Bonn

Prof. dr. H. B. van Linden van den Heuvell

Faculteit der Natuurwetenschappen, Wiskunde en Informatica



The author can be reached at
oleg.anton@gmail.com

ISBN: 978-94-91211-97-3

The research reported in this thesis was carried out at the Institute of Physics, van der Waals - Zeeman Institute, University of Amsterdam. This work was a part of the research program of the Stichting voor Fundamenteel Onderzoek der Materie (FOM), which is financially supported by the Nederlandse Organisatie voor Wetenschappelijk Onderzoek (NWO). A digital version of this thesis can be obtained from <http://dare.uva.nl/>.

CONTENTS

1. <i>Introduction</i>	9
1.1 Introduction	9
1.2 Overview of the statistics of Random Matrix Theory	12
1.2.1 Historical background of Random Matrix Theory	12
1.2.2 Gaussian Orthogonal Ensemble	13
1.2.3 Nearest neighbor eigenvalue spacing distribution and spectral rigidity	14
1.2.4 The distributions originating from coexistence of independent energy level sequences	18
1.2.5 Distributions for incomplete sequence of energy levels	20
1.2.6 Statistics of Random Matrix Theory for ultrasonic waves	22
1.2.7 Broken time reversal invariance	25
1.2.8 Moments of distributions	26
1.3 Overview of time reversal experiments	26
1.3.1 General scheme of the time-reversal experiment	26
1.3.2 From time reversal mirrors to time reversal within a closed chaotic cavity	29
1.3.3 Acoustic waves versus electromagnetic waves	31
1.3.4 Efficiency of the exciting pulse refocusing in time-reversal experiment and time-reversal window	31
1.4 This Thesis	35
2. <i>Statistics of resonances and time reversal reconstruction in aluminum acoustic chaotic cavities with time reversal invariance</i>	37
2.1 Introduction	37
2.2 Experimental setup	38
2.2.1 Material properties and design of samples	38
2.2.2 Sample support and transducer holders	40
2.2.3 Measurement instruments and procedures	42
2.3 Efficiency of excitation pulse reconstruction in time reversal experiments without breaking of time reversal invariance	45

2.4	Statistical properties obtained from experiments without breaking time reversal invariance	49
2.4.1	Division of energy between cavity waves: distributions of intensity transmission coefficients and resonance line widths	49
2.4.2	Random matrix statistics of resonance sequences obtained from experiments	51
2.5	Summary of experiments without breaking time reversal invariance	61
3.	<i>Simulation of elastic waves in the cavity</i>	63
3.1	Introduction	63
3.2	The samples and simulation	63
3.3	Simulation results	64
3.4	Discussion of the results: Nearest Neighbor Spacing Distribution and Spectral Rigidity determined from simulation	65
3.5	Conclusions	70
4.	<i>Statistics of resonances and time reversal reconstruction in aluminum acoustic chaotic cavities with feedback</i>	72
4.1	Introduction	72
4.2	Experimental setup for studies of the cavity with feedback loop	73
4.2.1	The sample and transducers	73
4.2.2	Measurements with feedback	76
4.3	Efficiency of excitation pulse reconstruction in time reversal experiments with a breaking of the time reversal invariance	76
4.4	Statistical properties obtained from experiments with feedback	77
4.4.1	Division of energy between cavity waves: distributions of intensity transmission coefficients and resonance line widths	77
4.4.2	Random matrix statistics of resonance sequences obtained from experiments	80
4.5	Summary on experiments with breaking of the time reversal invariance	84
5.	<i>Random matrix model of the chaotic cavity with time reversal invariance broken by the feedback loop</i>	88
5.1	Introduction	88
5.2	Derivation of the matrix to describe random matrix statistical properties of the elastic cavity influenced by a feedback loop	88
5.3	Input parameters of the simulation and the simulation procedure	95

5.4	Summary of random matrix model of the elastic cavity influenced by a feedback loop	99
6.	<i>Conclusions</i>	103
	<i>Appendix</i>	107
A.	<i>Moments, central moments, skewness, and kurtosis of the Nearest Neighbor Spacing Distributions of the main models of Random Matrix Theory</i>	108

ACRONYMS

AWG	Arbitrary Waveform Generator
GOE	Gaussian Orthogonal Ensemble
GUE	Gaussian Unitary Ensemble
NID	Normalized Intensity Distribution
NNSD	Nearest Neighbor Spacing Distribution
PC	Phase Conjugation
RMT	Random Matrix Theory
SR	Spectral Rigidity
TR	Time Reversal
TRM	Time Reversal Mirror

VARIABLES

in Chapter 1:

s	nearest neighbor resonance spacing
s_{avg}	average nearest neighbor resonance spacing in the considered energy (frequency) band
$P(s)$	various distribution functions
$N(E)$ or $N(f)$	staircase function (resonance counting function) depending on energy or frequency
Δ	spectral rigidity
$2L$	size of the energy (frequency) band used in calculation of spectral rigidity
E_C	central value in energy band used for calculation of spectral rigidity
A, B	parameters used for minimization when calculating the value of spectral rigidity
π	$\pi = 3.14159\dots$
γ	Euler's constant $\gamma = 0.57722\dots$
t_0	starting time of the time interval of the recorded oscillations to be replayed in time reversed order (assuming the original excitation pulse at $t = 0$)
t_1	ending time of the time interval of the recorded oscillations to be replayed in time reversed order (assuming the original excitation pulse at $t = 0$)
$\delta T = t_1 - t_0$	size of the time reversal window
A	point on the surface of the sample (acoustic resonator) where the input transducer (also referred as "acoustic source" or "source") is connected
B	point on the surface of the sample (acoustic resonator) where the output transducer (also referred as "receiver") is connected
τ_d	parameter used in detecting the position of the reconstructed spike in time (in analysis of the data from time reversal experiments)

in Chapter 2:

d	side of the aluminum cubes used for fabrication of the cubic resonators
Δt_0	first arrival time in determination of the longitudinal wave velocity
$2L$	size of the frequency band used in calculation of spectral rigidity
L_A	wave path in aluminum used in determination of the longitudinal wave velocity
s_{avg}	average nearest neighbor resonance spacing in the considered frequency band
t_1	time delay between the original excitation pulse and the end of the recorded oscillation track to be reversed (basically the same as in Chapter 1)
σ	normalization coefficients in analysis of the efficiency of time reversal reconstruction in time reversal experiments
I	intensity
I_{avg}	average intensity in the considered frequency band
w	resonance line width
w_{avg}	average resonance line width in the considered frequency band
s	nearest neighbor resonance spacing
s_{avg}	average nearest neighbor resonance spacing in the considered frequency band
p_1, p_2, p_3, p_4	coefficients of the smooth polynomial function used in unfolding procedure to fit the staircase function
s_j	resonance spacings
s_j^*	unfolded resonance spacings
f_j	resonant frequencies
f_j^*	unfolded resonant frequencies

in Chapter 3:

E	elastic modulus
$2L$	size of the frequency band used in calculation of spectral rigidity
s_{avg}	average nearest neighbor resonance spacing in the considered frequency band
ν	Poisson ratio

in Chapter 4:

- K amplification of the amplifier within the feedback loop
- k scaling coefficient used to scale time reversed oscillation tracks in time reversal experiment
- $2L$ size of the frequency band used in calculation of spectral rigidity
- I intensity
- I_{avg} average intensity in the considered frequency band
- s nearest neighbor resonance spacing
- s_{avg} average nearest neighbor resonance spacing in the considered frequency band

in Chapter 5:

$\vec{u}(\vec{x}, t)$	acoustic displacement field
ρ	mass density
λ	Lamé's first parameter
μ	Lamé's second parameter or shear modulus
\vec{x}	coordinate inside the cavity
t	time
$\vec{f}(\vec{x}, t)$	force density related to the excitation of the cavity waves by external forces (including the feedback loop influence)
c_{\parallel}	longitudinal wave velocity
c_{\perp}	transverse wave velocity
\hat{L}	space dependent part of the acoustic wave operator
$2L$	size of the frequency band used in calculation of spectral rigidity
s_{avg}	average nearest neighbor resonance spacing in the considered frequency band
A	point on the surface of the resonator where the input transducer is connected
B	point on the surface of the resonator where the output transducer is connected
C	point on the surface of the resonator where the feedback loop receives the signal
D	point on the surface of the resonator where the feedback loop releases the signal
α	transfer coefficient in modelling of the feedback loop
τ	delay time of the signal travelling through the feedback loop
ω_n	eigenfrequencies of the unperturbed cavity (without of the influence of the feedback loop)
$\vec{\psi}_n(\vec{x})$	eigenfunctions of the unperturbed cavity (without of the influence of the feedback loop)
$\varphi_n(t)$	time dependent amplitudes
β_{kj}	parameters in equations related to the strength of the influence of the feedback loop
ν_n	new eigenfrequencies (of the resonator influenced by the feedback loop)
B	parameter in statistical simulation related to the strength of the influence of the feedback loop
f_{AV}	average frequency in the frequency band in simulation of the resonance spacing distribution due to random matrix model

1. INTRODUCTION

1.1 Introduction

The propagation and scattering of acoustic ¹ waves as well as the properties of localized (resonant) modes are widely used to determine the elastic and viscous properties of liquid and solid materials. In many materials of practical importance (e.g. metals) acoustic waves can travel over distances much larger than the wavelength due to the very small damping of the acoustic vibrations. For example it is possible to hear the sound of the approaching train (tram) in the railway track long before it actually arrives.

In homogeneous materials the propagation of acoustic waves is strongly influenced by the boundaries, inhomogeneities, cracks etc. The mismatch in acoustic impedance which is a product of density and sound velocity at interfaces is in general much higher than the mismatch in the refractive index, i.e. the corresponding property of the electromagnetic waves. Acoustic waves also have a much smaller wavelength than electromagnetic ones at a given frequency due to the considerably smaller wave velocity.

Because of this high sensitivity to material properties on small length scales, acoustic waves are used in many practical applications such as nondestructive testing of materials and mechanical structures [1, 2]. These applications include e.g. monitoring quality and aging of construction materials in airplanes, tuning cars, testing computer hard drives, medical imaging, mapping the underground structures in relation with oil exploration, and all kinds of ultrasonic imaging.

Acoustic behavior of complex (almost) closed strong wave scattering systems will be considered in this thesis. To study scattering of waves in complicated structures one needs to consider statistical approaches rather than a detailed description of a particular case. One successful statistical approach originating from quantum mechanics [3, 4] is to describe properties of eigenvalues (i.e. resonant frequencies or energy levels) and eigenfunctions of the complex chaotic system by modelling the Hamiltonian of the system with an

¹ In this thesis the term acoustics is used for both acoustic waves in gaseous and liquid systems and elastic waves in solid systems

ensemble of random matrices with certain properties. Statistical properties of the eigenvalues of this ensemble of random matrices give statistical properties of the considered resonant frequencies or energy levels. This can also be applied to interpret the properties of acoustic waves in complex mechanical systems.

In general the associated wavefunctions of the resonant modes belong to several independent subspaces. E.g. each subspace may consist of wavefunctions localized in separate parts of real space or wave functions with common symmetry as in the case of a sequence of wavefunctions in a rectangular cavity described by two independent wavenumbers [3]. The combined resonance frequencies of all the modes are then most likely uniformly distributed with a Poisson (exponential) distribution for the spacing between neighboring resonance frequencies. This means that the statistical properties of the resonance frequencies in a small enough frequency band with constant density of resonance frequencies should be the same as for randomly chosen values uniformly distributed within this frequency band.

There is an important distinction between the spectra resulting from a combination of uncorrelated modes as described above and the spectrum of a single *chaotic* system. In classical physics chaos is defined as a system with exponentially diverging trajectories each of which tend to cover all the available phase space. This leads to a series of modes that can be identified by a single wavenumber in the wave system corresponding to chaotic ray trajectories. The resonance frequencies of such a classically chaotic system [5] should show level repelling [3] leading to a reduced probability of finding small frequency spacings. The spectral properties of chaotic classical and quantum mechanical systems are still studied intensely. In particular the spectral behavior when the limit to the quantum system is obtained from non-dissipative classical chaotic systems [6].

The statistical properties of resonance frequencies in chaotic systems can be modelled using Random Matrix Theory (RMT) [3]. The RMT is applicable to scattering of various kinds of waves, in particular also for acoustic waves [7]. For acoustic waves the Hamiltonian corresponds to the operator of the acoustic wave equation describing the displacement and velocity of the elastic motion. In RMT statistical properties of the levels (resonances) are obtained for different models of random Hamiltonian matrices with appropriate symmetries. Examples of such symmetries are the time reversal invariance of the underlying wave equation and geometrical symmetries in the cavity. For example a thin 2D plate of irregular shape when it has one or two symmetry planes normal to its surface, studied in [8, 9]. For more details on RMT see part 1.2.

Time reversal invariance holds for many phenomena in physics. In partic-

ular the standard classical wave equations display time reversal invariance. This is strictly true only for non dissipative systems, but as long as the dissipation is small, many features of time reversal invariance can still be identified. The breaking of the time reversal invariance in electromagnetic systems is well known and observed in magnetically active materials. For example Faraday rotators consisting of active magnetic materials break the symmetry between forward and backward propagating waves with respect to the direction of an applied magnetic field. In acoustic systems flow and motion of the media can break the time reversal invariance. Such phenomena have been studied in moving liquids in acoustic experiments [10, 11, 12, 13].

The breaking of time reversal invariance should also show up in the spectral properties of such systems. For example based on RMT one expects that level repelling occurs more in systems without time reversal invariance. For acoustic systems this has not been confirmed yet and it is of fundamental interest in the physics of classical wave systems.

Part of this thesis will focus on resonance statistics for the elastic cavity which has time reversal invariance broken in a controlled way. In a series of experiments outlined in Chapter 4 we implement the breaking of the time reversal invariance by introducing a feedback loop in a solid system instead of a flow in a liquid system. Part of the signal recorded on an additional transducer is amplified and re-emitted into the system through another additional transducer. Hence, the reciprocity and the time reversal invariance are broken (since the signal can travel in only one direction within the feedback loop). In these experiments we hope to identify the changes in the spectral properties (statistics of resonances) and compare them with main RMT models and with a novel approach to model random matrix statistics of a system with feedback (Chapter 5).

There is a suitable experimental method to determine the degree of time reversal invariance in the system. For a system with time reversal invariance the evolution of a propagating pulse can be traced back by reversing all outgoing waves in time [14]. In a time reversal experiment the scattered signal from a single source is recorded on several transducers placed around the source. The recorded signals are replayed then through the transducers in the reversed order of time. A spatial and temporal reconstruction of the original exciting pulse at the original source location occurs. However, the reconstructed pulse is a combination of the refocused signal and the ongoing evolution of the waves after the reconstruction.

The imperfection of the reconstruction is caused by the fact that only a part of the wavefront is reversed using a finite time window to record and reverse the signals. Issues related to reconstruction of the original excitation pulse using different parts of the recorded signal in a time reversal experiment

and detection of the reconstructed pulse are discussed in section 1.3.

In a cavity this mechanism of reversing all outgoing waves applies to even a single transmitter and detector pair [15]. In principle it is possible to use even a single transducer both as source and detector in sequence [16]. For more details on time reversal experiment see section 1.3.

1.2 Overview of the statistics of Random Matrix Theory

1.2.1 Historical background of Random Matrix Theory

RMT was originally developed to describe properties [4] of complex quantum many body systems (nuclei). An ensemble of random Hamiltonians with certain properties is considered in RMT instead of original Hamiltonian of the system which is usually unknown in detail [4]. It was the only practical way to estimate the role of different interactions in the nuclei and identify the symmetries of such systems without actually knowing the corresponding Hamiltonian. RMT was originally developed by the physicist Eugene Wigner in 1950 to describe the statistics of eigenvalues and eigenfunctions of complex quantum system (statistics of energy levels of nuclei). Later it was realized that RMT is applicable to scattering of various kinds of waves, in particular also to acoustic waves [7].

RMT gives in particular a model for the distribution of the spacing between the nearest neighbor levels. The most well known statistical distributions from the RMT refer to the following cases:

a. Random division of the energy band into intervals by energy levels. The distribution of the spacing between the nearest neighbor levels in this case is exponential (also referred as Poisson distribution).

b. The case of the random Hamiltonian preserving the time reversal invariance, when the Hamiltonian is modelled by the Gaussian Orthogonal Ensemble of matrices.

c. The case of the random Hamiltonian with broken time reversal invariance, when the Hamiltonian is modelled by the Gaussian Unitary Ensemble of matrices.

Case a) predicts a distribution of the distance between nearest neighbor levels with a high probability for the smallest separations. Cases b) and c) are distributions with a maximum peaked around the value close to the average spacing between the nearest neighbor levels. The difference between cases b) and c) is that in case c) the probability of small distances between eigenvalues (resonances, energy levels) is suppressed even more than in case b), revealing greater level repulsion.

We will discuss all three mentioned cases in more detail in the next sections of this chapter. In addition we also discuss the case of coexistence of independent level (resonance) sequences in the same energy (frequency) band and the case in which, due to finite resolution effects, an incomplete sequence of energy levels (resonances) is observed.

1.2.2 Gaussian Orthogonal Ensemble

The Gaussian Orthogonal Ensemble (GOE) is defined in RMT [3] as an ensemble of symmetric matrices that have identically distributed real random Gaussian elements and their statistical properties are invariant under orthogonal matrix transformations.

The detailed position of the eigenvalues of these matrices are varying for each realization. However quantities such as eigenvalue density and eigenvalue separation follow universal behavior. The distribution of the nearest neighbor eigenvalue spacing for the members of the GOE describes the distribution of intervals between energy levels (resonant frequencies) of a class of semiclassical Hamiltonian physical systems [17]. However, RMT models such as GOE are applicable to systems in which an understanding in terms of semiclassics has not been achieved yet, such as complex nuclei or other quantum many-body systems. So modelling a Hamiltonian with a random matrix has quite broad area of applications [4].

A symmetric matrix implies time reversal symmetry in the system. The invariance of the statistical properties of the matrix ensemble under orthogonal transformations describes an ensemble of Hamiltonian matrices that cannot be decomposed into a matrix with separated diagonal blocks. Such a block decomposition [4] leads to additional 'quantum numbers' and therefore to several independent sequences of energy levels. True non-regular (chaotic) resonances are described by only one 'quantum number', related to the only quantity that is conserved - energy. This holds for Hamiltonian systems with a classical chaotic counterpart [17]. Classical trajectories in the phase space of such systems are chaotically mixed so that energy is the only constant of motion.

In the experiments and models presented in Chapter 2 of this thesis the systems (elastic resonators) are in principle time reversal invariant. The statistics of the wave resonances determined in these experiments on chaotic cavities are expected to follow the GOE model. Deviations from this behavior may be expected when a feedback loop is introduced (Chapter 4).

To characterize the statistics of resonances and to compare them with RMT models we will use the nearest neighbor eigenvalue (energy level, resonance) spacing distribution (NNSD) and the spectral rigidity (SR). These

are discussed in greater detail in the subsection below.

To compare the measured distributions and/or theoretical models it is convenient to describe the distributions by a few characteristic parameters. For example the moments of the distributions (mean, variance and higher order moments) are well suited to compare the distributions and quantify their differences. We will use these parameters in addition to NNSD and SR in the analysis of the experimental and theoretical results presented in this thesis.

1.2.3 Nearest neighbor eigenvalue spacing distribution and spectral rigidity

Nearest neighbor eigenvalue spacing distribution

The nearest neighbor eigenvalue spacing distribution, NNSD, gives the probability density of finding the value of the spacing between neighboring energy levels (cavity resonances). NNSD is usually plotted against a variable scaled by the average spacing in the sequence, s/s_{avg} (see nearest neighbor resonance spacing s_j in a schematic graph of a spectrum in Fig. 1.1). The NNSD is normalized to unit area under the curve. If the energy levels (resonant frequencies) divide the given energy band into intervals randomly, case a) in 1.2.1, as in the case of regular (integrable) cavity waves, then the NNSD is a Poisson distribution (exponential distribution), $P_s^{\text{exp}}(s)$, as given below by Eqn. 1.1. Otherwise, if the observed resonances of chaotic cavity are described by the GOE model, case b) in 1.2.1, the NNSD has a shape with a maximum, as shown by the dashed curve in Fig. 1.3. In this case the NNSD is $P_s^{\text{goe}}(s)$, given by Eqn. 1.2.

$$P_s^{\text{exp}}(s) = \exp(-s/s_{\text{avg}}) \quad (1.1)$$

$$P_s^{\text{goe}}(s) = (\pi/2)(s/s_{\text{avg}}) \exp(-\pi s^2/(4s_{\text{avg}}^2)), \quad (1.2)$$

where s is the nearest neighbor resonance spacing and s_{avg} is the average nearest neighbor resonance spacing.

Spectral Rigidity

Another quantity characterizing the RMT (level, resonance) statistics is the spectral rigidity, SR. It depends on the relative order of the resonances (energy levels) and not only on spacings. It is defined through the staircase function $N(E)$ that counts the number of levels up to a value E . The spectral rigidity is a measure of the fluctuations of the staircase function $N(E)$ around a fitted line through $N(E)$.

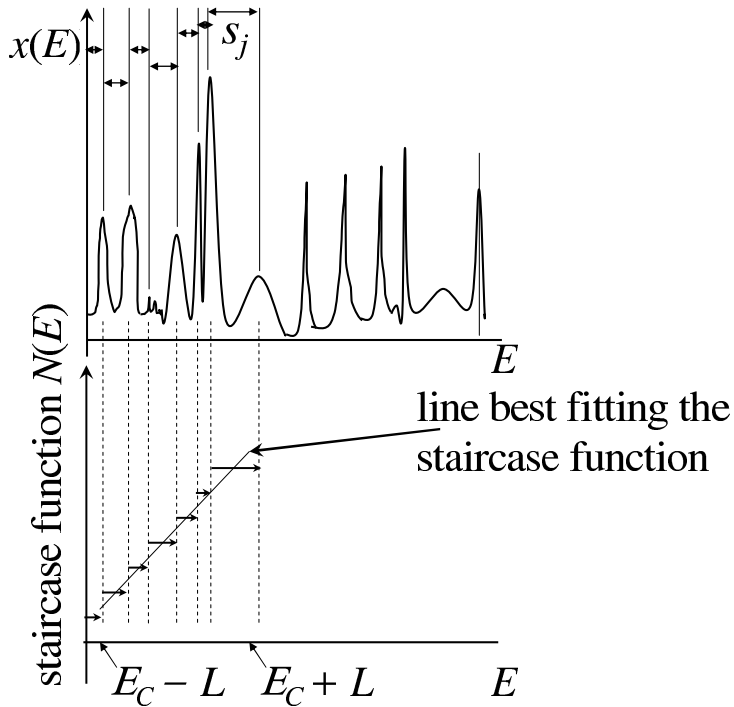


Fig. 1.1: Top graph gives a schematic example of resonances in the spectrum $x(E)$ as function of energy E . The nearest neighbor energy level (resonance) spacing s_j is shown. The sequence of energy levels (top graph) is used to define the staircase function $N(E)$ counting the number of energy levels below the energy E (bottom graph). The line ($y(E) = A + B(E - E_C)$) is the best fit of $N(E)$ in the energy band of size $2L$ centered at the energy value E_C . The staircase functions determined from the experimental data discussed further in this thesis are shown in Fig. 1.2.

The definition of the staircase function is illustrated in Fig. 1.1. The spectral rigidity, Δ , is defined then following [17] as:

$$\Delta = \left\langle \min_{A,B} \frac{1}{2L} \int_{-L}^L (N(E_C + \epsilon) - A - B\epsilon)^2 d\epsilon \right\rangle \quad (1.3)$$

or equivalently

$$\Delta = \left\langle \frac{1}{4L} \left[2 \int_{-L}^L N^2(E_C + \epsilon) d\epsilon - \frac{1}{L} \left(\int_{-L}^L N(E_C + \epsilon) d\epsilon \right)^2 - \frac{3}{L^3} \left(\int_{-L}^L N(E_C + \epsilon) \epsilon d\epsilon \right)^2 \right] \right\rangle, \quad (1.4)$$

where A and B are free parameters chosen to minimize Δ in Eqn. 1.3, $2L$ is the size of an energy band around the average energy value E_C . Brackets $\langle \rangle$ in Eqn. 1.3 and Eqn. 1.4 imply averaging over a number of energy bands of size $2L$ centered at different values of E_C .

Throughout this thesis we will use the function $N(f)$, giving the number of acoustic (elastic) resonances below frequency f (Fig. 1.2), instead of $N(E)$.

Also note that the equivalent form of the SR (Eqn. 1.4) is similar to the standard deviation of $N(E)$ per interval $2L$. Deviation of the function $N(E)$ around the best fitting line (Eqn. 1.3, Fig. 1.1) is the 'rigidity' of the spectra, measured by the SR. SR described by Eqn. 1.3 is the average square deviation of the staircase function from the line (defined by parameters A and B) best fitting the staircase function within the small energy band $E_C - L \dots E_C + L$, Fig. 1.1. So the sequence of resonances (eigenvalues, energy levels) is considered to be more rigid (i.e. has a larger rigidity) if the staircase function (resonance counting function) more significantly deviates from the best fitting line. The important property of the SR is: if energy levels (resonant frequencies) divide the given energy band into intervals randomly, then the SR is proportional to the total size of the included small energy band $2L$, increasing exactly as $2L/(15s_{\text{avg}})$. While for energy levels with statistical properties of a sequence of eigenvalues of the GOE the SR should saturate logarithmically (hence, remains smaller than $2L/(15s_{\text{avg}})$) with increasing L according to the prediction [17, 18] for GOE. Spectral rigidities for the case of random division of the energy band into intervals (or Poisson spectrum) and for GOE model are given below by Eqn. 1.5 and Eqn. 1.6 respectively [4]:

$$\Delta^{\text{exp}}(L) = \frac{2L}{15s_{\text{avg}}} \quad (1.5)$$

$$\Delta^{\text{goe}}(L) = \frac{1}{\pi^2} \left(\ln\left(4\pi \frac{L}{s_{\text{avg}}}\right) + \gamma - \frac{5}{4} - \frac{\pi^2}{8} \right) \quad (1.6)$$

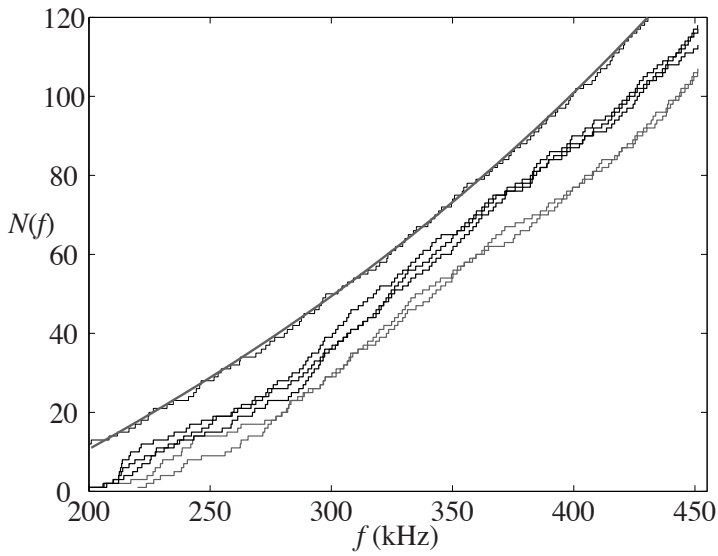


Fig. 1.2: Examples of the staircase functions $N(f)$ determined in an experiment described in Chapter 2. Top curves show the staircase function and the smooth cubic polynomial fitting it.

γ in Eqn. 1.6 is Euler's constant ($\gamma = 0.57722\dots$). The curves given by the above stated equations 1.5 and 1.6 are shown in Fig. 1.6.

Unlike the NNSD, the SR accounts not only for numbers of spacings larger or smaller than average one, but also for the order in which large and small spacings appear on the scale larger than several s_{avg} .

The NNSD and SR are not related to the natural increase in the number of resonances per frequency interval (number of energy levels per energy band). If the observed frequency band is large enough to have different s_{avg} at the beginning and at the end then this effect should be compensated for by the unfolding procedure [19]. Unfolding involves fitting of the staircase function $N(f)$ with smooth cubic polynomial (Fig. 1.2) and then re-scaling the frequency axis with the derivative of this polynomial so that the average spacing s_{avg} and therefore average number of resonances per frequency interval is constant in the frequency band (the same as the slope of the staircase function). After this procedure SR and NNSD can be evaluated as described above. Precise formulas that have been used to do the unfolding procedure are given in Chapter 2.

1.2.4 The distributions originating from coexistence of independent energy level sequences

The distributions originating from the coexistence of independent energy level sequences in the same energy band can be derived analytically [20, 21] by combining several independent energy level sequences in the observed energy band, or obtained via statistical simulation (see Fig. 1.3).

Fig. 1.3 contains 6 curves. Three of them are smooth continuous curves plotted using analytic formulas. NNSD for GOE (given by Eqn. 1.2) is shown as a dashed curve. NNSD for random division of the energy band into intervals by energy levels (given by Eqn. 1.1) is shown as a dash-dotted curve. The solid continuous curve shows the solution for NNSD according to [21] for the case of coexistence of level sequence distributed as eigenvalues of GOE and random sequence of energy levels with a 3:1 density ratio, uniformly distributed within the same energy band. This solution is given by the following equation [21]:

$$P_s^{3:1}(s) = \exp(-s/s_{\text{avg}})/4 \operatorname{erfc}(3\sqrt{\pi}(s/s_{\text{avg}})/8)/16 + \exp(-s/s_{\text{avg}})(16 + 9\pi(s/s_{\text{avg}}))/64(3/8 + 27\pi(s/s_{\text{avg}})/128), \quad (1.7)$$

where $\operatorname{erfc}(x)$ is the complementary error function,

$$\operatorname{erfc}(x) = (2/\sqrt{\pi}) \int_x^\infty \exp(-\xi^2) d\xi.$$

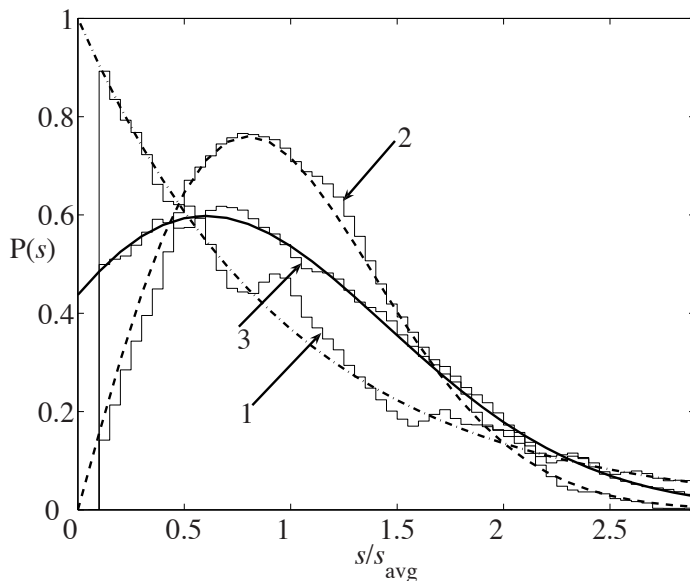


Fig. 1.3: The nearest neighbor spacing distribution for Gaussian Orthogonal Ensemble (dashed curve, $P_s^{\text{GOE}}(s)$, given by Eqn. 1.2) and Poisson distribution (dash-dotted curve, $P_s^{\text{exp}}(s)$, given by Eqn. 1.1). Solution for the nearest neighbor spacing distribution according to [21] for the case of coexistence of level sequence distributed as eigenvalues of Gaussian Orthogonal Ensemble and random sequence of energy levels with a 3:1 density ratio, uniformly distributed within the same energy band (solid curve, $P_s^{3:1}(s)$, given by Eqn. 1.7). Corresponding nearest neighbor spacing histograms for random and Gaussian Orthogonal Ensemble energy level sequences are shown as step-like functions 1 and 2 respectively. The nearest neighbor spacing distribution obtained as statistical simulation for the above-mentioned two level sequences coexisting is given by the step-like function 3.

Three other functions shown in Fig. 1.3 are histograms shown as step-like functions. They are marked with numbers 1, 2 and 3. Step-like function 3 represents the statistical simulation of the above mentioned coexistence of the energy level sequence due to GOE model and random energy level sequence. To do the statistical simulation two independent sequences of energy levels (with a given NNSD and known number of energy levels for each sequence) have been generated using MatLab (The Mathworks, Natick, MA, USA) routines. NNSD (histograms) for these two sequences of energy levels are shown as step-like functions 1 and 2. It is apparent from Fig. 1.3 that these step-like functions 1 and 2 are very close to the dash-dotted and dashed curves respectively (curves representing respectively $P_s^{\text{exp}}(s)$ given by Eqn. 1.1 and $P_s^{\text{GOE}}(s)$ given by Eqn. 1.2). As the next step, the NNSD of the spectra combined (see Fig. 1.4) in the same energy band has been evaluated. This NNSD is actually shown as step-like function 3 in Fig. 1.3. Step-like function 3 is very close to the solid continuous curve representing Eqn. 1.7, which confirms the outcome of the simulation.

1.2.5 Distributions for incomplete sequence of energy levels

For an accurate measurement of the spacing distribution between nearest neighbor resonances, all resonances in the system should be carefully identified. In practice the finite resolution of the experiment causes that a fraction of resonances are 'lost' in determining the statistics. Also damping and mismatch in coupling between the cavity and the transducers hampers the identification of all modes. For example, if the amplitude of the resonance is very small or it is located very close to another (more pronounced) resonance and the peak is selected as a resonance on the basis of having a large enough "peak to base" ratio, then this resonance could easily be missed.

The ability to identify the distributions when accounting for lost levels expands the applicability of the statistical analysis in realistic situations. The effect of lost levels on the level statistics has been studied for the quantum mechanical problem in [22] but not yet for acoustics in 3D metal cavities. Accounting for lost levels in [22] involved a complicated fitting procedure using several approximations. In this thesis the effect of lost levels in 3D metal chaotic cavities is considered by comparing the experimental data to statistical simulations.

Acoustic experiments have been performed [3] in which the issue of the lost levels plays an important role. However, only few quantitative descriptions of the lost levels have been published until now (e.g. article [23] by Enders et al. about states in heavy deformed nuclei and an article [24] by Nogueira et al. about acoustic plate resonators).

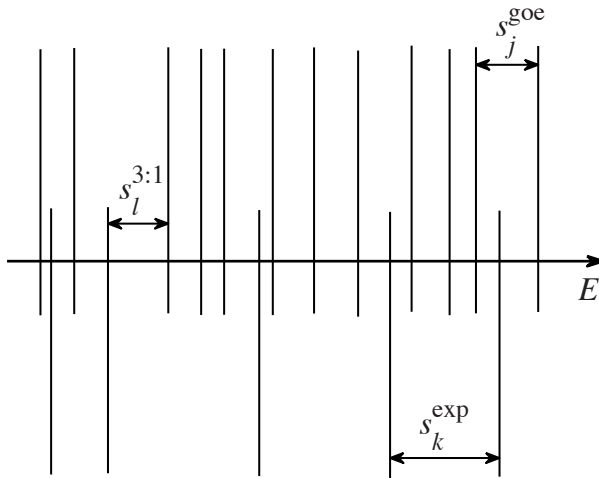


Fig. 1.4: The sequence of energy levels with nearest neighbor level spacing distributed as due to GOE model (top sequence, nearest neighbor spacing is s_j^{goe}) and the random sequence of energy levels (bottom sequence, nearest neighbor spacing is s_k^{exp}). $s_l^{3:1}$ is the nearest neighbor spacing of the simulated coexisting spectra. Its distribution is shown as statistical simulation in Fig. 1.3 (step-like function 3).

The distribution for an incomplete sequence of energy levels may be also efficiently obtained via statistical simulation (Fig. 1.5) similar to the case of coexisting spectra, discussed earlier in Fig. 1.3. We simulated the GOE distribution accounting for lost levels in the detection by averaging the NNSD over a set of generated GOE distributed level sequences. Each sequence consisted of 100 energy levels and a given fraction of lost levels was randomly removed before calculation of the NNSD. Distributions for the GOE model with lost levels obtained in such simulation are shown in Fig. 1.5. These distributions are very similar to those given in the paper [23] by Enders et al.

From Fig. 1.3 we see that NNSD approaches the Poisson (exponential) distribution after random levels are added to the pure GOE sequence of eigenvalues (illustrated by the step-like function 3 and solid curve in Fig. 1.3). Similar transformation of the NNSD happens when a fraction of the eigenvalue sequence is lost in the detection (Fig. 1.5), although the intercept of the NNSD (number of arbitrary small spacings) does not increase in this case.

These trends can also be seen in the spectral rigidity - the spectrum becomes more random (either due to adding randomly chosen levels or randomly removing the existing ones) and therefore more rigid (larger rigidity). An example is given in Fig. 1.6 where the SR is seen to increase for an incomplete sequence of energy levels. The dashed curve in Fig. 1.6 has been calculated as SR for the sequence of eigenvalues of large (5000x5000) random symmetric matrix when 25% of eigenvalues have been randomly removed from the sequence.

1.2.6 Statistics of Random Matrix Theory for ultrasonic waves

The GOE behavior in ultrasonic wave propagation has been found in volume (3D) rectangular aluminum blocks with slits, breaking the symmetry of the cavity [25]. The case of volume acoustic chaotic resonators with one symmetry plane has been studied as well. Weaver et al. [25, 26] found that the NNSD in this case is consistent with distribution for 2 independent GOE distributed sequences of resonances (assumed related to odd and even wavefunctions) coexisting in the frequency band. This implies that the total sequence of the resonant frequencies can be labelled with new 'quantum number' either $n_p = 0$ or 1 related to the conservation of parity in addition to the mentioned 'quantum number', related to conservation of energy.

The difference in spectral statistics for a cubic aluminum block (cavity) and the same cavity in which a small octant at a corner has been removed has been experimentally detected [27]. Similarly the gradual transition from a resonator that has a mirror-like symmetry to a fully chaotic resonator has

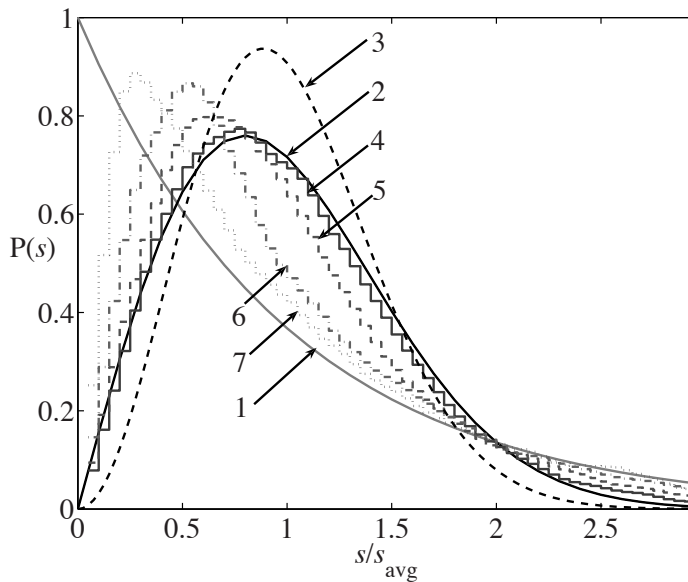


Fig. 1.5: The nearest neighbor spacing distribution for random arrangement of energy levels (exponential distribution, curve 1), Gaussian Orthogonal Ensemble (curve 2) and Gaussian Unitary Ensemble (curve 3). Statistical simulations shown here as step-like functions 4, 5, 6 and 7 correspond, respectively, to 10 %, 25 %, 50 % and 75 % of energy levels lost in generated sequence with nearest neighbor spacing distribution due to Gaussian Orthogonal Ensemble model.

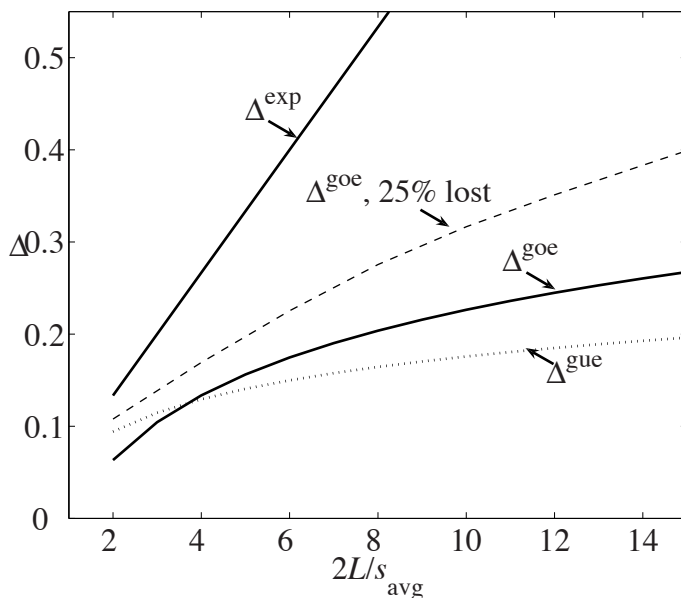


Fig. 1.6: Spectral rigidity for the Gaussian Orthogonal Ensemble model (solid curve, $\Delta^{\text{goe}}(L)$, given by Eqn. 1.6), Gaussian Unitary Ensemble model (dotted curve, $\Delta^{\text{gue}}(L)$, given by Eqn. 1.9) and the case of random division of the energy band into intervals by energy levels (solid line, $\Delta^{\text{exp}}(L)$, given by Eqn. 1.5). Dashed curve shows spectral rigidity for the case of the Gaussian Orthogonal Ensemble when 25 % of energy levels are randomly removed from the level sequence.

been studied and the corresponding evolution of the NNSD (approaching the GOE model) was observed experimentally in anisotropic quartz blocks [28]. More complex GOE based systems (2D resonators), made out of plates were studied in [8, 9]. In particular the NNSD in [8, 9] is actually caused by coexistence of independent GOE sequences of approximately equal densities in the same frequency band. Identification of the modes that belong to each subsequence (e.g. odd and even) was done by studying the sensitivities of resonance line widths to external parameters such as temperature and pressure [8].

This leads to the important conclusion that the symmetries (additional classical constants of motion or additional 'quantum numbers') of the Hamiltonian can be experimentally identified by observing the NNSD and the SR. The extra symmetries cause independent eigen spectra (energy level sequences) to overlap and the energy levels are allowed to fall closer to each other. The associated NNSD will tend to follow the Poisson distribution. Removing symmetries leads in general to a deviation of the NNSD from a Poisson distribution and approaching the GOE model, where energy levels do not tend to fall close to each other (Fig.1.3), and the SR saturates logarithmically (Fig. 1.6).

1.2.7 Broken time reversal invariance

The mentioned geometric symmetries that lead to new 'quantum numbers' are not the only symmetries involved. In principle also the time reversal invariance can be broken. Then the system can still be described by the random Hamiltonian approach now based on a Hermitian matrix. This applies to e.g. the cases where regular 'rotating' disturbance enters the wave equation [29, 10] and the system evolves in a closed cycle making the dynamics irreversible in time. The distribution of energy levels for this case is described by eigenvalue statistics for the matrix ensemble with statistical measures of elements invariant under unitary transformations, Gaussian Unitary Ensemble (GUE) [17, 18].

The NNSD and SR for the GUE model are given as follows [4]:

$$P_s^{\text{gue}}(s) = (32/\pi^2)(s/s_{\text{avg}})^2 \exp(-4s^2/(\pi s_{\text{avg}}^2)) \quad (1.8)$$

$$\Delta^{\text{gue}}(L) = \frac{1}{2\pi^2} \left(\ln(4\pi \frac{L}{s_{\text{avg}}}) + \gamma - \frac{5}{4} \right) \quad (1.9)$$

γ in Eqn. 1.9 (the same as in Eqn. 1.6) is Euler's constant ($\gamma = 0.57722\dots$).

The GUE distribution (Eqn. 1.8) is shown by curve 3 in Fig. 1.5. It shows even greater repelling of energy levels than in GOE case. The eigenspectrum becomes less rigid, meaning also that the logarithmic saturation of the SR occurs at the lower level (Fig. 1.6). So breaking of the time reversal invariance leads to even greater repelling of energy levels than in all earlier mentioned cases (GOE sequence of energy levels and several coexisting independent GOE sequences).

1.2.8 Moments of distributions

As it was mentioned before, the moments of the distributions will be used as well to characterize the resonance statistics in this thesis. Moments, central moments, skewness and kurtosis of the distributions are well suited to compare the distributions and quantify their differences. We will use these parameters in addition to NNSD and SR used traditionally to characterize eigenvalue statistics. In the existing literature [3, 4] moments of NNSD are not discussed while main emphasis is made on NNSD itself and SR.

More details in regard with moments, central moments, skewness and kurtosis for RMT distributions are given in Appendix A. All these parameters can be found as analytical expressions depending on the RMT model (Poisson, GOE, GUE). These expressions are summarized in tables and figures of Appendix A to be used further in Chapters 2 and 4 for comparison with the statistics obtained in the experiments.

1.3 Overview of time reversal experiments

1.3.1 General scheme of the time-reversal experiment

Time reversal invariance in acoustic systems leads to many experiments exploiting the reversibility of the wave solutions in the system [10, 11, 12, 13, 14, 15, 16, 30, 31, 32, 33, 34, 35, 36, 37].

In the context of this thesis time reversal experiments will be used to characterize time-reversal invariance in the system in the time domain as a compliment to the spectral techniques presented in the previous sections.

We will discuss the time-reversal experiment in more detail in the paragraphs below. Imagine an array of transducers that can act as detectors of oscillations delivered by waves and as well as sources of oscillations. Such an array together with the electronics required to record the detected oscillations and then play such recordings backwards will be referred further as time reversal mirror (TRM). Let this array surround an area around the source of waves at certain point A. When the signal is released by the source

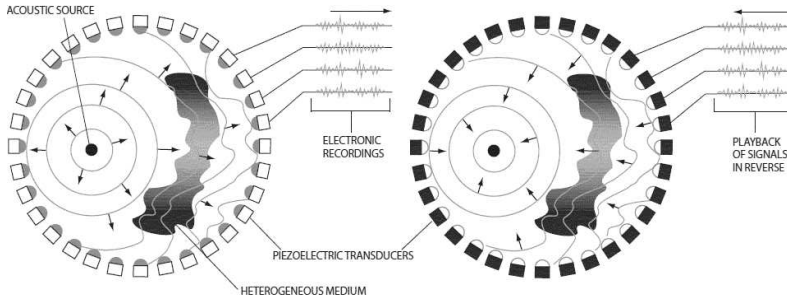


Fig. 1.7: Time reversal mirror in action. Recording of the scattered wave signal by elements of the time reversal mirror (left) and sending the signal back reversed in time (right). Figure from [30].

the wavefront spreads around A and after scattering in surrounding media reaches every transducer of the array. Every TRM receiver receives a long oscillation track which is afterwards recorded, reversed in time and released from the each TRM source at the same location in "reversed order", so that oscillations that arrived first are now released last. The recording of the scattered wave signal and sending it back (reversed in time) by TRM is illustrated in Fig. 1.7.

Now the wavefront may be recreated "propagating backwards" and due to time reversal symmetry of the wave equation deliver the exciting signal back to the original source location. The time reversal technique is based upon time reversal invariance of the wave equation: if one has a solution to the wave equation, then the time reversed solution (using negative time instead of time) of that solution is also a solution of the wave equation. This occurs because the standard wave equation contains only even order time derivatives. In some media time reversal invariance of the waves can not be assumed e.g. due to very high losses or special cases of interaction of the wave field with the media (like in case of moving liquid media for acoustic waves or electromagnetic isolators based on Faraday rotator for electromagnetic waves). But in many useful cases waves can be considered approximately time reversible including acoustic waves in metals, water or air, ultrasound

in human bodies and electromagnetic waves in free space (air).

In a typical TR experiment [14, 30, 38] a medium is excited by a short pulse e.g. at a source point A at time $t = 0$.

The resulting wave field is measured at TRM receiver points. A long oscillation track in a time interval $[t_0, t_1]$ is then time reversed electronically and transmitted at each TRM transducer in opposite order of time. Then, after a time delay of t_1 with respect to the start of the transmitted reversed oscillation track, the resulting wave field forms a localized peak of high intensity at the original source point A. This peak is the reconstruction of the short excitation pulse.

Possible interpretation of this effect in a ray picture is the following. Wave energy is transported along classical rays from point A to the receiver position B and the signal at B is a coherent superposition of waves having the same arrival time. The time-reversed signal thus produces wave fronts which travel back along the ray paths from B to A and, after all kinds of chaotic bouncing around, interfere constructively at the source point A after the time delay of t_1 .

Using TRM to focus the long scattered wave back into short exciting pulse at its source turns out to be quite robust focusing technique that is able to compensate automatically for many factors like spatial distribution of the mass density and sound wave speed, complex anisotropy and heterogeneity in materials as well as mode conversion between different type of waves occurring in the system. That is why such an experiment can have numerous practical applications as well as be the basis for fundamental experiments in pure physics.

TR focusing can be used in medical treatment of tumors and removal of kidney stones. In this treatments high-energy sound waves pass through your body without injuring it and (when focused properly) break the stone into small pieces. These small pieces move out of the body much more easily than a large stone [39]. Stones in kidney and tumors can be sufficiently located using other (non acoustic) techniques [14], like X-ray. But it is still problematic to efficiently focus the stone-destructive ultrasound waves through complex inhomogeneous body tissue without risk of damaging the healthy tissue surrounding the stones or tumors. Iterative TR procedure [14] can solve this problem. A time-reversal mirror with a modified playback algorithm [30] can nevertheless focus ultrasound even through complex porous dissipating skull bone onto a small target being a tumor.

The iterative TRM experiment has been proposed [32] to develop enhanced medical imaging techniques.

Time reversal approach can be applied to study of the quality of building materials, silicon wafers and hard drives, search for cracks in the railway

tracks and improve all kinds of non destructive testing techniques [40, 33]. The detection of small defects is particularly difficult [14] when the inspected object is composed of heterogeneous or anisotropic material. TR technique [14] is a very promising solution in such a case.

Application of time reversal technique to acoustic communication has been explored by Heinemann et al [35] and Derode et al [36]. Heinemann et al [35] used time reversal technique to efficiently communicate a signal to a desired spot within a reverberant acoustic enclosure (cavity). Derode et al [36] showed that on the contrary to intuition, the capacity to transport information in form of acoustic signals is enhanced in a chaotic scattering medium compared to a ballistic channel due to the focusing property of TR experiment.

Long-distance communication in the ocean and communication to submarines [30] can benefit from introduction of time reversal techniques. Also it is possible to use time-reversal approach to studies of the bottom of the ocean and the earth core using seismic waves [34].

Time reversal approach to telecommunications using electromagnetic waves in complex media is explored in [41].

And just think of the possibility of time reversal experiments on all kinds of waves that can happen in physics, like waves on the water, electromagnetic waves, waves in plasma and magnetic liquids, electron waves and complex matter waves (Bose Einstein condensates).

1.3.2 From time reversal mirrors to time reversal within a closed chaotic cavity

In an ideal TR experiment the signal is recorded over a closed surface surrounding the source as shown in Fig. 1.7. Further it is possible to see that TRM detector array not necessarily has to surround the source in all directions. It is enough to cover only a large area and collect the wavefront only over this area. There is always a coherent part [38] of the time-reversed field which will refocus at the source point A.

Furthermore only one receiver is enough [15] instead of an extended TRM if the waves are confined within a chaotic cavity, where due to scattering along chaotic (nonclosed) ray trajectories the distorted wavefront passes the receiver again and again many times. See illustration in Fig. 1.8.

Dynamical systems are considered chaotic in classical mechanics if they have the following properties: its dynamics is covering all the available phase space (e.g. velocity and coordinate of the particle which is a part of chaotic system take all possible values) and the trajectories are exponentially diverging.

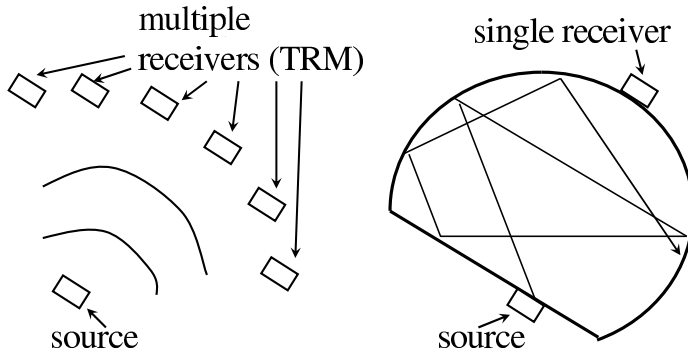


Fig. 1.8: Time reversal mirror setup (left) versus a setup enclosed in the chaotic cavity (right), where the rays bounce around in the closed space and pass through all possible locations inside the resonator.

This can also be seen for a closed space (cavity) from ray perspective. Let rays travel inside the cavity. In a regular cavity e.g. square or circle we see periodic ray trajectories. These keep the rays travelling periodically retracing the negligibly limited part of the cavity. In case of a chaotic shape there are no more periodic trajectories and any ray travelling inside the cavity sooner or later will get as close as possible to any point in the cavity (Fig. 1.8). Such situation is favorable for time reversal experiment with a single receiver because it always allows efficient "capture of all rays" emitted at arbitrary source location.

Draeger and Fink [15] demonstrated that TR experiment works also in a chaotic cavity using a single transducer. This work gives results of experiments and numerical simulations of the wave field in a mono-crystalline silicon wafer. The short excitation pulse was launched at a source point on the surface of a silicon wafer and the response was recorded at a single point on the boundary of the wafer. It was shown that time-reversed and re-emitted signal focuses at the source point.

Draeger and Fink [42] also studied the theoretical limits of time reversal experiments efficiency when using a single source and receiver enclosed in chaotic cavity.

1.3.3 Acoustic waves versus electromagnetic waves

Acoustics and electromagnetics probe at different time and length scales. They also look at different material properties.

Time reversal works particularly good in acoustics due to advanced sensor and source technology developed to handle acoustic waves specifically. It is also important that acoustic waves are quite slow related to electromagnetic waves. This makes it much easier to intercept the spreading acoustic waves of experimentally accessible wavelength, record the delivered oscillations in real time, time reverse the recorded oscillations and send them back in reversed order of time.

For this reason (available cheap and advanced electronics to handle acoustic waves) an acoustic TR experiment is much more convenient. It is important that the time dependence of the signal is fully resolved, that is, that both the intensity and the phase are recorded. For acoustic signals in the the MHz range, standard transducers can achieve this easily. But the same is highly non-trivial when for example using optical signals.

A technique similar to a TR experiment used in optics is called phase conjugation (PC). PC refers to the case where a time-reversal effect is achieved by reversing the sign of the phase of the optical signal. Similarities and differences of both techniques are discussed in detail in works by Fink et al [31] and Derode et al [43].

Furthermore, TR experiments have been done also with electromagnetic waves as well (Strohmer et al [44], Popovski et al [45] and Tourin et al [41]).

1.3.4 Efficiency of the exciting pulse refocusing in time-reversal experiment and time-reversal window

Here we will give a qualitative discussion. A more quantitative analysis of the quality and the properties of the chosen window etc. have been done in the literature (see e.g. work by Sprik and Tourin [37]).

The reconstruction of the initial short excitation pulse (TR focusing) can never be perfect due to a finite oscillation track (time-reversal window) recorded. By reducing the time-reversal window that is recorded and time reversed in experiment we reduce the efficiency of TR focusing. It was found in [15] that the time-reversed and re-emitted signal focuses at the source

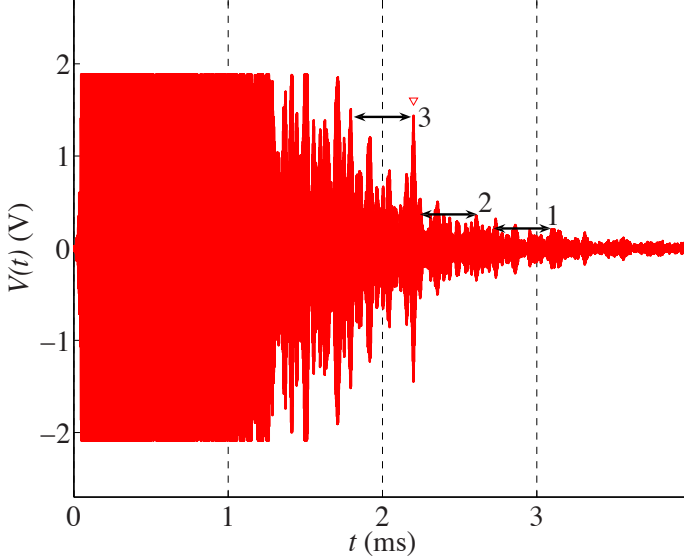


Fig. 1.9: Detecting the reconstructed exciting pulse in time reversal experiment. Cases 1 and 2 show the spikes that are not recognized as the time reversal reconstruction of the exciting pulse. Case 3 shows positive time reversal reconstruction identification. Time intervals of size τ_d are shown with arrows.

point with a signal-to-noise ratio proportional to the time-reversal window $\delta T = t_1 - t_0$.

However, the experiment still works as far as the reconstructed exciting pulse is still detectable on the background of the rest noisy response. At this point various detection techniques can be used. Present work uses the algorithm illustrated in Fig. 1.9. The reconstructed pulse is detected if there is a window of size τ_d before it that does not contain any peak of the same height.

By repeating the experiment with the same recorded oscillation time track length (time reversal window) but with different time delay t_1 of the end of time reversal window with respect to the original exciting pulse we can see a clear trend: detected reconstructed exciting pulse is delayed by the very same time delay t_1 (see Fig. 1.10 and Fig. 1.11). This is one more way that we use to verify the validity of the time reversal experiment and confirm that

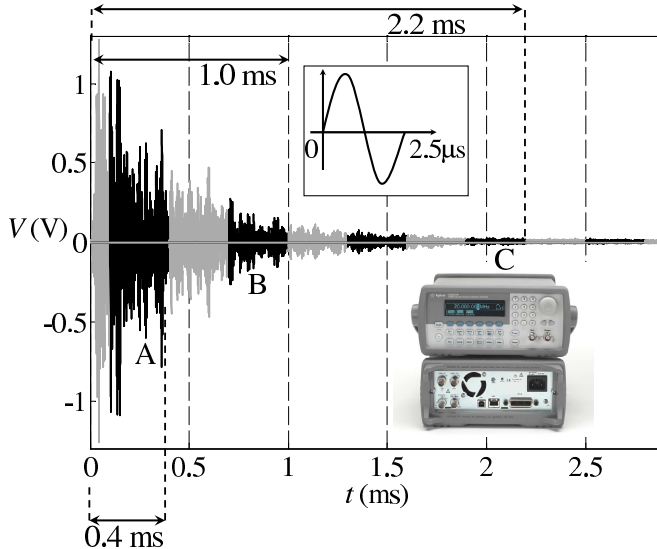


Fig. 1.10: Short $2.5 \mu s$ excitation pulse (upper inset), long response of the resonator including different $300 \mu s$ sections (time reversal windows) that are to be recorded and reversed in time (three of them are marked as cases A, B and C). t_1 (shown with arrows) takes values of 0.4 ms, 1.0 ms and 2.2 ms for time reversal windows in cases A, B and C respectively. Arbitrary waveform generator used in our experiment to generate the recorded oscillations backwards in time (lower inset). Plotted data are taken from experiments discussed further in Chapter 4.

the detected spike comes actually from TR focusing.

1.4 This Thesis

The possibility to study the relation between level (resonance) statistics and time reversal invariance in a single system motivated us to perform time reversal experiment [14] with ultrasonic waves in the aluminum volume samples. Time reversal experiments show directly how efficiently the wave dynamics in the model chaotic cavity (that conforms GOE statistics) can be reversed depending on how long the excitation pulse was dispersed while travelling along the chaotic trajectories in the cavity. We can compare then

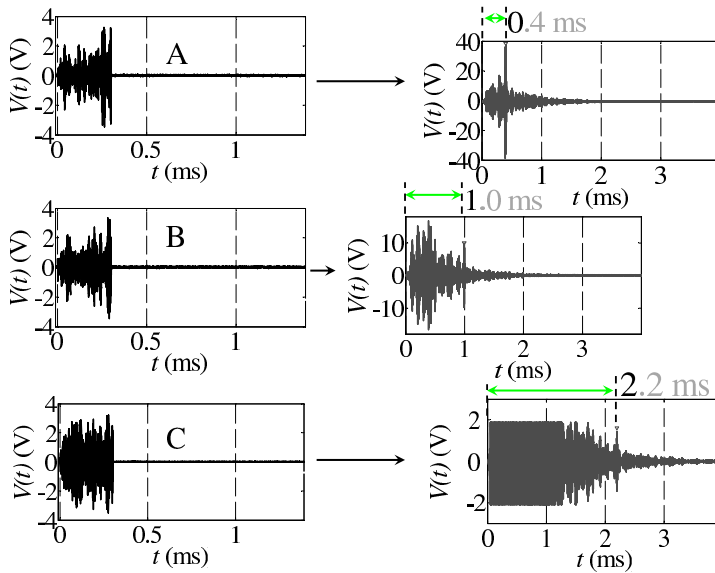


Fig. 1.11: Input time reversed signals marked earlier in Fig. 1.10 as cases A, B and C (left) and corresponding response oscillation tracks with detected reconstructions of the excitation pulse (right). Time delay t_1 (shown with arrows) takes values of 0.4 ms, 1.0 ms and 2.2 ms for time reversal windows in cases A, B and C respectively. Plotted data are taken from experiments discussed further in Chapter 4.

the resonance statistics in case of different degree of time reversal invariance measured by time reversal experiment.

As discussed before in present chapter, RMT was successful in predicting statistical properties of resonances in the systems where complex scattering of acoustic (elastic) waves takes place. Nevertheless there are still issues that have been paid very little attention so far, like quantitative estimations of the fraction of the lost resonances in analysis of elastic resonators. The fact that not all resonances have been detected ('lost modes') should be accounted for in a realistic experiment.

Missing resonances in plate resonators enclosed in the vacuum chamber (quite idealistic conditions) have been considered in [24]. But such particularly important practical case as RMT analysis of missing resonances in experiments on volume metal resonators at normal room conditions still remains unexplored. Such experiments were reported before [3] for aluminum volume (3D) resonators, however no quantitative estimation of the number of lost modes has been made.

Accounting for a fraction of resonances that are not detected plays an important role in analysis of our experiment. We will see that it is still possible to identify the essential features of the underlying statistical distributions in the experiment using simulated distributions (as in Fig. 1.5, part 1.2) for incomplete sequences of resonances.

Breaking the time reversal invariance in acoustic systems and the consequences for the spectral statistics are dealt with in this thesis by introducing well controlled feedback. The feedback loop allows only unidirectional transfer of the signal from one point on the surface of the resonator to another point. The results can be interpreted using standard RMT models and a novel approach to model random matrix statistics of a system with feedback (Chapter 5). Some fundamental questions related to the influence of the feedback loop on the RMT statistics of the elastic resonances are considered e.g. "can a feedback loop break the time reversal invariance of the waves in the elastic resonator sufficiently to make an impact on RMT statistics (NNSD and SR)?" or "what kind of impact can feedback loop do on RMT statistics?" So particularly interesting outcome is expected from TR experiment on a cavity with a feedback loop breaking the time reversal invariance of the system. The NNSD and SR found in experiment on such a system are of fundamental interest.

The further chapters of this thesis will address the above mentioned questions. RMT statistical properties of the unperturbed chaotic cavity (without influence of the feedback loop) determined from experiment and efficiency of time reversal experiment using this cavity are discussed in detail in Chapter 2. Namely NNSD (including moments, central moments, skewness and

kurtosis of the NNSD) and SR will be studied in Chapter 2. RMT statistical properties of the chaotic cavity can be determined both from cavity responses determined in experiment and from simulation of the elastic cavity response using simulation programs that simulate elastic equation in complex solid materials implementing adaptive finite difference method. Analysis of such simulation is discussed in Chapter 3. Investigation of RMT statistical properties and efficiency of time reversal experiment in case when the time reversal invariance of the elastic equation in the sample is broken by the feedback loop is discussed in Chapter 4. Chapter 5 describes possible random matrix model of the elastic chaotic cavity influenced by the feedback loop and outlines the statistical simulation of the corresponding NNSD as given by this model.

2. STATISTICS OF RESONANCES AND TIME REVERSAL RECONSTRUCTION IN ALUMINUM ACOUSTIC CHAOTIC CAVITIES WITH TIME REVERSAL INVARIANCE

2.1 *Introduction*

As pointed out in Chapter 1, statistical and time dependent (time reversal) properties are closely related. The statistical properties of the eigenfrequencies in wave systems such as the NNSD and SR are different for a system with and without time reversal invariance. The difference in time reversal invariance shows up in the time domain by e.g. performing Time Reversal reconstruction experiments. In systems without time reversal invariance the TR reconstruction should fail. In this chapter we investigate the spectral statistics (NNSD and SR) based on experiment and analyze the time reversal experiments for the same unperturbed cavity with time reversal invariance. The experiments were performed with elastic waves in solid aluminum cavities with low absorption properties. In later chapters we will extend this approach using the same cavity when attempting to break the reversal invariance by introducing a feedback loop.

The main goal of this chapter is to prove that the sample(s) behave according to the GOE model corresponding to a system with time reversal invariance. One may also expect that the statistics is influenced by the fact that in the experiments not all resonant modes are detected (i.e. lost resonances). This will be taken into account in detail in the current chapter. A comparison of the experimental and model distributions is carried out also using moments of NNSD. The moments, central moments, skewness and kurtosis will be evaluated as well for both the GOE (GUE, Poisson) cases and the experimentally determined distributions to obtain a full comparison of the RMT statistics obtained from experimental data to the random matrix models.

Two different kinds of experiments will be discussed. In the first kind the responses of the samples (elastic waves in aluminum blocks) to a short excitation pulse is measured. The statistical properties (such as intensity dis-

tribution, NNSD and SR as well as moments, central moments, skewness and kurtosis of the NNSD) will be determined from the analysis of the spectral density of the time dependent responses by Fourier analysis. The NNSD and SR will be compared to the GOE model accounting for the fraction of lost levels in the detection. In the second kind of experiment - the time reversal experiment - different parts of the cavity response will be recorded and sent back through the system reversed in time to test the time reversal invariance.

The experimental setup is described in Sec. 2.2. Sec. 2.2 includes discussion of material properties, design of the samples, sample support, transducer holders and measurement instruments. The efficiency of the reconstruction of the excitation pulse in the time reversal experiments is discussed in Sec. 2.3. The statistical properties obtained from experimental data are considered in Sec. 2.4. In particular the statistics of the division of the excitation pulse energy between the cavity modes and the associated RMT statistics will be studied in Sec. 2.4. Conclusions on experiments without breaking of the time reversal invariance are given in the summary section (Sec. 2.5).

2.2 Experimental setup

2.2.1 Material properties and design of samples

A set of identical aluminum cubes with a side length of 20 mm were used to construct different chaotic cavities. The cubes were further machined to lower the symmetry and to make them more chaotic [3]. An asymmetrically placed well was drilled in cavities Nr. 1 and Nr. 2 to remove the cubic symmetry. An extra side corner was removed from cavity Nr. 2 (see Fig. 2.2 and Fig. 2.3) to lower the symmetry even further. Cavity Nr. 1 has one symmetry plane. Cavity Nr. 2 does not have any symmetry properties like rotation axes or reflection planes. So it is not expected to have independent GOE sequences of resonances in RMT sense. Hopefully it will only have chaotic sets of geometric ray trajectories due to its chaotic shape and will turn out to be a suitable sample to study the statistics of resonances.

The longitudinal wave velocity was determined for the aluminum used by detecting the first arrival of the acoustic pulse through the stack of plates (cubes) of different width (Fig. 2.1). There is also an agreement between the five lowest resonances of the symmetric cubic resonator (without the drilled well or the removed side corner) of the same aluminum and calculations [46]. These give values for the longitudinal and transverse sound velocities of 6410 m/s and 3200 m/s respectively.

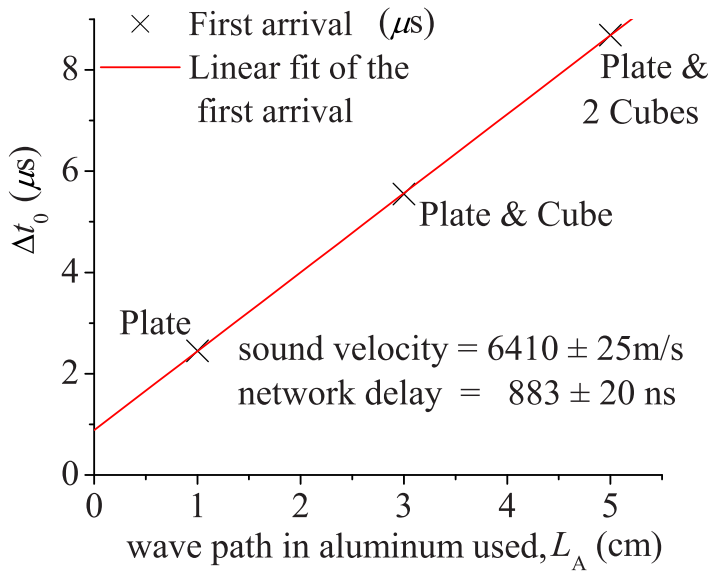


Fig. 2.1: Determination of the longitudinal (fast) wave speed by fitting the first arrival time through the aluminum sample of given width.

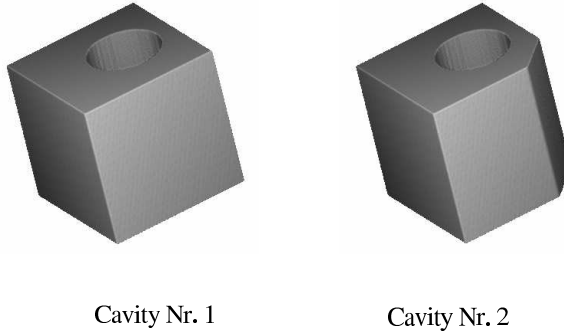


Fig. 2.2: The cavities used in the experiment are made out of aluminum cubes with a cube side size of $d=20$ mm. The symmetry of the cubes is broken by additional features such as an asymmetrically placed cylindrical well (both cavities Nr. 1 and Nr. 2) and a removed side corner (cavity Nr. 2). The radius of the well is 5 mm and its depth is 18 mm. The center of the well divides two orthogonal sides of the square face of the cube as 0.5:0.5 and approximately 0.6206:0.3794. The removed side corner reduces each of two adjacent sides of the square face of the cube by 5 mm.

2.2.2 Sample support and transducer holders

To reduce the losses in the system a very light low mass support is used for the cubes. A slab of low mass density packing material supports three small polystyrene pieces which touch the cavity (one of two aluminum blocks shown in Fig. 2.2) only in three points from the bottom (Fig. 2.3). Small changes in the position of the support did not influence the transmission spectrum and the measurements are as close as possible to the aluminum cavity with free boundary conditions.

To satisfy the best possible alignment of the piezoelectric transducers that are used for signal generation and detection, the optical mirror holders with regulating screws are used as shown in the Fig. 2.3. Slight tuning of the alignment of the transducer holder with the regulating screws enables to

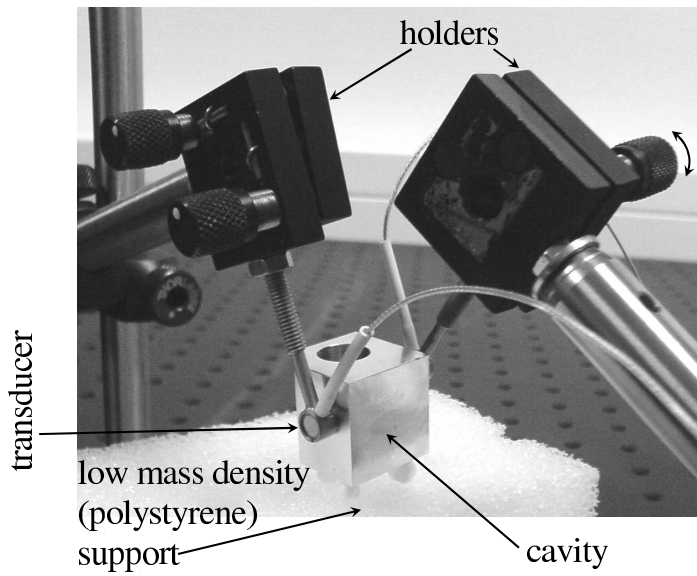


Fig. 2.3: Picture of the sample, transducers connected to it and transducer holders.

reach the highest possible output signal.

2.2.3 Measurement instruments and procedures

The schematics of the experimental setup are shown in Fig. 2.4. An Agilent 33220A 20 MHz Function/Arbitrary Waveform Generator (AWG) generates signals driving the piezoelectric source transducer connected to the cavity using oil as coupling agent. AWG generates a voltage pulse of one period of 400 kHz sine shape (Fig. 2.5) to excite the sample. A Thurlby Thandar Instruments WA 301 Wideband Amplifier is used as the driver amplifier. By changing the excitation pulse amplitude we can discriminate between detection noise and resonant response peaks in the spectrum. The long cavity responses (with reverberation time of about 5 ms) are received by the 2-nd piezoelectric transducer. The second piezoelectric transducer is also coupled to the cavity using oil. Its signal is amplified by an EG&G Princeton Applied Research 5113 model pre-amplifier and recorded by a LeCroy Wave Surfer 424 model 200 MHz digitizing oscilloscope with time step of $0.1 \mu\text{s}$. PICO-HF 1.2 piezoelectric transducers were used. They were manufactured by Physical Acoustics Corporation (MISTRAS Group Holding Company).

The computer connected to the oscilloscope saves the recorded signals by means of Lab View Software (National Instruments Corp., Austin, TX, USA). A 65 536 point Fast Fourier transform of the reverberation response is calculated by Matlab routines (The Mathworks, Natick, MA, USA). Further calculations involve identification of resonances and give the statistical properties discussed before in RMT overview in the Introduction chapter and further in Sec. 2.4.

Fig. 2.5 shows examples of the short excitation pulse driving the source transducer and the corresponding 5 ms long response recorded by the digitizing oscilloscope. The spectral densities calculated from such signals are shown in Fig. 2.6. The spectral density of the excitation pulse recorded by the digitizing oscilloscope is shown in Fig. 2.6 together with the spectral density of the elastic cavity oscillations detected at the receiving piezoelectric transducer, amplified by the preamplifier and recorded by the digitizing oscilloscope.

Both the radius of the well and the width of the aluminum prism removed from the corner of cavity Nr.2, as well as the diameters of the transducers that are attached to the samples are very close to 5 mm. This is approximately half the wavelength of the transverse plane wave in aluminum at 200-450 kHz. The spectral density of the excitation pulse is peaked in this band (Fig. 2.6). The wavelength range of the 200...450 kHz band used is approximately $1.6d \dots 0.7d$ for the fast (longitudinal) wave and $0.8d \dots 0.35d$ for the

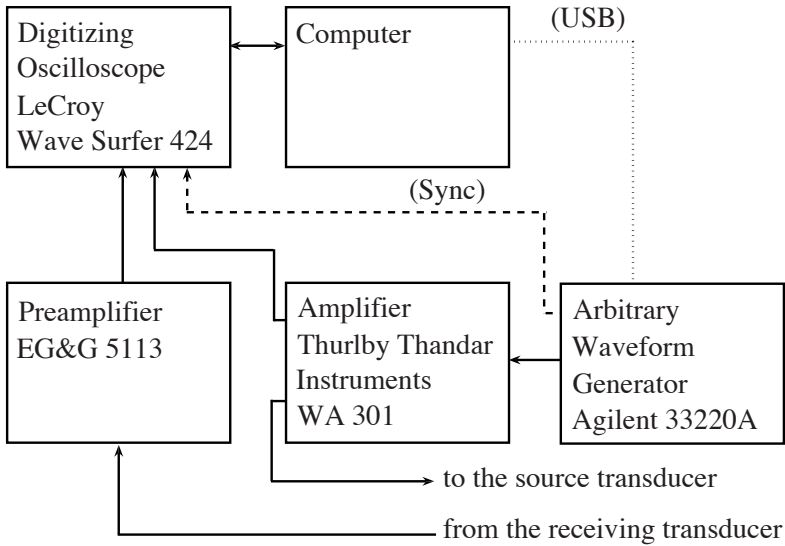


Fig. 2.4: Schematics of the experimental setup.

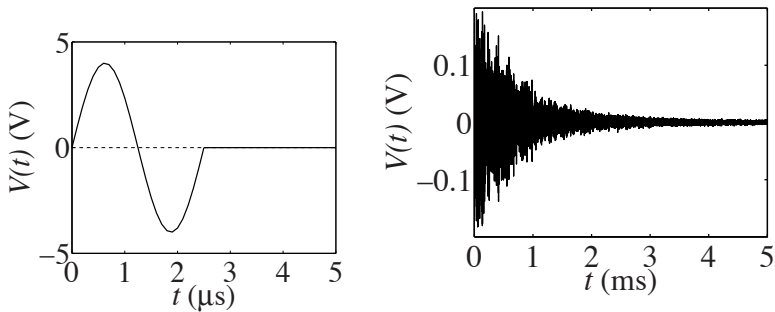


Fig. 2.5: The excitation pulse driving the source transducer (Fig. 2.4), one period of 400 kHz sine shape (left), and the cavity response (right) received by the receiving transducer (Fig. 2.4), amplified by the preamplifier and recorded by the digitizing oscilloscope.

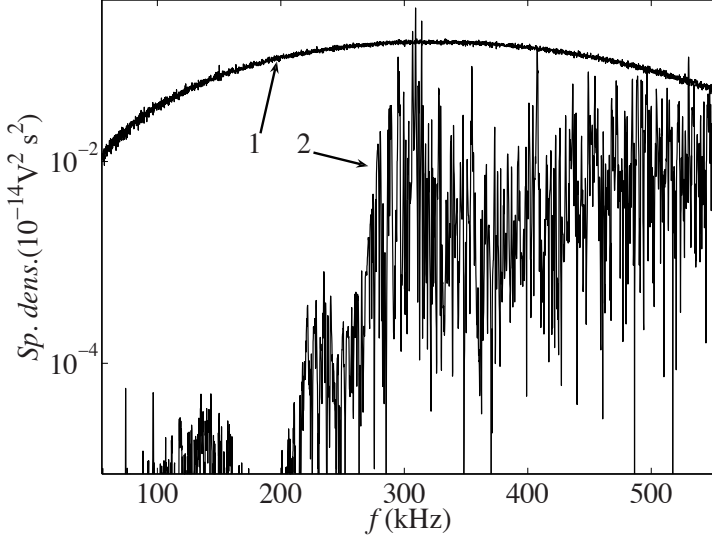


Fig. 2.6: Spectral densities of the short $2.5 \mu\text{s}$ pulse (one period of 400 kHz sine shape) used to excite the cavity oscillations (curve 1) and the 5 ms long response (curve 2) plotted over a broad frequency range. From the measurement on cavity Nr. 2.

slow (transversal) wave. Here d is the size of aluminum cavities (see Fig. 2.2). Therefore, the main contribution to the detected density of resonances may come from "transverse-like" cavity oscillations. The "transverse-like" cavity modes should have a displacement component normal to the surface that can be detected by compressional piezoelectric transducers. They are also the most likely to be excited by the source and received by the receiver which both have the diameter of approximately $0.25d$, which matches half the wavelength of the transverse wave inside the used frequency band. Resonances and corresponding wavefunctions of the complex metallic 3D block can in general not be divided strictly into "transverse-like" and "longitudinal-like" ones e.g. due to transverse-longitudinal wave coupling (transformation) at the complex cavity boundary. But transducers due to their size are more efficient in detecting displacement variations within the wavelength range corresponding to transverse waves at given frequencies. Even if so, this does not mean that "longitudinal-like" resonances are not detected.

In the band above 0.45 MHz (Fig. 2.6) a more dense structure of reso-

nances arises and unavoidably there is a situation reached when the resonance line width is of the order of the average resonance spacing, so that individual cavity modes can not be resolved any more.

2.3 Efficiency of excitation pulse reconstruction in time reversal experiments without breaking of time reversal invariance

There is a natural decay of acoustic energy density in the cavities due to absorption in the aluminum, the loss to the piezoelectric transducers, and some coupling to the support and surrounding air that causes departure from time reversal invariance. We will see that in the experiments the oscillations can be observed for a time considerably longer than the Heisenberg time. The Heisenberg time is defined as the inverse of the average nearest neighbor resonance spacing, $1/s_{\text{avg}}$. It is a measure of the total recording time of the elastic oscillations required in order to resolve the average spacing between the neighboring resonances in the frequency domain. Both time-reversal experiment and the extraction of statistical properties can be performed using the time scale well beyond the Heisenberg time and thus will provide a basis to characterize these properties in one system.

The time reversal experiment, as e.g. described in [14] in general and worked out for a closed chaotic system in [15] can be a clear measure of time reversal invariance for acoustic waves in a chaotic cavity. As outlined in [15], a single transmitter-receiver pair is sufficient to perform a time-reversal experiment in a closed space (cavity). In this experiment each part of the cavity response shown in Fig. 2.7 is recorded separately. Then each track has been scaled to appropriate integer numbers, which were downloaded into the memory of the AWG. So the AWG could replay the recorded oscillation track in the reversed time direction (oscillations that arrived first are being released last). Each of the responses to the 300 μs long reversed tracks (Fig. 2.7) give a clear reconstruction of the original short pulse (Fig. 2.8). The arrows in Figs 2.7 and 2.8 demonstrate that after the generation of the particular reversed oscillation track (track 4) one has to wait a time t_1 until the refocused image of the excitation pulse. This time t_1 is equal exactly to the time elapsed from the original excitation pulse until the end of track 4 (Fig. 2.7). Thus we explicitly see time reversed wave propagation in our aluminum cavities. The oscillation track that has been reversed and corresponding reconstruction of the excitation pulse are marked with the same number in Figs 2.7 and 2.8. We observe the reconstruction peak on the background of noisy decaying signal (Fig. 2.8) due to the fact that only

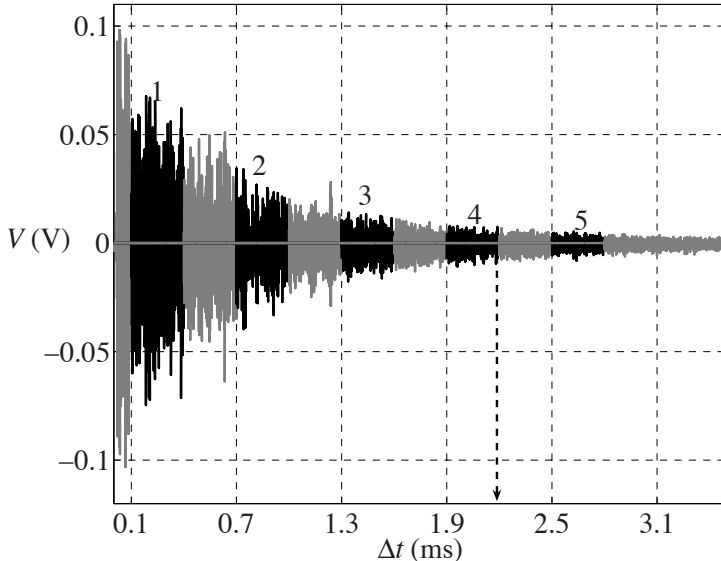


Fig. 2.7: Cavity response upon the exciting pulse at $t=0$, for cavity Nr. 2. Time delay t_1 between the original excitation pulse and the end of the recorded oscillation track 4 is shown by the dashed arrow.

short finite part of the response is being time reversed.

Fig. 2.9 shows the amplitude of the reconstructed pulse, normalized to σ_i , the mean square average of the signal amplitude in the reversed $300 \mu s$ long oscillation track used for excitation. σ_i is proportional to the square root of the energy contained in $300 \mu s$ signal section driving the exciting transducer. Such normalization is necessary because the recorded $300 \mu s$ tracks shown in Fig. 2.7 have different average amplitude. σ_{max} in Fig. 2.9 is the maximum of all thirteen σ_i related to thirteen points in Fig. 2.9. The normalized amplitude characterizes the efficiency of energy focusing in the time reversal experiment with a given time delay t_1 of the end of the recorded oscillation track with respect to the excitation pulse. We can expect from Fig. 2.9 that the amplitude of the reconstructed pulse decays exponentially with delay time. This can be explained simply as absorption of acoustic energy during the time it is stored in the cavity, before the energy is refocused into a reconstructed pulse. However, for the normalized amplitude of the reconstructed pulse shown in Fig. 2.9 this behavior does not extend down to

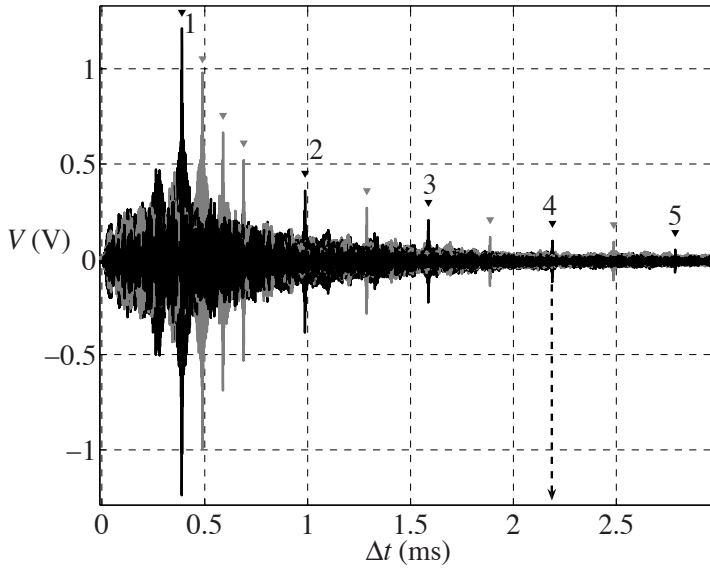


Fig. 2.8: The reconstruction of the dispersed input pulse by time reversal of the recorded signal for cavity Nr. 2. The experiment shows to be working for time delays much longer than the Heisenberg time determined further in Sec. 2.4. Dashed arrow shows delay time t_1 of the reconstructed pulse 4 relative to the start of the replay of track 4 in reverse order of time.

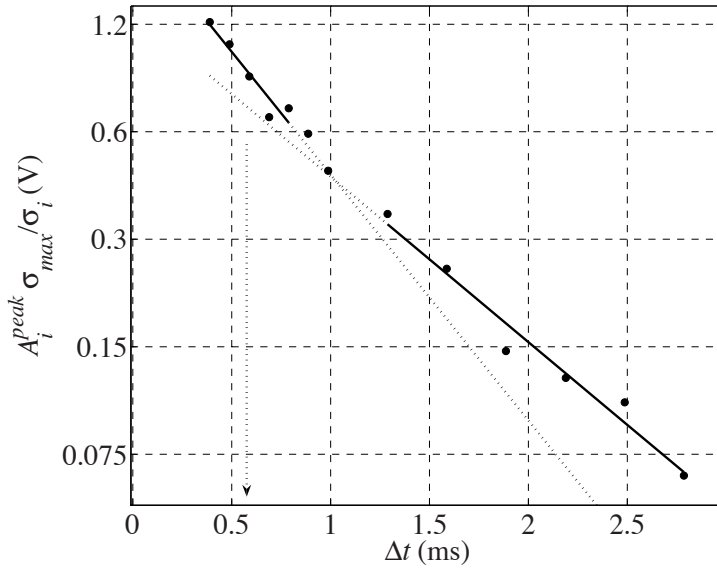


Fig. 2.9: Normalized amplitude of the refocused excitation pulse depending on the time delay of the reversed oscillation track. Closed circles show result of the experiment on cavity Nr. 2. Solid lines show linear least square fits using the first five and the last five points. Dotted lines are simply extensions of the solid lines.

smaller delay times (at least does not extend with the same decay constant). The small delay times correspond to shorter and therefore may be less chaotic trajectories. The estimate of the Heisenberg time is marked with an arrow in Fig. 2.9.

Change in the slope shown in Fig. 2.9 can be related to the fact that longer scattering times correspond to better approach to equilibrium energy distribution between cavity modes. This can influence the reversibility of the wave dynamics. Similar phenomena were considered in work [47].

The length of the reversed tracks was made as short as possible ($300 \mu\text{s}$), just enough to insure good detection of the maximum of the reconstruction peak. This enables to judge the efficiency (per input energy) of the refocused pulse as a function of the time delay.

2.4 Statistical properties obtained from experiments without breaking time reversal invariance

2.4.1 Division of energy between cavity waves: distributions of intensity transmission coefficients and resonance line widths

If a finite amount of energy in each excitation pulse in the chosen frequency band is shared randomly between the cavity waves at different frequencies, then the distribution of the intensity transmission coefficient in the appropriately small frequency band is expected to be exponential. The transmission coefficient at a certain frequency is calculated as a ratio of the spectral density of the output signal to the spectral density of the input pulse at this frequency (see spectral densities of the input and output signals shown in Fig. 2.6).

We performed the statistical analysis using responses of the same samples used in previous section in time reversal experiment. The normalized intensity distribution (NID) obtained for cavity Nr. 1 is shown in Fig. 2.10. The results agree with an exponential dependence if the distribution is evaluated in a small enough frequency band (60 kHz wide, contains about 30 resonances). For broader frequency bands the distribution is a mixture of exponentially distributed intensities with different average values, resulting in an overall non-exponential intensity distribution. Different average intensity values in the broader frequency bands are caused by e.g. different amplification of the amplifier and slightly different sensitivity of the piezoelectric transducers at different frequencies.

The distribution of the intensity transmission coefficients and resonance widths are related to each other and overall related to the distribution of

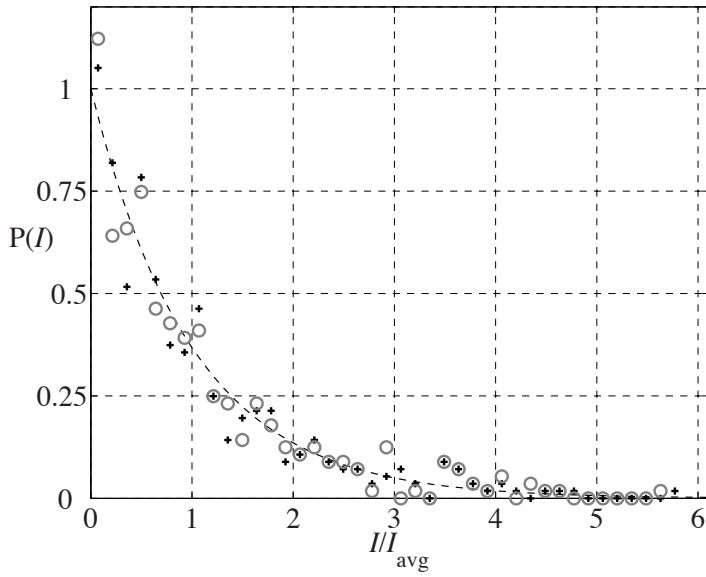


Fig. 2.10: Typical normalized intensity distribution for 60 kHz wide frequency band. The cross and round symbols give distributions for different signal amplitudes. From the measurement on cavity Nr. 1 in 0.27...0.33 MHz band. I_{avg} is the average intensity in the band. The dashed curve shows exponential distribution.

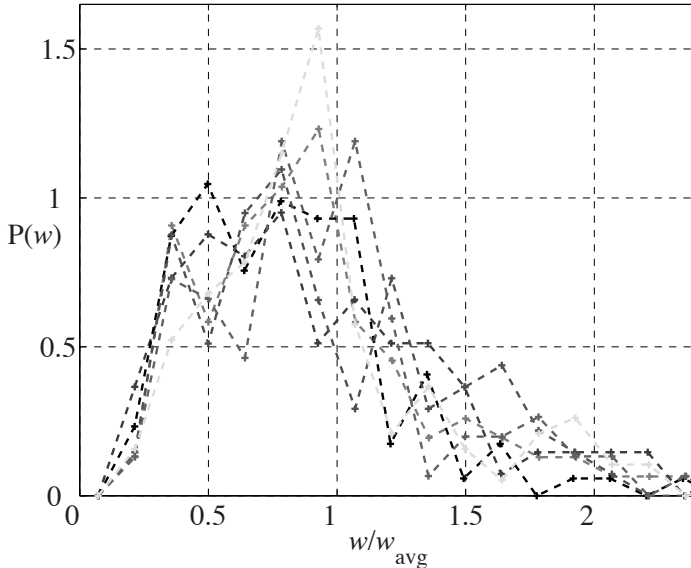


Fig. 2.11: Resonance line width distributions for measurements at different positions of source and receiver for cavity Nr. 2. w_{avg} is the average resonance line width.

pulse intensity between different kinds of cavity waves. In case the detected resonances form a single GOE sequence of resonances or are a major part of it, the resonance width distribution is expected to be peaked around a single average value. This is more or less in agreement with the distributions obtained for cavity Nr. 2 at different locations of source and receiver. They are shown in Fig. 2.11.

The value of the average resonance width w_{avg} is about 300-400 Hz. So the ratio of the average resonance width to the average nearest neighbor resonance spacing determined from experimental data is approximately 0.2.

2.4.2 Random matrix statistics of resonance sequences obtained from experiments

The statistics mentioned in the previous paragraph describes how the finite pulse intensity is shared among the cavity modes. Now we proceed to calculating the RMT statistics from the measured cavity responses. As mentioned

in the introduction, it involves studying how the values of resonant frequencies are distributed themselves or more precise how do they divide fixed finite frequency band into intervals. We take a broad frequency band of 200..250 kHz with an almost constant resonance density and calculate the NNSD. The result calculated from the experimental time traces for cavity Nr. 2 is shown in Fig. 2.12. We see that the results do not agree with the pure model of the GOE, but do agree much better with the distribution where a loss of 25 % of the resonances is accounted for. The error bars in Fig. 2.12 are based on measurements performed for different positions of receiver and source on the surface of the sample. From the NNSD we obtain an average nearest neighbor spacing for both cavities of about 1.8 kHz. This gives an estimate for Heisenberg time: $t_H \approx 556 \mu s$. However, there can be more resonances missing, or independent sequences of resonances present in the case of cavity Nr. 1. Lost resonances can lead to a smaller value of the average nearest neighbor spacing and a larger apparent Heisenberg time.

Figure 1.2 shows the experimentally determined staircase function $N(f)$ for different alignment of the transducers (from experiment on cavity Nr. 2) at certain fixed positions of source and receiver. The best alignment enables the best coupling of the transducers to the sample. Therefore, it allows one to observe the largest amount of resonances. Thus the resulting staircase function is used in the determination of NNSD and SR.

The density of elastic resonances increases as a polynomial function of frequency. It is essential [19] to have the same density of elastic resonances and the same s_{avg} at low and high frequencies for calculation of NNSD and SR. To compensate for slow increase of density of resonances with frequency an unfolding procedure [19] has been applied to the staircase functions. The unfolding procedure involves fitting of the staircase function with a smooth cubic polynomial (Fig. 1.2). Top curves in Fig. 1.2 show the staircase function and smooth cubic polynomial fitting it.

Unfolding of the staircase function $N(f)$ has been performed in this thesis by the following steps:

1. Fitting $N(f)$ in the studied frequency range with a smooth polynomial function:

$$N^*(f) = p_1 f^3 + p_2 f^2 + p_3 f + p_4 \quad (2.1)$$

2. Given $n - k$ spacings $s_j = f_j - f_{j-1}$, $j = k + 1..n$ between neighboring resonances at $n - k + 1$ frequencies f_i , $i = k..n$ are scaled as

$$s_j^* \sim s_j \frac{dN^*}{df} \Big|_{f=(f_j+f_{j-1})/2} \quad (2.2)$$

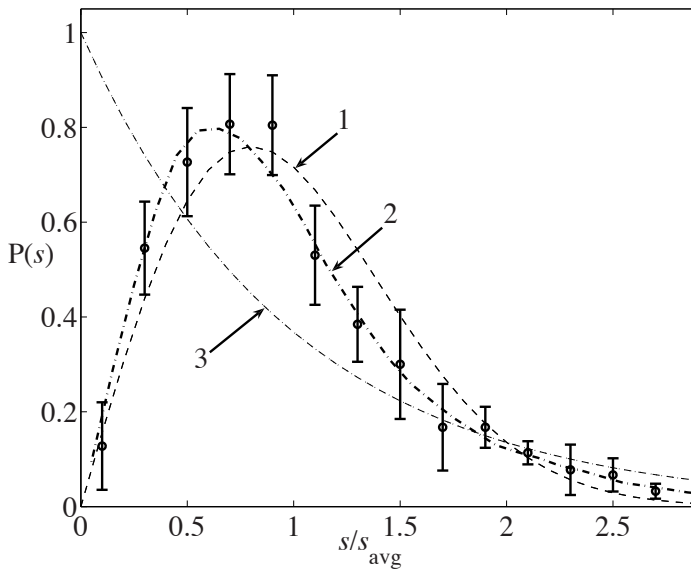


Fig. 2.12: The nearest neighbor resonance spacing distribution (NNSD) for cavity Nr. 2. The distribution obtained from experimental data is shown as points with error bars. Curve 1 shows the distribution expected due to GOE model. Curve 2 accounts for 25% of eigenvalues lost in GOE model distribution. The Poisson distribution is shown by curve 3.

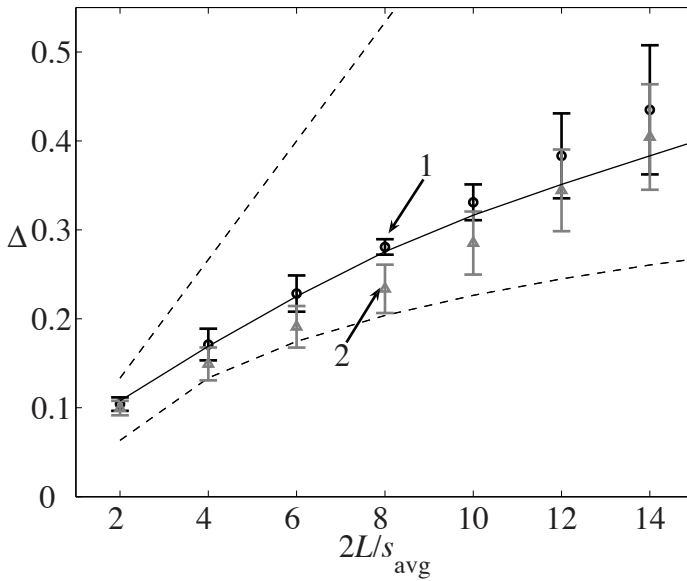


Fig. 2.13: The spectral rigidity for cavity Nr. 1 (circles with error bars, marked as "1") and cavity Nr. 2 (triangles with error bars, marked as "2") as functions of $2L$, the frequency band used in Eqn. 1.3 or Eqn. 1.4. The GOE model that involves logarithmic saturation of SR and the case of random division of the frequency band into intervals by resonances are shown as dashed curve and dashed line respectively. Solid curve shows the case of GOE with 25% of eigenvalues lost.

Using Eq. 2.1 the expression for the rescaled spacings may be rewritten as:

$$s_j^* = s_j \frac{3p_1(f_j + f_{j-1})^2/4 + p_2(f_j + f_{j-1}) + p_3}{3p_1(f_n + f_{n-1})^2/4 + p_2(f_n + f_{n-1}) + p_3} \quad (2.3)$$

3. The new sequence of frequencies used to determine SR is calculated as

$$f_k^* = f_k \quad (2.4)$$

$$f_i^* = f_k + \sum_{j=k+1}^i s_j^*, \quad i = k + 1..n \quad (2.5)$$

The new staircase function obtained from the new sequence of frequencies f_i^* is used in the determination of NNSD and SR.

From the Fig. 2.13 we see that the SR agrees satisfactorily with a GOE model [17] for averaging over the frequency bands $2L$ of 2..10 average spacings in case of cavity Nr. 2. It is, however, slightly larger than predicted by the model probably due to a fraction of lost resonances. The spectral rigidity calculated from the data of the same experiment for cavity Nr. 1 is systematically larger than in case of cavity Nr. 2. Both values agree better with the GOE model (that involves logarithmic saturation of SR) than with the case of random division of the frequency band into intervals (straight dashed line in Fig. 2.13). The solid curve in Fig. 2.13 shows the case of the GOE model with 25% of eigenvalues lost. This curve has been calculated as the SR for sequence of eigenvalues of a large (5000x5000) random symmetric matrix where 25% of the eigenvalues have been randomly removed from the sequence. This curve offers a reasonably good fit to the spectral rigidities determined from the experiment. The error bars in Fig. 2.13 (the same as in Fig. 2.12) are based on measurements performed for different positions of receiver and source on the surface of the sample. It is possible to see from Fig. 2.13 that triangles mainly fall below the solid curve (representing the SR accounting for lost resonances). This implies that 25% is a bit exaggerated estimation. The real fraction of the lost resonances can be lower.

Now moments and central moments, skewness and kurtosis of the NNSD (as mentioned in Chapter 1) will be considered. These quantities can be used to characterize the NNSD quantitatively. They will be used in discussions of the experimental data in the coming chapters as well (Chapters 4, 5 and 6).

Moments and central moments of different order, skewness and kurtosis for NNSD corresponding to the three most common RMT models (Poisson, GOE and GUE) mentioned in Chapter 1 are summarized in Appendix A (Chapter A). So we can compare the moments, central moments, skewness

and kurtosis of the three model distributions to the same values calculated from the NNSD discussed in present chapter.

In the figures discussed further in the present section the moments are shown for spacing distributions (NNSD) from each experiment on cavity#2 separately (not averaged over different positions of source and receiver on the surface of the sample). Moments of the distributions corresponding to different positions of source and receiver on the surface of the sample are shown in Figures 2.14 and 2.15 with different signs. So each sign (e.g. triangle or circle) in Figures 2.14 and 2.15 corresponds to a distribution calculated from a certain experiment characterized by certain positions of source and receiver on the surface of the sample.

Figure 2.14 shows the moments for the three models for the NNSD (Exponential or Poisson, GOE and GUE) together with the moments calculated from experimental data (green signs). The red, green and blue curves in Figure 2.14 are calculated using formulas from the last column of Table A.1.

Figure 2.15 shows the central moments for the three models for NNSD (Exponential or Poisson, GOE and GUE) together with central moments calculated from experimental data (green signs). The red, green and blue curves in Figure 2.15 are plotted using values from Table A.2.

Skewness and Kurtosis are summarized in Figures 2.16 and 2.17. The red, green and blue lines in Figures 2.16 and 2.17 are plotted using values from Table A.3.

It is visible from Figures 2.14, 2.15, 2.16 and 2.17 that values obtained from experimental data fall in between values due to GOE model and values for random arrangement of resonance frequencies (Poisson or Exponential model). This may be explained as a consequence of the fraction of the lost resonances (apparent from NNSD and SR discussed before in this chapter). The theoretical models are based on all existing modes.

The measurements use a limited number of transducer positions to obtain the experimental distributions. This is by itself an interesting issue. When using a limited number of probing positions it is possible to observe some noticeable errors in average NNSD and SR (given in Fig. 2.12 and Fig. 2.13). This makes analysis (e.g. determination of the fraction of lost resonances) less precise.

We dealt with a considerable amount of lost resonances in our experiments. This amount is higher than found in earlier reports like [24] by Nogueira et al. However, these experiments [24] were performed under idealized circumstances. Firstly, aluminum plate resonators were used instead of the volume ones in present work. Secondly, a vacuum chamber enclosing the sample was used to increase the isolation and therefore increase quality factors of the resonances. Thirdly, probably better support mechanism was

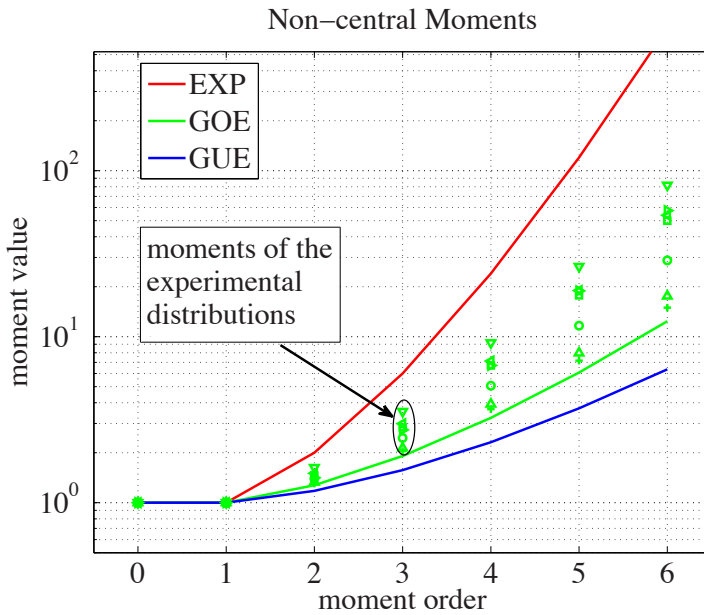


Fig. 2.14: Red, green and blue curves show the moments for the three models for the NNSD (Exponential or Poisson, GOE and GUE respectively). Green signs show values of the same moments calculated from experimental data for cavity#2. Different signs refer to different experiments corresponding to different positions of source and receiver on the surface of the sample.

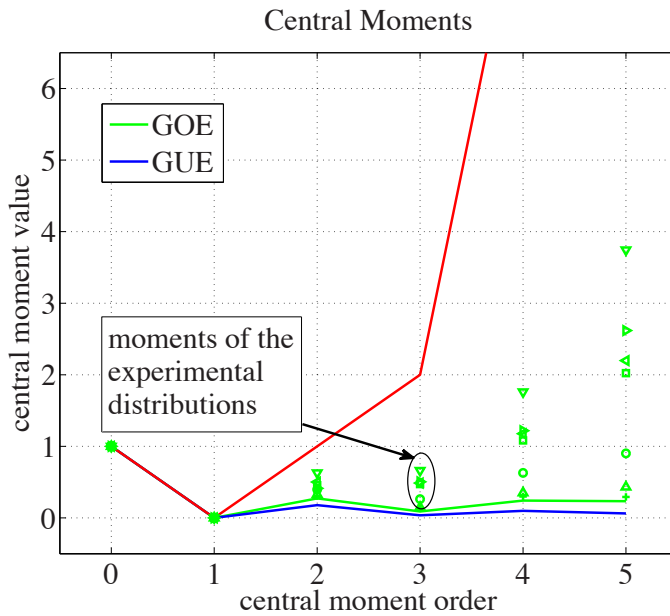


Fig. 2.15: Red, green and blue curves show central moments for the three models for NNSD (Exponential or Poisson, GOE and GUE respectively). Green signs show values of the same central moments calculated from experimental data for cavity#2. Different signs refer to different experiments corresponding to different positions of source and receiver on the surface of the sample.

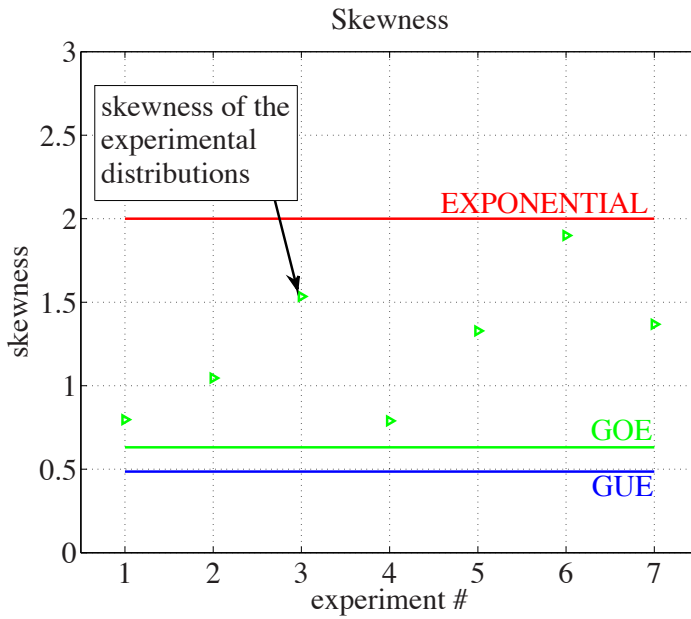


Fig. 2.16: Skewness for the NNSD models (Exponential or Poisson, GOE and GUE) is shown with red, green and blue lines respectively. Skewness of distributions obtained from experiments on cavity#2 is shown with green triangle signs. Different values of "experiment#" on the x axis (from 1 to 7) refer to different experiments corresponding to different positions of source and receiver on the surface of the sample.

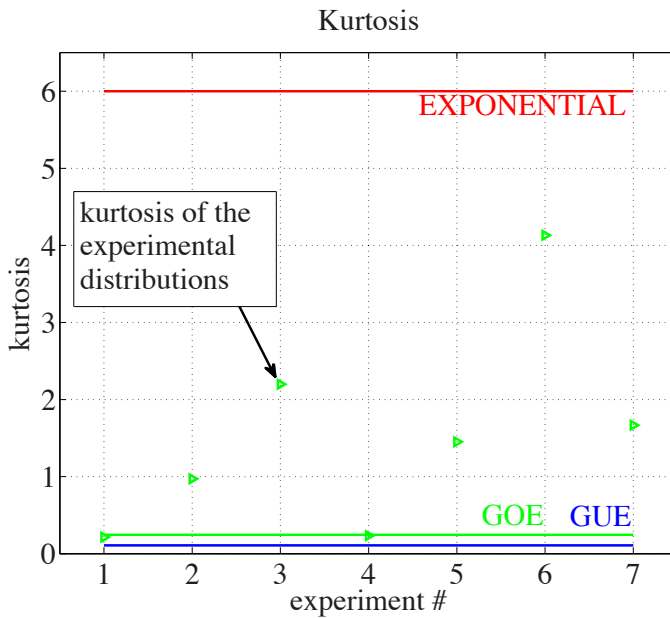


Fig. 2.17: Kurtosis for the NNSD models (Exponential or Poisson, GOE and GUE) is shown with red, green and blue lines respectively. Kurtosis of distributions obtained from experiments on cavity#2 is shown with green triangle signs. Different values of "experiment#" on the x axis (from 1 to 7) refer to different experiments corresponding to different positions of source and receiver on the surface of the sample.

used as well.

We report experiments that have been done at normal room conditions in air with support of the sample not entirely optimized. Therefore, a bit worse resonance detection conditions are indeed in place. However, our approach opens the possibility to explore experiments making use of RMT statistics on arbitrary samples under non-optimized conditions. This is important for validating the RMT statistical approach for probable future applications in mechanical engineering.

2.5 Summary of experiments without breaking time reversal invariance

The distributions of the intensity transmission coefficients studied in the narrow frequency bands confirm random division of pulse intensity between the cavity waves for both studied cavities. Division of the frequency band into intervals by cavity resonances for cavity Nr. 2, characterized by the NNSD, is found in agreement with the prediction of RMT for GOE. Perfect agreement, however, is achieved when accounting for a fraction of the lost resonances (about 25%). The corresponding SR shows behavior close to the GOE model that involves logarithmic saturation of the SR. The curve that shows SR in case of GOE model with 25% of eigenvalues lost offers even better fit to the spectral rigidities determined from the experiment. So both NNSD and SR can be identified as predicted by the GOE statistics, however a relatively large fraction of the lost resonances (25%) has to be assumed to achieve such an agreement. The SR calculated from the data of the experiment for a symmetric cavity (cavity #1) is systematically larger than in the comparable case of an asymmetric cavity (cavity #2). This agrees with the concept of coexistence of odd and even independent sequences of resonances.

The normalized amplitude of the reconstructed pulse in the time reversal experiment deviates from exponential dependence on the time delay if the last one is getting smaller and approaches the Heisenberg time (inverse of the average nearest neighbor resonance spacing).

The two aluminum samples can be used further to study random matrix statistical properties and time reversal experiment efficiency for the case of broken time reversal invariance which will be studied in Chapters 4 and Chapter 5 in detail.

We also found that moments and central moments of different order, skewness and kurtosis for the NNSD determined from experiment fall close to the values corresponding to the GOE model. These values actually fall

in between the GOE values and values corresponding to random arrangements of resonance frequencies, Poisson model. This may be considered as a consequence of the lost resonances.

Before using the samples in experiments where time reversal invariance is actively broken, we would like to have further evidence to support that the aluminum cavities are indeed following GOE statistics, despite the fact that the lost resonances modify the statistics calculated from the observed experimental data. Therefore we performed numerical simulations on an ideal representation of the cavities. These simulations are presented in the next chapter.

3. SIMULATION OF ELASTIC WAVES IN THE CAVITY

3.1 Introduction

We found a relatively high fraction of lost resonances in the experimental results in the previous chapter. So additional evidence is required to confirm that the sequences of resonances in the studied aluminum cavity can indeed be modeled by GOE statistics. In this chapter we will investigate the spectral statistics in the aluminum cavities for the full elastic wave solutions using simulated cavity responses. The simulations were performed using the program Wave3000 [48] that has been developed by Kaufman et al. to calculate ultrasonic responses in complex solid materials using an optimized adaptive finite difference method in the time domain. The simulations enable an efficient and direct way to study the influence of e.g. the position of transducers on the statistics of the resonance frequencies (fluctuations in resonance spacing distributions and spectral rigidity).

For comparison, the calculated responses are analyzed in the same way as the experimentally obtained results in the previous chapter. The sequences of resonance frequencies obtained from the spectral density of the simulated responses are used to calculate the NNSD and SR. The simulated results are compared to the predictions [3, 4] of RMT for chaotic systems with time reversal symmetry (GOE model).

3.2 The samples and simulation

The exact model representations (Fig. 2.2) of the cavities used in the experiments discussed in Chapter 2 were defined as input to the Wave3000 program [48].

The sound velocities for the aluminium used in the experiments of Chapter 2 were estimated as 6.41 km/s and 3.20 km/s for longitudinal and transverse waves respectively. Therefore the corresponding wavelengths ranges of the chosen frequency band 200..450 kHz used in the measurement are approximately $1.6d..0.7d$ in wavelength of the longitudinal wave and $0.8d..0.35d$ in wavelength of the transversal wave. Very small damping in aluminum was

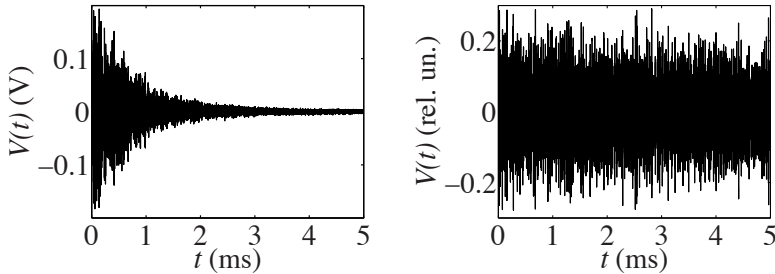


Fig. 3.1: Measured (left) and simulated (right) cavity responses at certain positions of the source and receiver.

included in the material properties used in the simulation. However the effect of it is not possible to notice in the typical simulated cavity response shown in Fig. 3.1.

The following simulation parameters were used: elastic modulus $E = 7.2 \cdot 10^{10}$ Pa and Poisson ratio $\nu = 0.33$, what corresponds to transverse and longitudinal wave velocities 3200 m/s and 6410 m/s respectively. The time step used was $0.0301 \mu\text{s}$ and grid size was 0.2 mm. This corresponds to a total of 10^6 grid points and 166113 time steps.

3.3 Simulation results

Responses of the cavities to short excitation pulses were simulated for nine different positions of the source and receiver. Fig. 3.1 shows examples of the measured (discussed in Chapter 2) and simulated cavity responses. The details of the cavity geometries, the coupling to the environment, and the exact response of the transducers are too complex to expect a detailed match between experiment and simulation. In particular the reverberation time is much shorter in the experimental results. However, the statistical properties of the spectra should be the same.

The spectral densities of the cavity responses were calculated, resonances were identified and the staircase functions $N(f)$ were determined. Then the spectral statistics (NNSD and SR) was calculated for each sequence of resonances in the same way as in the previous (experimental) chapter. The NNSD and SR were averaged then over different resonance sequences corresponding to different positions of the source and receiver.

To verify the simulation parameters, a simulation of the symmetric cubic

metal block (without well drilled in it or corner removed) has been done. Fig. 3.2 shows spectral densities of the responses of the symmetric cubic aluminum block simulated for the aluminum parameters mentioned above. Three different curves given in Fig. 3.2 correspond to different receiver positions. The comparison to the resonance frequencies obtained by Demarest [46] is also given in Fig. 3.2. The resonance frequencies listed in Demarest [46] are used at the value of the Poisson ratio $\nu = 0.33$ and a transverse wave velocity equal to 3200 m/s, what corresponds to the aluminum used in the experiment (discussed in the previous chapter) and simulation.

It can be seen, however, from the spectral density of the responses of the symmetric cube that a few small sharp peaks are present (although not represented in all three spectral density curves in Fig. 3.2) in addition to much better pronounced peaks identified as resonances studied in work [46] by Demarest. These small peaks can be an artifact of the simulation. Such spurious modes in higher frequency band may influence the statistics of resonances and therefore cause the departure from the random matrix model.

3.4 Discussion of the results: Nearest Neighbor Spacing Distribution and Spectral Rigidity determined from simulation

The NNSD calculated from the spectral density of the simulated responses of cavity Nr. 2 is shown in Fig. 3.3. Error bars shown in Fig. 3.3 appear from averaging the distribution over different positions of source and receiver (nine different positions). The simulation does not show the effect of missing resonances, something inherently present in the experiment (Chapter 2). However the NNSD determined from simulation shows larger repelling of resonant frequencies than in the GOE model distribution. We see from Fig. 3.3 that the NNSD determined from simulation has higher peak value while both the NNSD from simulation and the GOE model distribution are normalized to the unit area under the curve. The NNSD calculated from the spectral density of the simulated responses of cavity Nr. 1 shows similar behavior.

The SR (Δ) calculated from the simulated responses for cavity Nr. 2 is shown in Fig. 3.4. Error bars in Fig. 3.4 appear from averaging the SR over different positions of source and receiver (nine different positions). Calculated SR is in agreement with the GOE model. However, unlike the dependence determined from experiment, the simulation data gives a bit lower values of the SR than predicted by the model. This is better shown in Fig. 3.5. The SR calculated from simulation for each particular position of source and receiver is shown in Fig. 3.5. We see that these dependencies either exactly coincide

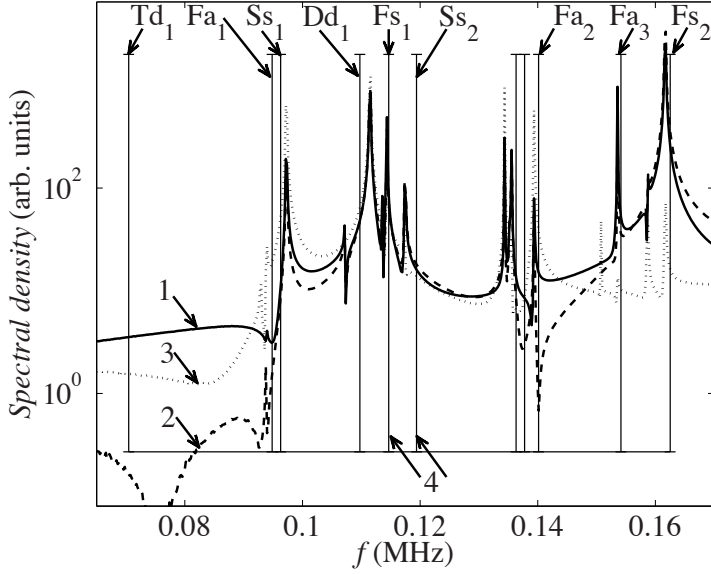


Fig. 3.2: Spectral densities of the responses of the symmetric cubic aluminum block simulated by Wave3000 program. Curves 1, 2 and 3 correspond to different positions of the receiver. Vertical lines (4) represent lowest resonances of the cubic block of aluminum according to [46]. Capital letters D, T, S and F refer to the initial of the group to which the vibration mode belongs [46]: 'dilation', 'torsion', 'shear' and 'flexure'. A lower case subscript refers to the subgroups: s refers to 'symmetric', a refers to 'antisymmetric' and d refers to 'doublet'. An additional subscript orders the modes in certain subgroup by frequency (1,2,3...).

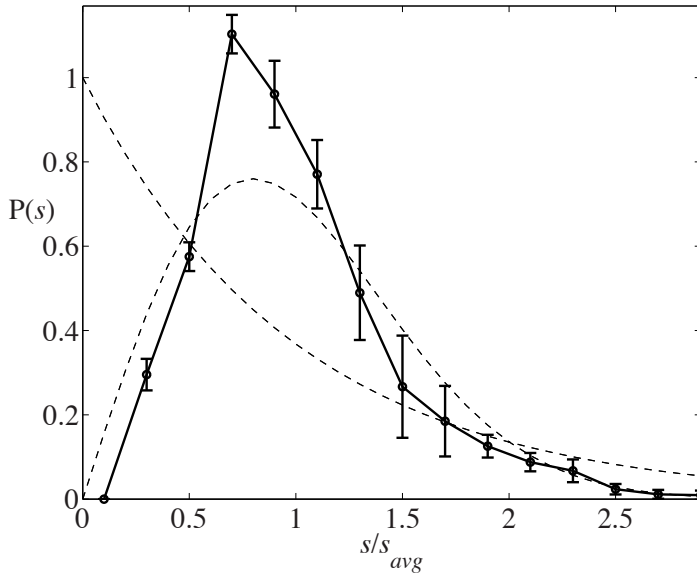


Fig. 3.3: NNSD calculated for cavity Nr. 2 from responses obtained in Wave3000 simulation program for different positions of source and receiver (round signs with error bars). Exponential (Poisson) distribution corresponding to random division of the frequency band into intervals by resonances and distribution due to GOE model are shown as dashed curves.

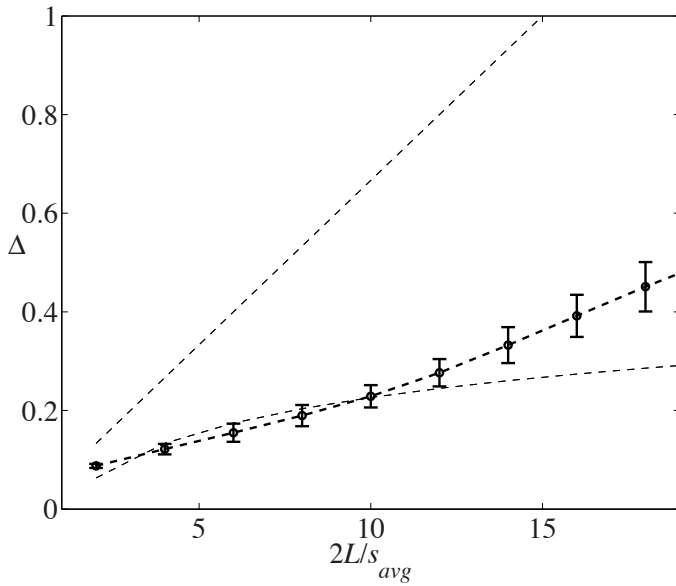


Fig. 3.4: Spectral rigidity for cavity Nr. 2 (round signs with error bars). From responses obtained in Wave3000 simulation program. Spectral rigidities corresponding to random division of the frequency band into intervals by resonances and GOE model are shown respectively as dashed line and dashed curve without error bars.

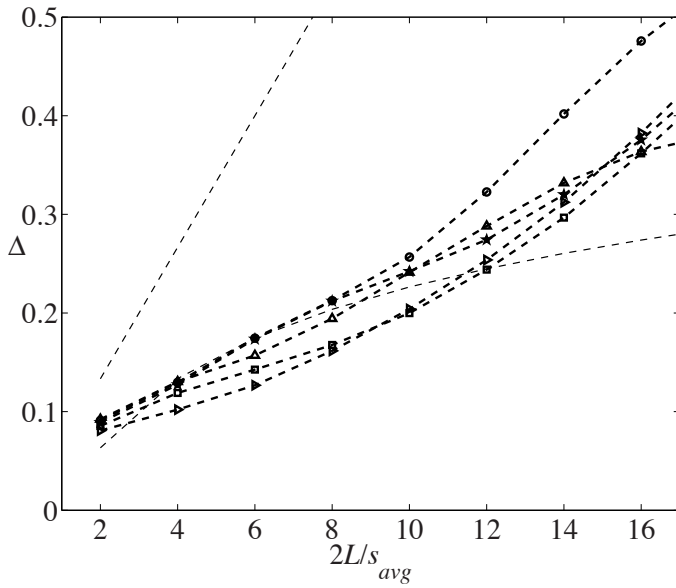


Fig. 3.5: Spectral rigidity for cavity Nr. 2. From responses obtained in Wave3000 simulation program. Different curves with signs in this picture show results for different positions of source and receiver. Spectral rigidities corresponding to random division of the frequency band into intervals by resonances and GOE model are shown respectively as dashed line and dashed curve without signs.

with GOE model for frequency bands $2L < 10s_{avg}$ or take lower value.

3.5 Conclusions

Simulation with the Wave3000 program allows satisfactory reproduction of the cavity responses. The spectral density of the response of the symmetric cubic aluminum resonator (without well drilled in it or corner removed) allows a correct identification of 10 consequent resonances of the cubic resonator as given by the analytical model [46].

The simulated acoustic wave dynamics shows noticeably larger repelling of resonances than determined from the responses in the experiment. The NNSD determined from the simulation data is better peaked around average value than predicted by the GOE distribution. SR averaged over frequency bands $2L$ smaller than $10s_{avg}$ has a bit lower value than predicted by the GOE model. The behavior of NNSD and SR due to a fraction of lost resonances in GOE model is not found in the case of the Wave3000 simulation (unlike for NNSD and SR determined from experimental data discussed in Chapter 2).

In particular, SR determined from the spectra of the Wave3000 simulated responses satisfactory follows the GOE curve for averaging over bands $2L$ of size of 2 to 10 average spacings. The corresponding SR determined from experimental data (discussed in Chapter 2) has larger values than given by the GOE model and significantly deviates from the GOE curve: it falls above the GOE curve and agrees with GOE model with the lost levels. The reduced spacing value corresponding to the maximum of NNSD determined from the Wave3000 simulated responses is close to that of the pure GOE distribution (without the lost resonances). The only discrepancy between the GOE model and NNSD determined from simulated responses is the actual height of the maximum of NNSD obtained from simulated responses. This can not be explained satisfactory at the moment.

But it can be seen from the spectral density of the responses of the symmetric cube that small sharp peaks are present in addition to large (much better pronounced) ones that have been identified with 10 consequent known elastic resonances from work [46] for the Poisson ratio of 0.33 corresponding to aluminum. These small sharp peaks, that can be artifact of the simulation, can alter the distribution when identified as resonances. So the departure from the GOE distribution can happen if such peaks are present in the higher frequency band and are counted as resonances. But it is important to mention that NNSD determined from simulated responses in present chapter does not behave as GOE distribution with randomly added resonance fre-

quencies (considered in Chapter 1). So if the small peaks, being the artifact of the simulation, are present in higher frequency band used to study statistics then they appear around real cavity resonances in non-random fashion. This implies that they can be for example higher harmonics of the identified resonances that appear due to some kind of numerical nonlinearities.

Indeed NNSD and SR calculated from the responses simulated with Wave3000 program do not require accounting for the fraction of lost resonances to be fitted with predictions for the GOE statistics. So the sample is suitable for further studies of the resonance statistics in case of broken time reversal invariance. However the lost resonances remain an experimental issue (discussed in Chapter 2) that can make the outcome of the experiment less clear.

NNSD and SR have still noticeable error bars arising from the different positions of source and receiver on the surface of the samples. The NNSD and SR as well as sequences of resonances used in calculation are different for different positions of the transducers on the surface of the sample. This was also observed in the analysis of the experimental data (Chapter 2). But in Chapter 2 different sequences of resonances for different positions of the transducers can be explained by the fraction of lost resonances. In present chapter obviously the error bars of NNSD and SR appear for a different reason (e.g. small peaks in spectral density that can be an artifact of the simulation).

4. STATISTICS OF RESONANCES AND TIME REVERSAL RECONSTRUCTION IN ALUMINUM ACOUSTIC CHAOTIC CAVITIES WITH FEEDBACK

4.1 *Introduction*

This chapter addresses the case of elastic waves in a chaotic cavity where the time reversal (TR) invariance is broken by a feedback loop. Considerable effort in acoustics has been devoted to study the influence of motion in liquids on TR invariance. For example the rotation in a vortex motion of a liquid breaks the TR invariance for the propagation of acoustic waves [10, 11, 12, 13]. An analogous phenomenon should be present in solids and would be of practical interest in such mechanical systems as blenders, airplane engines and so on.

An alternative and appealing method we devised to study the effects of TR invariance is to detect the acoustic signal at one location on the surface of the cavity and re-inject the signal after delay and amplification into another location on the surface of the cavity. Depending on the amplification (forward and/or backward) and the signal delay this feedback loop can influence the TR invariance and reciprocity in the acoustic system. The connecting cable and the amplifier introduce a delay in the feedback. When only forward waves travelling from the pick-up source through the amplifier are re-injected, the forward and backward paths for the waves are different and the reciprocity of wave propagation and therefore TR invariance of the wave equation are broken. The wave solution with negative time is no longer a solution. However, paths not travelling through the loop still have their reciprocity intact. Similar idea of one-directional wave signal transfer was explored in work [49] by Stoffregen et al about specially designed microwave billiards.

It should be mentioned that reciprocity still can be observed in the system with TR invariance broken. Reciprocity is equality of responses obtained by sending the same signal both from point A to point B and from B to A in opposite direction. The example of preserving the reciprocity in time reversal non-invariant system is a symmetric vortex in a liquid with the source and

receiving transducers located on the opposite sides of the vortex at equal distances from the center of the vortex. The wave equation has no time reversal invariance but still the reciprocity can be observed between these two points. We consider that the above-mentioned situation is never the case in our experiment. So the feedback loop considered in this thesis breaks both TR invariance and reciprocity.

The amplification coefficient K in the feedback loop strongly influences the feedback process. Self oscillation in the cavity may occur for K much larger than the loss in cables and piezoelectric transducers. Recently the effects of such a strong feedback in a chaotic cavity has been studied in the context of an acoustic laser (see the work [50] by Richard Weaver, Oleg Lobkis and Alexey Yamilov).

Multi channel feedback network for radio waves has been studied in [51] using S - matrix description both in case of low amplification in the feedback loop (far from self-oscillating regime) and in self-oscillating regime.

In this chapter we will study how and to what extent the efficiency of the time reversal experiment and RMT statistics (cavity resonances) are influenced by the feedback loop with K remaining below the self oscillation condition. The outcome of the TR experiments and the statistical properties of the cavity spectra obtained from cavity responses for a system with feedback will be discussed further in present chapter.

Section 4.2 gives a brief description of the experimental setup by pointing main features of the experiential setup and measurement procedures with a feedback loop. Section 4.3 tells about efficiency of excitation pulse reconstruction in TR experiments with different amplification in the feedback loop. The efficiency of the excitation pulse reconstruction in TR experiment is considered a measure of TR invariance. Section 4.4 gives statistical properties (NID, NNSD and SR) obtained from experiments with the feedback loop. Summary and conclusions are given in section 4.5.

4.2 *Experimental setup for studies of the cavity with feedback loop*

4.2.1 *The sample and transducers*

For comparison with the results described in Chapter 2 we use the same aluminum Cavity Nr. 2 as used in the experiments on TR and statistics (Fig. 4.1, left shows the shape of the cavity (aluminum block)). The time reversal invariance of elastic waves travelling inside the cavity will be broken by an additional feedback loop. The schematic of the feedback loop is

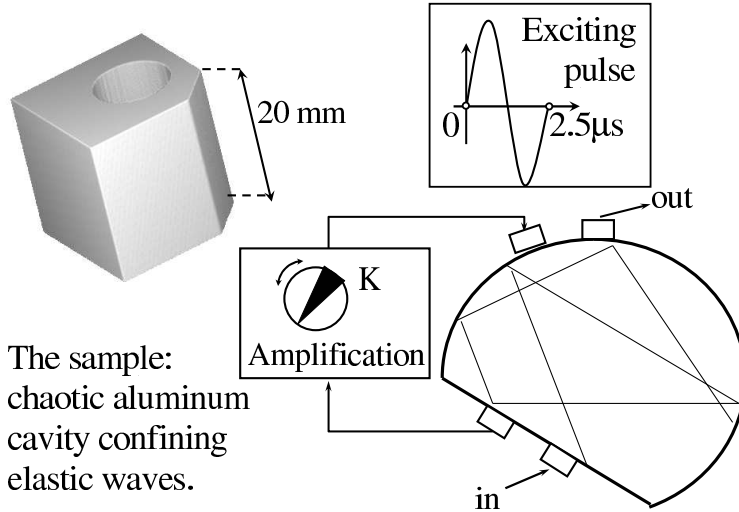


Fig. 4.1: The actual shape of the sample (aluminum block) used in experiment with time reversal invariance broken by a feedback loop (left in the figure), excitation pulse (top right in the figure) played by the input transducer and schematic of the feedback loop (bottom right in the figure).

shown in Fig. 4.1. The time reversal invariance of the wave dynamics in the cavity for waves travelling through the loop is broken because the amplifier included in the feedback connection transmits only in one direction. The frequency bandwidth of the amplifier is set constant to the frequency band of approximately 10 kHz - 400 kHz and the amplification coefficient K can be changed.

To reduce losses in the system a very light low mass polystyrene support is used (Fig. 4.2). Four transducers are attached to the cavity (aluminum block). Two of them are to be used for the measurement of the cavity response in the same way as described in Chapter 2 (Experiments on the cavity without breaking of the time reversal invariance). They shall be referred to further as input and output transducers. The remaining two transducers are glued to the sample and do not change the position during the measurements. These two transducers are connected to form feedback loop between them and to break the time reversal invariance of the elastic waves in the sample

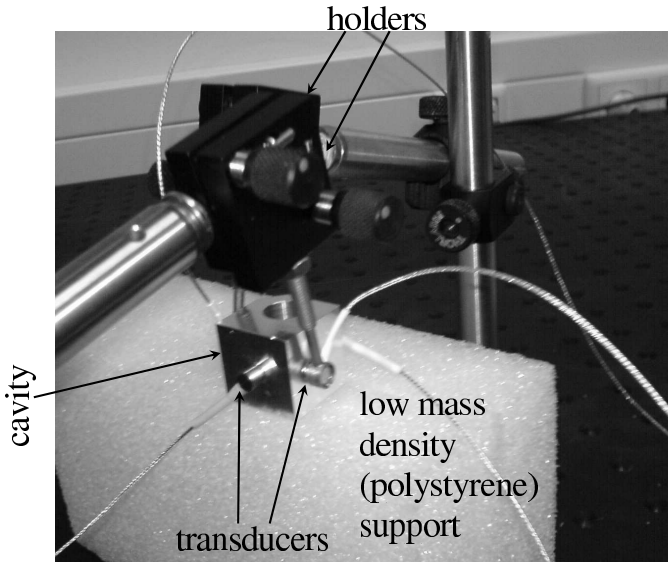


Fig. 4.2: Picture of the sample, transducers connected to it and transducer holders. Transducer holders hold transducers used to measure the response of the cavity to a short excitation pulse, the same as in Chapter 2, describing the experiment without the feedback loop. An additional pair of transducers is glued to the aluminum block as shown in this figure. This pair of transducers is used to connect a feedback loop between them.

(Figures 4.1 and 4.2).

The schematics of the experimental setup mainly remains the same as in Chapter 2 (Experiments on the aluminum block without breaking the time reversal invariance). The only difference is the feedback loop connected to the sample via two additional transducers.

4.2.2 Measurements with feedback

Time reversal experiments and analysis of the statistics (NID, NNSD and SR) obtained from the cavity responses are performed for several distinct positions of input and output transducers in the same way as without a feedback loop. However a such sequence of measurements (several positions of the input and output transducers) is repeated now for the feedback loop amplifier switched off and for a few values of the feedback amplification

coefficient K (Fig. 4.1).

The range of K available in experiment is limited for the following reason: for small K the receiving transducer gets a decaying response composed of many modes at different resonant frequencies. When increasing the amplification K further and further beyond the value of 2200 eventually the regime is reached when the receiving transducer receives an oscillation at one of the resonant frequencies with high amplitude (so that other modes contribute a negligibly small output signal). In such a case, when self-oscillation is reached, the calculation of random matrix statistics is impossible. This will be discussed again in Chapter 5, the chapter about the possible random matrix model for the cavity influenced by the feedback loop.

The case of high amplification (reaching the self-oscillation regime) has been studied in [50], although not in sense of random matrix statistics.

4.3 Efficiency of excitation pulse reconstruction in time reversal experiments with a breaking of the time reversal invariance

Fig. 4.3 shows the efficiency of the time reversal pulse reconstruction as function of the time delay between the end of the oscillation track replayed backward in time and the exciting pulse. 300 μ s long oscillation tracks have been used (in the same way as explained previously in chapters 1 and 2). The circle signs show the results for the feedback loop switched off. Results are given also for the same oscillation tracks replayed backwards with active feedback loop with feedback coefficients K of the voltage amplifier equal to 1000 (squares) and 2200 (crosses). Fig. 4.3 shows that the active feedback loop has a negligible effect on the TR reconstruction for small time delays (0.4-0.6 ms). But the active feedback loop noticeably suppresses the reconstruction of the excitation pulse for larger time delays (0.7-1.0 ms). Such an effect of the suppression of the TR reconstruction increases with an increase of the amplification coefficient K as can be seen from Fig. 4.3. So we see explicitly from Fig. 4.3 that time reversal focusing of the part of the response back into the short excitation pulse (time reversal reversal reconstruction) becomes less and less efficient with increasing feedback: the normalized amplitude of the reconstructed pulse goes down with increasing K .

However, for very long time delays (about 2 ms) and a large amplification coefficient K the voltage spike, representing the reconstruction of the excitation pulse in TR experiment, is obscured by the background peaks. As a result the TR reconstruction peak detection algorithm, developed to be used in this thesis and described in Chapter 1, does not work properly. Also these

background noisy peaks make the determination of the reconstructed pulse amplitude less reliable for the long time delays.

Moreover for large time delays the TR experiment becomes sensitive to many minor issues like aging and temperature dependence of transducer-oil-aluminum coupling so the daily drift is influencing the amplitude of the detected reconstruction spike (if there is not enough time to repeat the experiments at different positions of source and receiver for different amplification in the feedback loop without experiencing the effect of the daily drift). For time delays of 2 ms and larger the daily drift of the amplitude of the reconstruction spike was measured as large as 10%. For the delays shorter than 1.6 ms it never exceeded 3%.

$k \leq 1$ in Fig. 4.3 is a coefficient used to scale the input signal for lower time delays, so that the reconstructed spike will not be high enough to cause the changes in sensitivity (due to the high signal amplitude) of the receiving transducer.

4.4 Statistical properties obtained from experiments with feedback

4.4.1 Division of energy between cavity waves: distributions of intensity transmission coefficients and resonance line widths

Fig. 4.4 gives NID in 60 kHz wide frequency band. The results mainly agree with an exponential distribution corresponding to the input pulse energy being shared randomly between the cavity waves.

4.4.2 Random matrix statistics of resonance sequences obtained from experiments

The NNSD for the different amplification K in the feedback loop is given in Fig. 4.5, Fig. 4.6 and Fig. 4.7. It is possible to see that the feedback loop leads to changes in the distribution more significant than the error bars shown in the figures. SR for the different amplification K in the feedback loop is given in Fig. 4.8. The error bars in Fig. 4.5, Fig. 4.6, Fig. 4.7 and Fig. 4.8 are based on measurements performed for different positions of source and receiver (input and output transducers) on the surface of the aluminum block. Transducers with a feedback loop connected between them remain glued to the sample at the same locations through the full cycle of measurements.

Unfortunately the trend related to the active feedback loop is not clearly visible from NNSD given in Fig. 4.5, Fig. 4.6 and Fig. 4.7. As indicated in Chapters 1 and 2 and Appendix A, a moment analysis of the distribution may

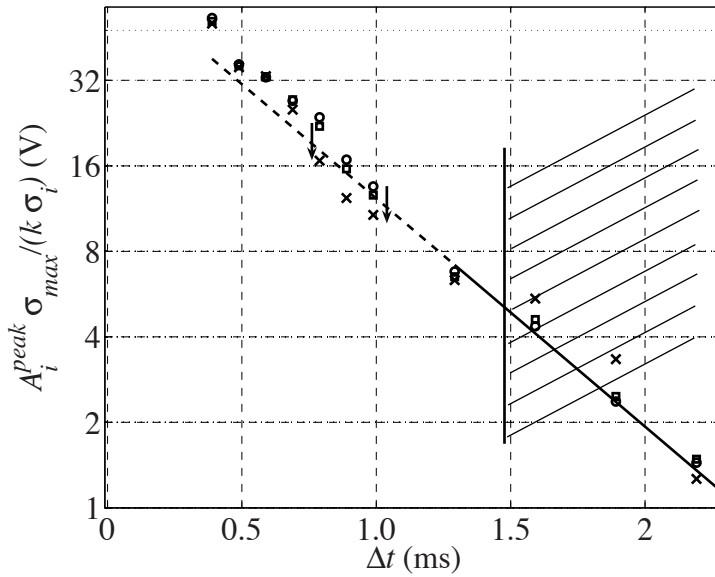


Fig. 4.3: Normalized amplitude of the excitation pulse refocused in TR experiment depending on the time delay of the reversed oscillation track with respect to the excitation pulse. Circles correspond to a blocked feedback loop (amplification coefficient K is equal to zero). Squares and crosses correspond to amplification coefficients 1000 and 2200 respectively. The area hatched with diagonal lines represents the time delays for which the reconstructed pulse is very badly detectable and the daily drift of the reconstructed pulse plays certain role.

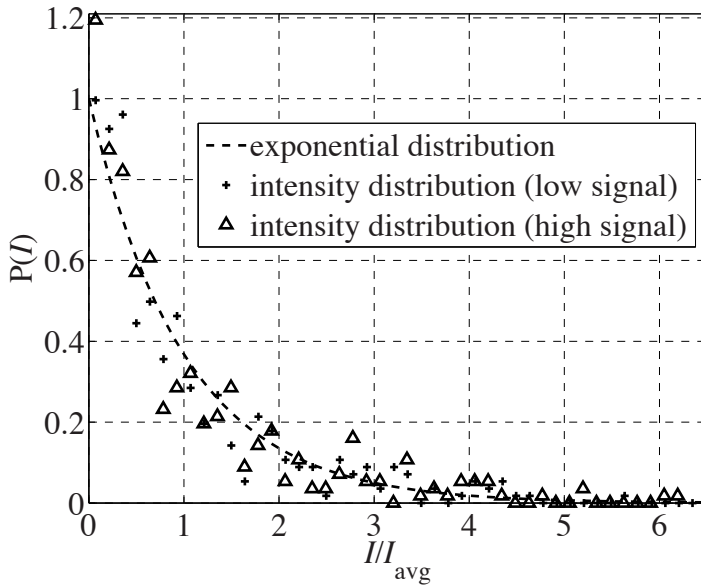


Fig. 4.4: Normalized intensity distribution (NID) in the frequency band 210 kHz ... 270 kHz for the amplification $K=2200$ in the feedback loop. Different signs correspond to different (low/high) voltage amplitude of the exciting pulse (1.25 V and 2.5 V respectively).

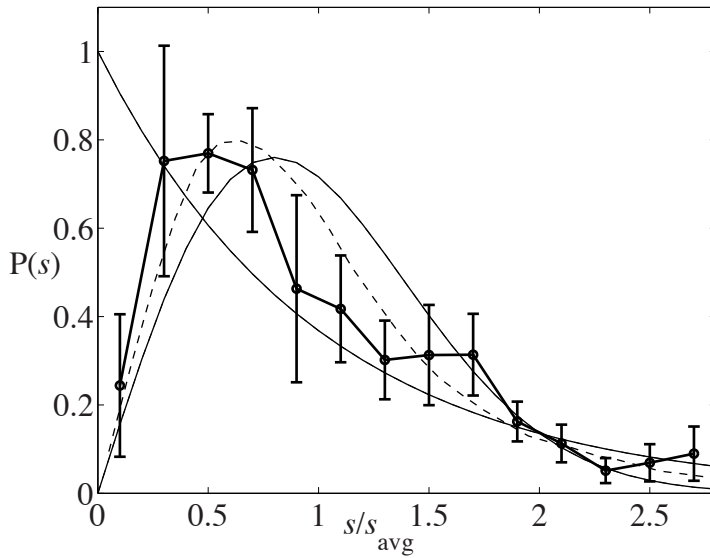


Fig. 4.5: NNSD for the amplification $K = 0$ in the feedback loop (points with error bars connected with lines). Poisson case (exponential distribution) is shown by solid decaying curve. GOE model distribution is shown by solid curve with a maximum. Dashed curve shows GOE model with 25% of resonances lost.

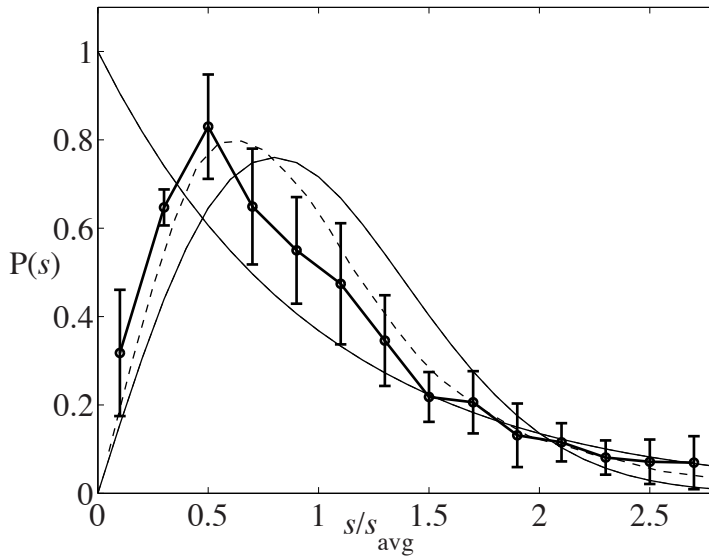


Fig. 4.6: NNSD for the amplification $K = 1000$ in the feedback loop (points with error bars connected with lines). Poisson case (exponential distribution) is shown by solid decaying curve. GOE model distribution is shown by solid curve with a maximum. Dashed curve shows GOE model with 25% of resonances lost.

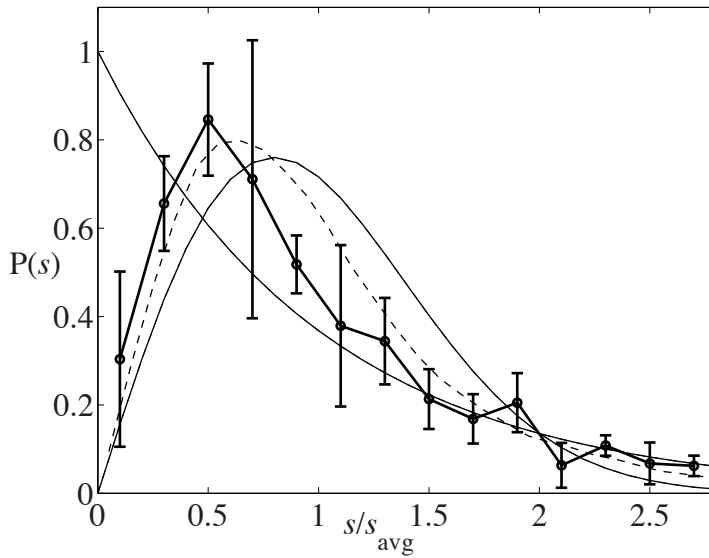


Fig. 4.7: NNSD for the amplification $K = 2200$ in the feedback loop (points with error bars connected with lines). Poisson case (exponential distribution) is shown by solid decaying curve. GOE model distribution is shown by solid curve with a maximum. Dashed curve shows GOE model with 25% of resonances lost.

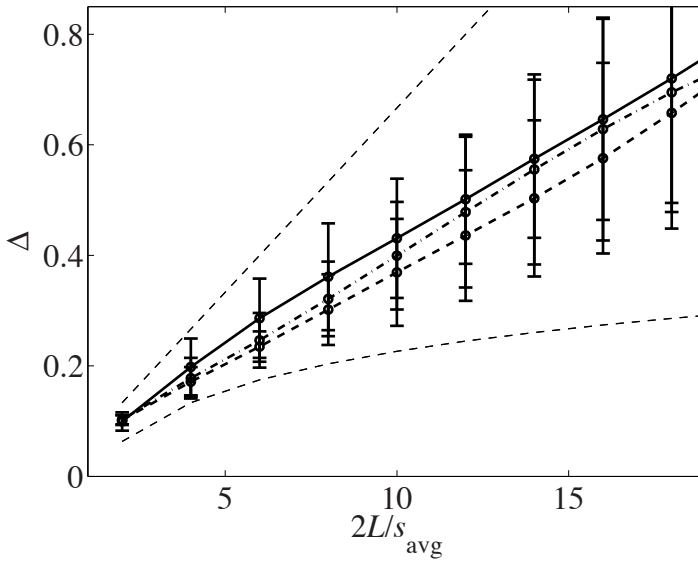


Fig. 4.8: SR (delta statistics) for the amplification $K=0$ in the feedback loop (points with error bars connected by the solid line) and for amplifications $K = 1000$ and $K = 2200$ (points with error bars connected by dash and dash dotted lines respectively). Theoretical predictions for uncorrelated sequence of resonances (the same as in case of randomly chosen resonance frequencies) and GOE model are shown by dashed line and dashed curve respectively.

help to clarify the difference. In particular moments, skewness and kurtosis of the experimentally determined distributions can be calculated. Skewness is a measure of the asymmetry of the distribution around the mean and kurtosis indicates the nature of the spread around the mean (whether small or large deviations of the random variable around the mean contribute to the spread around the mean). Precise definitions of these values are given in Appendix A. The moment analysis for the main model NNSD functions (GUE, GOE and Poisson or exponential) is given in detail in the Appendix A (Chapter A).

The skewness and kurtosis of the NNSD for the case of active feedback loop (broken time reversal invariance) are summarized in Figures 4.9 and 4.10. Skewness and kurtosis values for NNSD due to GUE, GOE and Poisson models (shown by horizontal lines in Figures 4.9 and 4.10) are taken from Table A.3 in Appendix A (Chapter A).

Figures 4.9 and 4.10 show that skewness and kurtosis approach closer to the values of the Poisson model (marked as 'EXP') with increasing of the influence of the feedback loop. Hence, the NNSD is approaching the case of randomly chosen resonant frequencies (Poisson or exponential NNSD).

So it is apparent from figures 4.9 and 4.10 that although the feedback loop breaks the time reversal invariance in the system, the distribution is not approaching the GUE model. However such behavior as shown in figures 4.9 and 4.10 may be explained also by the growing amount of lost resonances with increasing influence of the feedback loop. E.g. because some of the modes are inhibited by the loop, some are on the contrary amplified and many of the modes remain uninfluenced (this will be discussed again in Chapter 5, the chapter about possible random matrix model describing the resonance statistics of the cavity with feedback). So more modes are obscured by the growth of the modes that are amplified by feedback.

4.5 *Summary on experiments with breaking of the time reversal invariance*

The TR experiments show that the feedback loop suppresses the reconstruction of the excitation pulse for different time delays of the recorded (and replayed backwards) oscillation track with respect to the original excitation pulse. The suppression of the time reversal reconstruction increases with increasing amplification coefficient K of the amplifier in the feedback loop. Thus time reversal experiment becomes less efficient due to increasing influence of the feedback loop.

The NID obtained from 60 kHz wide frequency band mainly agree with

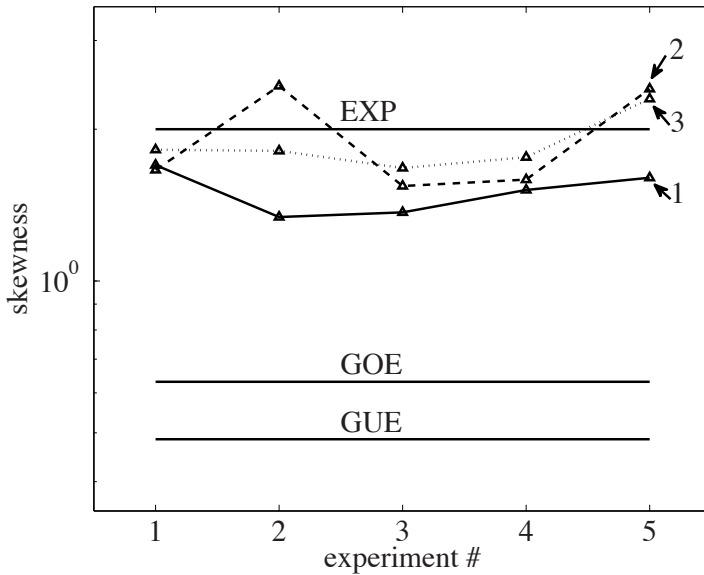


Fig. 4.9: Skewness of the NNSD obtained from experimental data for zero amplification K in the feedback loop (curve 1), $K = 1000$ (curve 2) and $K = 2200$ (curve 3). Every value of "experiment#" on the x axis (from 1 to 5) corresponds to certain positions of the input and output transducers on the surface of the sample. Skewness values for NNSD due to GUE, GOE and Poisson models are shown by horizontal lines marked respectively as 'GUE', 'GOE' and 'EXP'.

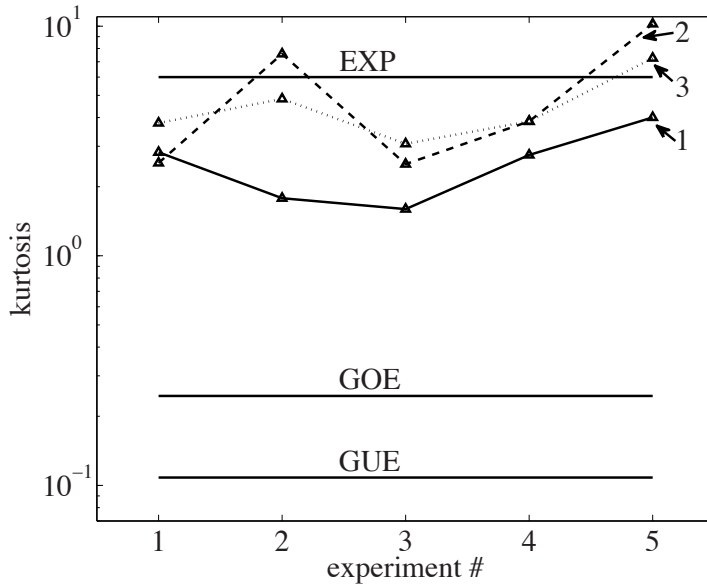


Fig. 4.10: Kurtosis of the NNSD obtained from experimental data for zero amplification K in the feedback loop (curve 1), $K = 1000$ (curve 2) and $K = 2200$ (curve 3). Every value of "experiment#" on the x axis (from 1 to 5) corresponds to certain positions of the input and output transducers on the surface of the sample. Kurtosis values for NNSD due to GUE, GOE and Poisson models are shown by horizontal lines marked respectively as 'GUE', 'GOE' and 'EXP'.

the exponential distribution corresponding to the input pulse energy being shared randomly between the cavity waves.

It is found also that the active feedback loop influences the NNSD statistics. The effect of the feedback loop on SR (delta statistics) is found negligibly small compared to the error bars based on measurements at several different positions of source and receiver.

It can be seen also that skewness and kurtosis of the NNSD, determined from the data of several experiments, approach closer to the values due to the Poisson model (exponential NNSD) with an increase of the influence of the feedback loop, what implies that NNSD is approaching the case of randomly chosen resonant frequencies. This means that arrangement of the resonances becomes more random with increasing influence of the feedback loop in the experiment.

However a part of this behavior may be explained also by the growing amount of lost resonances with increasing influence of the feedback loop in case if more modes are obscured by the growth of the modes that are amplified by feedback.

5. RANDOM MATRIX MODEL OF THE CHAOTIC CAVITY WITH TIME REVERSAL INVARIANCE BROKEN BY THE FEEDBACK LOOP

5.1 Introduction

It is not possible (not practical) to define a feedback loop in numerical simulation programs that use a finite difference method like Wave 3000. Thus, this chapter will consider another approach that allows to obtain the NNSD using the matrix model built specifically for the elastic cavity influenced by the feedback loop. We shall use the agreement of the RMT statistics for the unperturbed cavity (cavity not influenced by the feedback loop) with the GOE model as an assumption. The main goal of the present chapter is to obtain resonance frequencies of the cavity influenced by the feedback loop when the resonances of the unperturbed cavity are known and obey GOE statistics.

5.2 Derivation of the matrix to describe random matrix statistical properties of the elastic cavity influenced by a feedback loop

We start with the standard Navier-Cauchy wave equation [38] that describes acoustic displacement field $\vec{u}(\vec{x}, t)$ within a block of solid isotropic material.

$$\rho \ddot{\vec{u}} = (\lambda + \mu) \nabla (\nabla \cdot \vec{u}) + \mu \Delta \vec{u} + \vec{f}(\vec{x}, t) \quad (5.1)$$

Here ρ is the mass density, λ is the first Lamé parameter and μ is the second Lamé parameter or shear modulus. $\vec{f}(\vec{x}, t)$ is the force density related to the excitation of the cavity waves by external forces (e.g. piezoelectric transducers in experiments described earlier in this thesis). \vec{x} is a coordinate inside the cavity and t is time. This equation implies that the elastic properties of the solid material (Lamé parameters) do not vary in space inside the cavity (solid block).

The wave equation 5.1 can be rewritten using $c_{\parallel} = \sqrt{(\lambda + 2\mu)/\rho}$ and $c_{\perp} = \sqrt{\mu/\rho}$ (the velocities respectively of the longitudinal and transverse plane waves in infinite uniform space of the considered solid material):

$$\frac{\ddot{\vec{u}}}{c_{\parallel}^2} = \left(\frac{c_{\parallel}^2 - c_{\perp}^2}{c_{\parallel}^2} \right) \nabla (\nabla \cdot \vec{u}) + \frac{c_{\perp}^2}{c_{\parallel}^2} \Delta \vec{u} + \frac{\vec{f}(\vec{x}, t)}{\rho c_{\parallel}^2}$$

Now let us consider the differential operator of this wave equation as the sum of the time dependent (the inverse of the longitudinal wave speed squared times the second derivative with respect to time) and the space dependent (\hat{L}) parts:

$$\left(\frac{1}{c_{\parallel}^2} \frac{\partial^2}{\partial t^2} - \hat{L} \right) \vec{u}(\vec{x}, t) = \frac{\vec{f}(\vec{x}, t)}{\rho c_{\parallel}^2} = \vec{F}(\vec{x}, t) \quad (5.2)$$

Here $\hat{L} \equiv (1 - \xi) \nabla (\nabla \cdot) + \xi \Delta$ and $\xi \equiv c_{\perp}^2/c_{\parallel}^2$.

In case of active feedback loop it is essential that \vec{F} is written in the form dependent on the displacement field $\vec{u}(\vec{x}, t)$ as $\vec{F}(\vec{u}, \vec{x}, t)$.

Let us consider first the cavity without the external excitation forces and without the feedback loop ($\vec{F} = \vec{0}$). In this case the separation of the time and space variables is possible using the relation $\vec{u}(\vec{x}, t) = T(t)\vec{X}(\vec{x})$. This allows using the form of the displacement field $\vec{u}(\vec{x}, t)$ shown below to find the eigenvalues corresponding to the eigenfunctions $\vec{\psi}_n(\vec{x})$ of the unperturbed cavity.

$$\vec{F} = \vec{0} \quad : \quad \vec{u}(\vec{x}, t) = \sum_n \left(A_n e^{i\omega_n t} + B_n e^{-i\omega_n t} \right) \vec{\psi}_n(\vec{x})$$

Now after substituting this form of $\vec{u}(\vec{x}, t)$ into the equation 5.2 we can write down the eigenfrequencies and eigenfunctions of the unperturbed cavity as eigenvalues and eigenfunctions of the operator \hat{L} :

$$\hat{L}\vec{\psi}_n = -k_n^2 \vec{\psi}_n, \quad k_n^2 = \frac{\omega_n^2}{c_{\parallel}^2}$$

In our further simulation of the statistical properties of the cavity influenced by the feedback loop we consider eigenfrequencies of the unperturbed cavity ω_n known and having statistical properties as of a sequence of GOE eigenvalues.

The displacement field $\vec{u}(\vec{x}, t)$ when excitation forces and feedback loop are active can be represented in general as the sum of the eigenfunctions $\vec{\psi}_n(\vec{x})$ of the unperturbed cavity with time dependent amplitudes $\varphi_n(t)$:

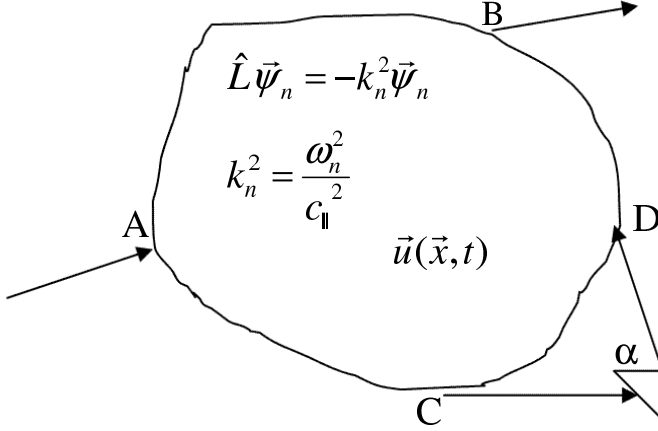


Fig. 5.1: Schematic of the cavity with an active feedback loop described by equation 5.4 or equation 5.5.

$$\vec{u}(\vec{x}, t) = \sum_{n=1}^N \varphi_n(t) \vec{\psi}_n(\vec{x}) \quad (5.3)$$

The short excitation pulse and the feedback loop can be described as a combined excitation force $\vec{F}(\vec{u}, \vec{x}, t)$ of the following form:

$$\vec{F}(\vec{u}, \vec{x}, t) = \vec{F}_0 \delta(t) \delta(\vec{x} - A) + \hat{\alpha} \vec{u}(C, t - \tau) \delta(\vec{x} - D) \quad (5.4)$$

The first term $\vec{F}_0 \delta(t) \delta(\vec{x} - A)$ describes a short excitation pulse at the moment $t = 0$ launched at point A ($\vec{x} = A$) similar e.g. to [42]. The second term $\hat{\alpha} \vec{u}(C, t - \tau) \delta(\vec{x} - D)$ describes the feedback loop: the oscillations recorded at point C are played at point D (Fig. 5.1) after a delay time τ , which is a delay time of the signal travelling through the feedback loop. The quantity $\hat{\alpha}$ is simply a matrix of proportionality coefficients.

However, it is natural to write the feedback loop term in a form given by Eq. 5.5, where only the normal component of the displacement is received (played) by the transducers at points C and D . This is actually the case for the transducers used in the experiment discussed in the previous chapters.

$$\vec{F}(\vec{u}, \vec{x}, t) = \vec{F}_0 \delta(t) \delta(\vec{x} - A) + \alpha (\vec{n}_C \cdot \vec{u}(C, t - \tau)) (\delta(\vec{x} - D) \cdot \vec{n}_D) \quad (5.5)$$

Here \vec{n}_C and \vec{n}_D are unit vectors normal to the surface of the cavity (solid block) at points C and D respectively, where the transducers of the feedback loop are connected. α here is a scalar proportionality coefficient.

Equation 5.4 (or equation 5.5) offers a possibility to add a feedback loop to the wave equation 5.2. Now substituting the $\vec{u}(\vec{x}, t)$ as sum (5.3) into (5.2) with $\vec{F}(\vec{u}, \vec{x}, t)$, given by (5.4) as the sum of the above-mentioned non-zero excitation term and the feedback loop term, we get:

$$\sum_{n=1}^N \left\{ \left(\frac{\varphi_n''(t)}{c_{\parallel}^2} + \frac{\omega_n^2 \varphi_n(t)}{c_{\parallel}^2} \right) \vec{\psi}_n(\vec{x}) \right\} = \vec{F}_0 \delta(t) \delta(\vec{x} - A) + \hat{\alpha} \delta(\vec{x} - D) \left(\sum_{j=1}^N \vec{\psi}_j(C) \{ \varphi_j(t) - \varphi_j'(t) \tau \} \right) \quad (5.6)$$

Here we assumed already $\tau \ll 1/\omega_n$ and wrote down the approximation $\varphi_j(t) - \varphi_j'(t)\tau$ instead of $\varphi_j(t - \tau)$.

Further we multiply both sides of the equation 5.6 by $\vec{\psi}_k(\vec{x})$ and integrate over the volume of the cavity (solid block): $\int \vec{\psi}_k(\vec{x}) \cdot \dots dV$. The following relations are used: $\int \vec{\psi}_k(\vec{x}) \cdot \vec{\psi}_n(\vec{x}) dV = \delta_{kn}$ (Kronecker delta symbol), $\int \vec{\psi}_k(\vec{x}) \delta(\vec{x} - A) dV = \vec{\psi}_k(A)$ and $\int \vec{\psi}_k(\vec{x}) \delta(\vec{x} - D) dV = \vec{\psi}_k(D)$. After taking the above stated relations into account we get the following system of equations ($k = 1..N$) for the time dependent amplitudes $\varphi_k(t)$:

$$\varphi_k''(t) + \omega_k^2 \varphi_k(t) - \sum_{j=1}^N \{ \beta_{kj} (\varphi_j(t) - \varphi_j'(t)\tau) \} = \gamma_k \delta(t) \quad (5.7)$$

Here $\gamma_k = \vec{F}_0 c_{\parallel}^2 \vec{\psi}_k(A)$. The β_{kj} are defined as follows:

$$\beta_{kj} = c_{\parallel}^2 \vec{\psi}_k(D) \hat{\alpha} \vec{\psi}_j(C)$$

for the case of general proportionality coefficients $\hat{\alpha}$ (Eqn. 5.4). For transducers sensing only the component of the displacement normal to the surface of the cavity (Eqn. 5.5) the β_{kj} can be defined as follows:

$$\beta_{kj} = \alpha c_{\parallel}^2 (\vec{\psi}_k(D) \cdot \vec{n}_D) (\vec{\psi}_j(C) \cdot \vec{n}_C)$$

Now equations 5.7 can be used to determine new eigenfrequencies of the cavity (cavity under influence of the feedback loop). It is clear from Eqn. 5.7

that when the feedback loop is absent ($\beta_{kj} = 0$) only a collection of N independent harmonic oscillator equations is left. The eigenfrequencies are then the eigenfrequencies of the original cavity without the feedback loop. However in case of non-zero β_{kj} and τ equations 5.7 are coupled to each other. This naturally leads to the new eigenfrequencies (denoted further as v_k) departing from original values ω_k (eigenfrequencies of the cavity without the feedback loop).

In the simple case of N equal to 1 and $\tau = 0$ the influence of the feedback loop is quite straightforward. Equations 5.7 take on the simple form:

$$\varphi_1''(t) + \omega_1^2 \varphi_1(t) - \beta_{11} \varphi_1(t) = \gamma_1 \delta(t)$$

In this case the new resonance frequency is defined as $v_1^2 = \omega_1^2 - \beta_{11}$. The solution for $\varphi_1(t)$, after applying the initial conditions $\varphi_1(-0) = 0$, $\varphi_1(+0) = 0$, $\varphi_1'(-0) = 0$ and $\varphi_1'(+0) = \gamma_1$ at $t = 0$, when a delta pulse is applied, takes the following form: $\varphi_1(t) = (\gamma_1/v_1) \sin(v_1 t)$. The first derivative $\varphi_1'(t)$ experiences a jump of γ_1 at $t = 0$. This can be seen easily from integrating both sides of the differential equation for $\varphi_1(t)$ over time within an arbitrary small interval around $t = 0$.

It is possible to get a similar solution for $N = 2$ and $\tau = 0$:

$$v_{1/2}^2 = \frac{\omega_1^2 + \omega_2^2 - \beta_{11} - \beta_{22} \pm \sqrt{(\omega_1^2 - \omega_2^2 - \beta_{11} + \beta_{22})^2 - 4\beta_{12}\beta_{21}}}{2}$$

$$\varphi_1(t) = \frac{(v_2^2 - \omega_1^2 + \beta_{11})\gamma_1 + \beta_{12}\gamma_2}{(v_2^2 - v_1^2)v_1} \sin(v_1 t) - \frac{(v_1^2 - \omega_1^2 + \beta_{11})\gamma_1 + \beta_{12}\gamma_2}{(v_2^2 - v_1^2)v_2} \sin(v_2 t)$$

$$\varphi_2(t) = \frac{(v_2^2 - \omega_2^2 + \beta_{22})\gamma_2 + \beta_{21}\gamma_1}{(v_2^2 - v_1^2)v_1} \sin(v_1 t) - \frac{(v_1^2 - \omega_2^2 + \beta_{22})\gamma_2 + \beta_{21}\gamma_1}{(v_2^2 - v_1^2)v_2} \sin(v_2 t)$$

So the new wave functions $\vec{\psi}_1$ and $\vec{\psi}_2$ corresponding to v_1 and v_2 are:

$$\vec{\psi}_1 = \left(\frac{(v_2^2 - \omega_1^2 + \beta_{11})\gamma_1 + \beta_{12}\gamma_2}{\Lambda_1 (v_2^2 - v_1^2) v_1} \vec{\psi}_1(\vec{x}) + \frac{(v_2^2 - \omega_2^2 + \beta_{22})\gamma_2 + \beta_{21}\gamma_1}{\Lambda_1 (v_2^2 - v_1^2) v_1} \vec{\psi}_2(\vec{x}) \right)$$

$$\vec{\psi}_2 = \left(-\frac{(v_1^2 - \omega_1^2 + \beta_{11})\gamma_1 + \beta_{12}\gamma_2}{\Lambda_2 (v_2^2 - v_1^2) v_2} \vec{\psi}_1(\vec{x}) - \frac{(v_1^2 - \omega_2^2 + \beta_{22})\gamma_2 + \beta_{21}\gamma_1}{\Lambda_2 (v_2^2 - v_1^2) v_2} \vec{\psi}_2(\vec{x}) \right)$$

$$\vec{u}(\vec{x}, t) = \Lambda_1 \sin(v_1 t) \vec{\psi}_1(\vec{x}) + \Lambda_2 \sin(v_2 t) \vec{\psi}_2(\vec{x})$$

In case of $\tau > 0$ equations 5.7 contain terms proportional to derivatives of the functions $\varphi_j(t)$. These terms correspond to damping terms in classical mechanics. For example in case $N = 1$ and $\tau > 0$ equations 5.7 take the following form:

$$\varphi_1''(t) + \beta_{11}\tau\varphi_1'(t) + \omega_1^2\varphi_1(t) - \beta_{11}\varphi_1(t) = \gamma_1\delta(t)$$

The solution is then can be given as follows:

$$\varphi_1(t) = \frac{\gamma_1}{\sqrt{\omega_1^2 - \beta_{11} - (\beta_{11}\tau)^2/4}} e^{-\beta_{11}\tau t/2} \sin(\sqrt{\omega_1^2 - \beta_{11} - (\beta_{11}\tau)^2/4} t)$$

Equations 5.7 can be written in the full phase space fashion using additional functions $\varphi_{N+k}(t)$ being the derivatives of $\varphi_k(t)$:

$$\begin{cases} \varphi_k'(t) = \varphi_{N+k}(t) \\ \varphi_{N+k}'(t) = \sum_{j=1}^N \{(\beta_{kj} - \delta_{kj}\omega_k^2)\varphi_j(t) - \beta_{kj}\tau\varphi_{N+j}(t)\} + \gamma_k\delta(t) \end{cases}, \quad k = 1..N$$

This can be written as the following matrix equation:

$$\begin{pmatrix} \varphi_1'(t) \\ \varphi_2'(t) \\ \vdots \\ \varphi_{N-1}'(t) \\ \varphi_N'(t) \\ \hline \varphi_{N+1}'(t) \\ \varphi_{N+2}'(t) \\ \vdots \\ \varphi_{2N-1}'(t) \\ \varphi_{2N}'(t) \end{pmatrix} = \begin{pmatrix} 0 & 0 & \cdots & 0 & 0 & | & 1 & 0 & \cdots & 0 & 0 \\ 0 & 0 & \cdots & 0 & 0 & | & 0 & 1 & \cdots & 0 & 0 \\ \vdots & \vdots & \ddots & \vdots & \vdots & | & \vdots & \vdots & \ddots & \vdots & \vdots \\ 0 & 0 & \cdots & 0 & 0 & | & 0 & 0 & \cdots & 1 & 0 \\ 0 & 0 & \cdots & 0 & 0 & | & 0 & 0 & \cdots & 0 & 1 \\ \hline & & & [\beta_{kj} - \delta_{kj}\omega_k^2] & & & & [-\beta_{kj}\tau] & & & \end{pmatrix} \begin{pmatrix} \varphi_1(t) \\ \varphi_2(t) \\ \vdots \\ \varphi_{N-1}(t) \\ \varphi_N(t) \\ \hline \varphi_{N+1}(t) \\ \varphi_{N+2}(t) \\ \vdots \\ \varphi_{2N-1}(t) \\ \varphi_{2N}(t) \end{pmatrix} + \begin{pmatrix} 0 \\ \vdots \\ 0 \\ \hline \gamma_1\delta(t) \\ \vdots \\ \gamma_{N-1}\delta(t) \\ \gamma_N\delta(t) \end{pmatrix} \quad (5.8)$$

The $2N \times 2N$ matrix in equation 5.8 consists of the following 4 blocks: matrix of zeros (top left), unit matrix of $N \times N$ size (top right), $[\beta_{kj} -$

$\delta_{kj}\omega_k^2]$ (bottom left) and $[-\beta_{kj}\tau]$ (bottom right), assuming that index k is the number of the row and index j is the number of the column within the block.

According to the theory of differential equations solutions for $\varphi_k(t)$ in equation 5.8 are linear combinations of exponents $e^{\lambda_i t}$, where λ_i are eigenvalues of the $2N \times 2N$ matrix in equation 5.8. It can be shown that in the absence of the feedback loop ($\beta_{kj} = 0$) the eigenvalues of such a $2N \times 2N$ matrix take the following $2N$ values: $-i\omega_N, -i\omega_{N-1}, \dots, -i\omega_1, i\omega_1, \dots, i\omega_{N-1}, i\omega_N$, i.e. values of the resonant frequencies of the original cavity times imaginary unit i and corresponding conjugated values. This is the case when equation 5.7 represents N independent harmonic oscillator equations.

When β_{kj} and τ are taken as small nonzero values the eigenvalues of the big matrix in equation 5.8 start to shift along the imaginary axis as well as depart from this axis by acquiring also very small real part (but in such a manner that conjugated eigenvalues are also eigenvalues). Positive imaginary parts of the new eigenvalues are new resonant frequencies ν_k of the cavity influenced by the feedback loop. The simulation described further will allow us to see how the statistical properties of the new eigenfrequencies ν_k differ from the statistical properties of the old eigenfrequencies ω_k .

The above-mentioned very small real part of each eigenvalue governs the slow decay or growth of the corresponding mode ν_k . This exponential growth (damping) with the small real part of the eigenvalue as a growth (decay) constant is caused by the feedback loop. As it has been calculated earlier in this chapter, this growth (decay) constant in case $N = 1$ and $\tau > 0$ is equal to $-\beta_{11}\tau/2$, the product of the feedback coupling strength and the feedback loop delay τ .

The natural damping of the modes is neglected in equations 5.8 and 5.7. We assume it to be small and not affected sufficiently by the feedback loop as long as K is small enough and as a consequence α and β_{kj} are small enough. This is the reason why the range of the values of amplification K used in experiment, discussed in Chapter 4, is limited. The upper limit for values of K arises from the fact that mode growth due to the feedback loop can compensate the natural damping and cause the system to go to the self-oscillation regime.

When amplification K is sufficiently large then the amplitude of one of the modes can start quickly growing exponentially and eventually the system can switch to the regime when the receiving transducer receives continuous oscillation with a large amplitude at the self-oscillation frequency instead of receiving decaying response composed out of many distinguishable modes at different resonant frequencies.

β_{kj} , which enters equations 5.8 and 5.7, is dependent not only on K

($\alpha \propto K$), but also on normal components of the wavefunctions (of the cavity without feedback loop) at points C and D (points at which the transducers of the feedback loop are connected). α in fact should be considered as $\alpha = K\zeta$, where ζ is related to the loss in piezoelectric transducers and efficiency of coupling of the piezoelectric transducers glued at the points C and D in experiment. So the range of experimentally available values of K should be dependent also on the normal components of the wavefunctions at points C and D , loss in piezoelectric transducers and efficiency of coupling of the glued transducers.

5.3 Input parameters of the simulation and the simulation procedure

The following simulation parameters are used:

1. Original frequencies ω_k , uniformly distributed in the section $[f_{AV} - 0.5..f_{AV} + 0.5]$ with GOE distribution of the frequency spacing. These are obtained from eigenvalues of the large symmetric matrix (Fig. 5.2) and have GOE statistical properties (Figures 5.3 and 5.4).

2. Time delay of the feedback loop τ . The value of this parameter is estimated from the measurements discussed in Chapter 2. It can be seen from Figure 2.1 that the delay value can be estimated as less than a microsecond. This parameter depends on how long the signal is delayed by travelling through the feedback loop. The value of τ is considered reasonably smaller than the period of oscillation for the studied resonant modes.

3. B , a parameter related to β_{kj} , describes the strength of the influence of the feedback loop. β_{kj} are defined by the wavefunction components at points D and C . $\beta_{kj} = \alpha c_{\parallel}^2 (\vec{\psi}_k(D) \cdot \vec{n}_D) (\vec{\psi}_j(C) \cdot \vec{n}_C) = B d(k) c(j)$, where $d(k)$ and $c(j)$ are values proportional to the wave function components along \vec{n}_D and \vec{n}_C at points D and C respectively. These values $d(k)$ and $c(j)$ are taken as gaussian distributed (what is natural for chaotic wave system) with standard deviation of 1. B is a scaling coefficient. So $B = \alpha c_{\parallel}^2 \sqrt{\langle (\vec{\psi}_k(D) \cdot \vec{n}_D)^2 \rangle} \sqrt{\langle (\vec{\psi}_j(C) \cdot \vec{n}_C)^2 \rangle}$.

Parameters γ_k are not considered in the simulation for the reason that they represent the strength of the excitation signal. Eigenfrequencies (as with present feedback loop as without it) do not depend on the excitation signal (γ_k do not appear in the $2N \times 2N$ matrix: see equation 5.8).

Using the above mentioned ω_k , B and τ as input for the $2N \times 2N$ matrix from equation 5.8 it is possible to calculate the positive imaginary parts of the eigenvalues of this matrix, the new eigenfrequencies ν_k .

The new eigenfrequencies ν_k are approximately uniformly distributed in

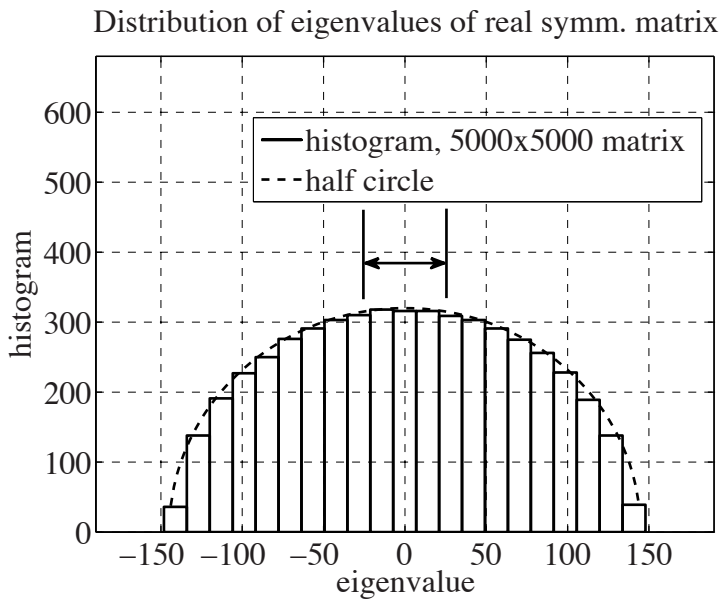


Fig. 5.2: Distribution of the eigenvalues of 5000x5000 random symmetric matrix (agrees with Wigner's semicircle law). Range of 1000 selected eigenvalues used to obtain eigenfrequencies of the aluminum block without feedback loop ω_k is shown with the arrow.

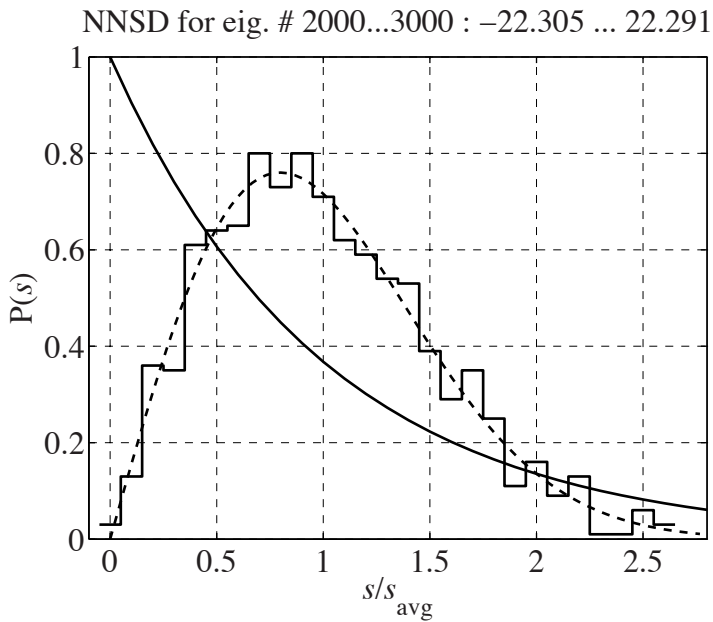


Fig. 5.3: NNSD for 1000 selected eigenvalues (see Figure 5.2) of 5000x5000 random symmetric matrix, Poisson (exponential) distribution (solid curve) and GOE model (dashed curve). There is naturally a full agreement with the GOE curve.

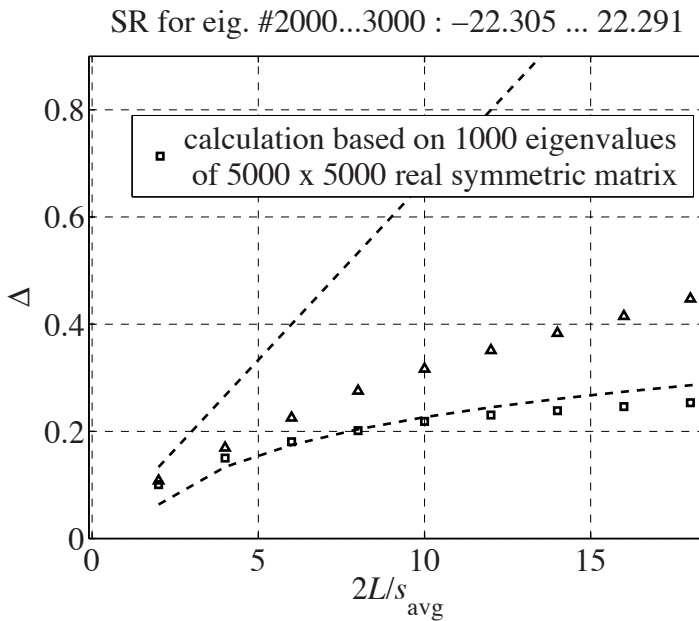


Fig. 5.4: SR (delta statistics) for sequence of 1000 eigenvalues of 5000x5000 random symmetric matrix (squares). SR model for sequence of randomly placed values (uncorrelated level sequence) and GOE model correspond to dashed line and dashed curve respectively. Triangles illustrate the same calculation for sequence of 1000 eigenvalues of 5000x5000 random symmetric matrix when 25% of eigenvalues are randomly lost.

the section $[f_{AV} - 0.5..f_{AV} + 0.5]$, the same as input eigenfrequencies ω_k . A very few of ν_k values "jump out" of this section and this effect is neglected. NNSD for the new eigenfrequencies ν_k , obtained for certain values of the simulation parameters, are shown in Figures 5.5, 5.6 and 5.7.

It can be seen from NNSD shown in Figure 5.5, as well as from NNSD obtained for other values of the simulation parameters (Figures 5.6 and 5.7), that the number of small spacings increases and the number of average spacings decreases due to the influence of the feedback loop. Such transformation makes NNSD approach the Poisson (exponential) model. This is more or less in agreement with data given in Figures 4.9 and 4.10.

5.4 Summary of random matrix model of the elastic cavity influenced by a feedback loop

The model matrix, the eigenvalues of which give eigenfrequencies of the elastic cavity influenced by the feedback loop, can be derived for small values of τ (time delay of the signal travelling through the feedback loop). It can be seen from the NNSD obtained due to this model matrix for different values of simulation parameters that the number of small resonance spacings (relative to the average spacing) increases and the number of average spacings decreases due to the influence of the feedback loop. This means that the trend here is similar to the one found in Chapter 4 when distributions calculated from experimental data were discussed. Increase in small eigenvalue (resonance) spacings and decrease in average eigenvalue (resonance) spacings makes the distribution closer to exponential (earlier referred as Poisson model). However exact fitting of the distributions obtained from experimental data using the random matrix model discussed in the present chapter is considerably complicated due to unknown factors ($\sqrt{\langle (\vec{\psi}_k(D) \cdot \vec{n}_D)^2 \rangle}$ and $\sqrt{\langle (\vec{\psi}_j(C) \cdot \vec{n}_C)^2 \rangle}$) involved in expression for the parameter B measuring the strength of the influence of the feedback loop. And unknown fraction of the lost (undetected) resonances can be also present in distributions obtained from experimental data.

The considered random matrix model also shows that the feedback loop may have influence on decay constants (linewidth, quality factor) of the individual resonances.

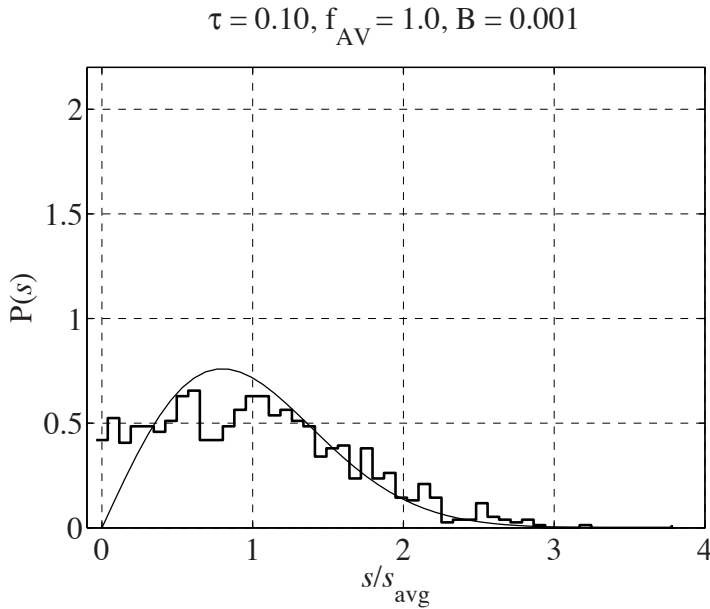


Fig. 5.5: NNSD for the case of active feedback loop (shown as step like function) obtained from statistical simulation as described in the present chapter. The GOE model is shown by the solid continuous curve. The exact values of simulation parameters are shown above the figure. τ is the delay time in the feedback loop, f_{AV} is the average frequency in the considered band and B is the parameter related to the strength of the influence of the feedback loop, $B \propto K \sqrt{\langle (\vec{\psi}_k(D) \cdot \vec{n}_D)^2 \rangle} \sqrt{\langle (\vec{\psi}_j(C) \cdot \vec{n}_C)^2 \rangle}$ (according to the definition given in the present section). Averaging denoted by the brackets $\langle \rangle$ is performed over indices k and j (different wavefunctions). C and D are points where the transducers of the feedback loop are placed.

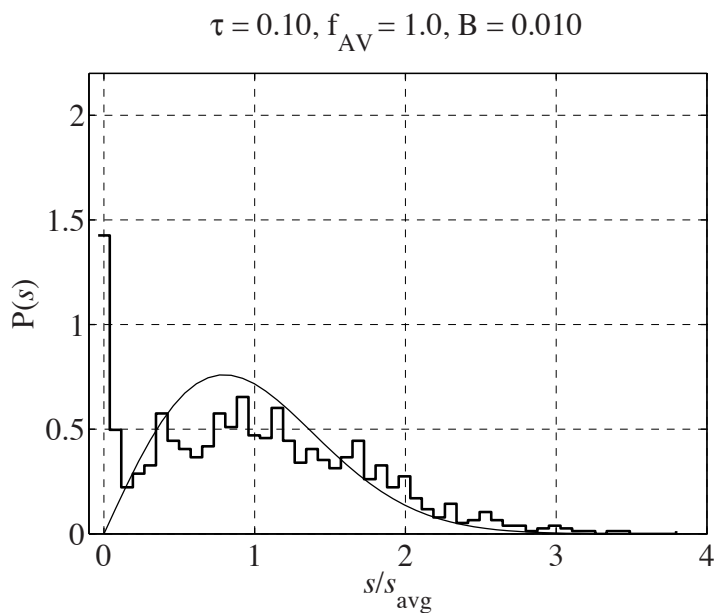


Fig. 5.6: NNSD for the case of active feedback loop (shown as step like function) obtained from statistical simulation as described in the present chapter. The GOE model is shown by the solid continuous curve. The exact values of simulation parameters are shown above the figure (the same parameters as explained in the caption to Figure 5.5).

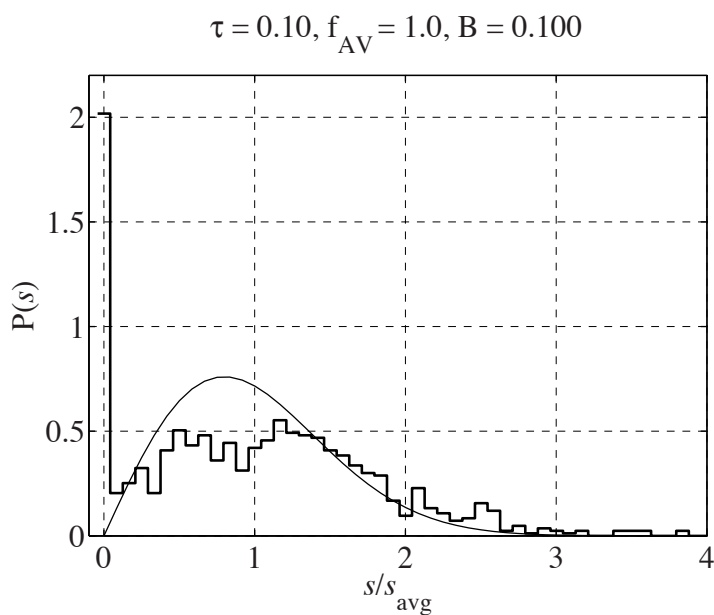


Fig. 5.7: NNSD for the case of active feedback loop (shown as step like function) obtained from statistical simulation as described in the present chapter. The GOE model is shown by the solid continuous curve. The exact values of simulation parameters are shown above the figure (the same parameters as explained in the caption to Figure 5.5).

6. CONCLUSIONS

Calculations based on experimental data for the case without the feedback loop (experiments on unperturbed aluminum blocks "Cavity #1" and "Cavity #2"), discussed in Chapter 2, show that the distributions of the intensity transmission coefficients studied in the narrow frequency bands confirm random division of pulse intensity between the cavity waves for both studied cavities.

Division of the frequency band into intervals by cavity resonances for the unperturbed cavity #2, characterized by the NNSD, is found in agreement with the prediction of RMT for GOE. Perfect agreement, however, is achieved when accounting for a fraction of the lost resonances (about 25%). The corresponding SR shows behavior close to the GOE model that involves logarithmic saturation of the SR. The curve that shows SR in case of GOE model with 25% of eigenvalues lost offers even better fit to the spectral rigidity determined from the experimental data of Chapter 2. So both NNSD and SR can be identified as predicted by the GOE statistics, however a relatively large fraction of the lost resonances (25%) has to be assumed to achieve such an agreement. The SR calculated from the data of the experiment on a symmetric cavity (cavity #1) is systematically larger than in the comparable case of an asymmetric cavity (cavity #2). This agrees with the concept of coexistence of odd and even independent sequences of resonances.

The normalized amplitude of the reconstructed pulse in the time reversal experiment discussed in Chapter 2 deviates from exponential dependence on the time delay if the last one is getting smaller and approaches the Heisenberg time (inverse of the average nearest neighbor resonance spacing).

We also found that moments and central moments of different order, skewness and kurtosis of the NNSD determined from experiment discussed in Chapter 2 fall close to the values corresponding to the GOE model. These values actually fall in between the GOE values and values corresponding to random arrangements of resonance frequencies, Poisson model. This may be considered as a consequence of the lost resonances.

We dealt with a considerable amount of lost resonances in our experiments discussed in Chapter 2. This amount is higher than found in earlier reports like [24] by Nogueira et al. However, these experiments [24] were performed

under idealized circumstances. Firstly, aluminum plate resonators were used instead of the volume ones in present work. Secondly, a vacuum chamber enclosing the sample was used to increase the isolation and therefore increase quality factors of the resonances. Thirdly, probably better support mechanism was used as well.

We report experiments that have been done at normal room conditions in air with support of the sample not entirely optimized. Therefore, a bit worse resonance detection conditions are indeed in place. However, our approach opens the possibility to explore experiments making use of RMT statistics on arbitrary samples under non-optimized conditions. This is important for validating the RMT statistical approach for probable future applications in mechanical engineering.

Simulation with the Wave3000 program [48] discussed in Chapter 3 allows satisfactory reproduction of the cavity responses. The spectral density of the response of the symmetric cubic aluminum resonator (without well drilled in it or corner removed) allows a correct identification of 10 consequent resonances of the cubic resonator as given by the analytical model [46].

The simulated elastic wave dynamics for cavity #2 shows noticeably larger repelling of resonances than determined from the responses in the experiment. The NNSD determined from the simulation data is better peaked around average value than predicted by the GOE distribution. SR averaged over frequency bands smaller than $10s_{\text{avg}}$ has a bit lower value than predicted by the GOE model. The behavior of NNSD and SR showing a fraction of lost resonances is not found in the case of the Wave3000 simulation (unlike for NNSD and SR determined from experimental data discussed in Chapter 2).

In particular, SR determined from the spectra of the Wave3000 simulated responses satisfactory follows the GOE curve for averaging over bands of size of 2 to 10 average spacings. The corresponding SR determined from experimental data (discussed in Chapter 2) has larger values than given by the GOE model and significantly deviates from the GOE curve: it falls above the GOE curve and agrees with GOE model with the lost levels. The reduced spacing value corresponding to the maximum of NNSD determined from the Wave3000 simulated responses is close to that of the pure GOE distribution (without the lost resonances). The only discrepancy between the GOE model and NNSD determined from simulated responses is the actual height of the maximum of NNSD obtained from simulated responses. This can not be explained satisfactory at the moment.

But it can be seen from the spectral density of the responses of the symmetric cube that small sharp peaks are present in addition to large (much better pronounced) ones that have been identified with 10 consequent res-

onances from work [46] for the Poisson ratio of 0.33 corresponding to aluminum. These small sharp peaks, that can be artifact of the simulation, can alter the distribution when identified as resonances. So the departure from the GOE distribution can happen if such peaks are present in the higher frequency band and are counted as resonances. But it is important to mention that NNSD determined from simulated responses in Chapter 3 does not behave as GOE distribution with randomly added resonance frequencies (considered in Chapter 1). So if the small peaks, being the artifact of the simulation, are present in higher frequency band used to study statistics then they appear around real cavity resonances in non-random fashion. This implies that they can be for example higher harmonics of the identified resonances that appear due to some kind of numerical nonlinearities.

NNSD and SR have still noticeable error bars arising from the different positions of source and receiver on the surface of the samples. The NNSD and SR as well as sequences of resonances used in calculation are different for different positions of the transducers on the surface of the sample. This was also observed in the analysis of the experimental data (Chapter 2). But in Chapter 2 different sequences of resonances for different positions of the transducers can be explained by the fraction of lost resonances. In Chapter 3 obviously the error bars of NNSD and SR appear for a different reason (e.g. small peaks in spectral density that can be an artifact of the simulation).

Indeed NNSD and SR calculated from the responses simulated with Wave3000 program do not require accounting for the fraction of lost resonances to be fitted with predictions for the GOE statistics. So the studied sample (cavity #2) fits for further studies of the resonance statistics in case of experimentally broken TR invariance, however a fraction of the lost resonances which remains an experimental issue (discussed in Chapter 2) can make the outcome of the experiment less clear.

Cavity #2 was used further to study random matrix statistical properties and time reversal experiment efficiency for the case of broken time reversal invariance (Chapter 4) which was attempted to achieve in experiment by connecting two additional transducers to the surface of the sample and connecting the feedback loop between them (so that the signal can travel only in one direction through the feedback loop).

It has been found from TR experiments discussed in Chapter 4 that the feedback loop suppresses the reconstruction of the excitation pulse for different time delays of the recorded (and replayed backwards) oscillation track with respect to the original excitation pulse. The suppression of the time reversal reconstruction increases with increasing amplification coefficient K of the amplifier in the feedback loop. Thus time reversal experiment becomes less efficient due to increasing influence of the feedback loop.

The NID obtained from 60 kHz wide frequency band in case of the active feedback loop mainly agree with the exponential distribution corresponding to the input pulse energy being shared randomly between the cavity waves.

It is found also that the active feedback loop influences the NNSD statistics. The effect of the feedback loop on SR (delta statistics) is found negligibly small compared to the error bars based on measurements at several different positions of source and receiver.

It can be seen also that skewness and kurtosis of the NNSD, determined from the data of several experiments, approach closer to the values due to the Poisson model (exponential NNSD) with an increase of the influence of the feedback loop, what implies that NNSD is approaching the case of randomly chosen resonant frequencies. This means that arrangement of the resonances becomes more random with increasing influence of the feedback loop in the experiment. However a part of this behavior may be explained also by the growing amount of lost resonances with increasing influence of the feedback loop in case if more modes are obscured by the growth of the modes that are amplified by feedback.

The model matrix for the elastic cavity influenced by the feedback loop can be derived for small values of τ (time delay of the signal travelling through the feedback loop). Imaginary parts of the eigenvalues of such a matrix derived in Chapter 5 represent eigenfrequencies of the chaotic elastic cavity influenced by the feedback loop. It can be seen from the NNSD obtained due to this model matrix for different values of simulation parameters that the number of small resonance spacings (relative to the average spacing) increases and the number of average spacings decreases due to the influence of the feedback loop. This means that the trend here is similar to the one found in Chapter 4 when distributions calculated from experimental data were discussed. Increase in small eigenvalue (resonance) spacings and decrease in average eigenvalue (resonance) spacings makes the distribution closer to exponential (earlier referred as Poisson model). However exact fitting of the distributions obtained from experimental data using the random matrix model discussed in Chapter 5 is considerably complicated due to unknown factors ($\sqrt{\langle (\vec{\psi}_k(D) \cdot \vec{n}_D)^2 \rangle}$ and $\sqrt{\langle (\vec{\psi}_j(C) \cdot \vec{n}_C)^2 \rangle}$) involved in expression for the parameter B measuring the strength of the influence of the feedback loop. And unknown fraction of the lost (undetected) resonances can be also present in distributions obtained from experimental data.

The considered random matrix model also shows that the feedback loop may have influence on decay constants (linewidth, quality factor) of the individual resonances.

APPENDIX

A. MOMENTS, CENTRAL MOMENTS, SKEWNESS, AND KURTOSIS OF THE NEAREST NEIGHBOR SPACING DISTRIBUTIONS OF THE MAIN MODELS OF RANDOM MATRIX THEORY

Moments of the Nearest Neighbor resonance Spacing Distributions (NNSD) for main models from Random Matrix Theory (RMT) can be derived as simple analytical functions of the order of the moment. Table A.1 gives results of calculation of such functions for three main RMT distribution models (Exponential or Poisson, GOE and GUE).

Zero and first order moments, $\int_0^\infty P(s)ds$ and $\int_0^\infty sP(s)ds$ are both equal to 1 for all three models (Exponential or Poisson, GOE and GUE) due to the normalization of the distribution functions $P(s)$ and variable s (average nearest neighbor spacing s_{avg} in present chapter is set to 1). It can be also clearly seen from the Table A.1. So it is obvious that for zero order central moment we have $\int_0^\infty P(s)ds = 1$ again for all three above-mentioned models for distribution functions $P(s)$ and the first order central moment is equal to 0 in all cases: $\int_0^\infty (s - 1)P(s)ds = 0$. The values of the rest of the central moments (e.g. central moments of 2-nd, 3-rd, 4-th and 5-th order) can be found as shown in Table A.2.

Skewness S and kurtosis K can be defined by Equation A.1 and Equation A.2 using central moments $C_n = \int_0^\infty (s - 1)^n P(s)ds$.

Tab. A.1: Moments of the NNSD models.

Model (name)	Distribution $P(s)$	Moments			
		$\int_0^\infty P(s)ds$	$\int_0^\infty sP(s)ds$	$\int_0^\infty s^2P(s)ds$	$\int_0^\infty s^n P(s)ds$
Poisson	e^{-s}	1	1	2	$\Gamma(n + 1)$
GOE	$\frac{\pi}{2}se^{-\frac{\pi}{4}s^2}$	1	1	$\frac{4}{\pi} = 1.273$	$(\frac{2}{\sqrt{\pi}})^n \Gamma(\frac{n+2}{2})$
GUE	$\frac{32}{\pi^2}s^2e^{-\frac{4}{\pi}s^2}$	1	1	$\frac{3\pi}{8} = 1.178$	$(\frac{\sqrt{\pi}}{2})^{n-1} \Gamma(\frac{n+3}{2})$

Tab. A.2: Central moments of the NNSD models.

Model (name)	Central Moments	
	$\int_0^\infty (s-1)^2 P(s) ds$	$\int_0^\infty (s-1)^3 P(s) ds$
Poisson	1	2
GOE	$\frac{4}{\pi} - 1 = 0.273$	$2 - \frac{6}{\pi} = 0.090$
GUE	$\frac{3\pi}{8} - 1 = 0.178$	$2 - \frac{5\pi}{8} = 0.037$

Model (name)	Central Moments	
	$\int_0^\infty (s-1)^4 P(s) ds$	$\int_0^\infty (s-1)^5 P(s) ds$
Poisson	9	44
GOE	$\frac{32}{\pi^2} - 3 = 0.242$	$\frac{4}{\pi^2} (\pi(5 + \pi) - 25) = 0.234$
GUE	$\frac{\pi}{4} - 3 + \frac{15\pi^2}{64} = 0.099$	$4 + \frac{5\pi}{4} - \frac{51\pi^2}{64} = 0.062$

Tab. A.3: Skewness S and Kurtosis K of the NNSD models.

Model (name)	Distribution $P(s)$	Skewness S	Kurtosis K
Poisson	e^{-s}	2	6
GOE	$\frac{\pi}{2} s e^{-\frac{\pi}{4} s^2}$	$\frac{2 - \frac{6}{\pi}}{(\frac{4}{\pi} - 1)^{3/2}} = 0.6311$	$\frac{\frac{32}{\pi^2} - 3}{(\frac{4}{\pi} - 1)^2} - 3 = 0.2451$
GUE	$\frac{32}{\pi^2} s^2 e^{-\frac{4}{\pi} s^2}$	$\frac{2 - \frac{5\pi}{8}}{(\frac{3\pi}{8} - 1)^{3/2}} = 0.4857$	$\frac{\frac{\pi}{4} - 3 + \frac{15\pi^2}{64}}{(\frac{3\pi}{8} - 1)^2} - 3 = 0.1082$

$$S = \frac{C_3}{(C_2)^{3/2}} \tag{A.1}$$

$$K = \frac{C_4}{(C_2)^2} - 3 \tag{A.2}$$

Skewness S and kurtosis K for all three above mentioned distributions models $P(s)$ are summarized in Table A.3.

Figure A.1 shows moments for the three models for NNSD (Exponential or Poisson, GOE and GUE). Curves in Figure A.1 are calculated using formulas from the last column of Table A.1.

Figure A.2 shows central moments for the three models for NNSD (Exponential or Poisson, GOE and GUE). Curves in Figure A.2 are plotted using Table A.2.

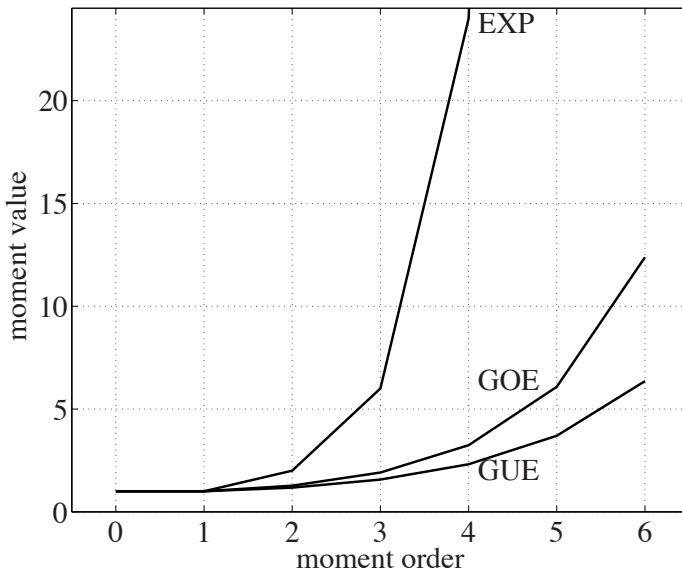


Fig. A.1: Curves marked as 'EXP' 'GOE' and 'GUE' show the moments for the three models for NNSD (Exponential or Poisson, GOE and GUE respectively).

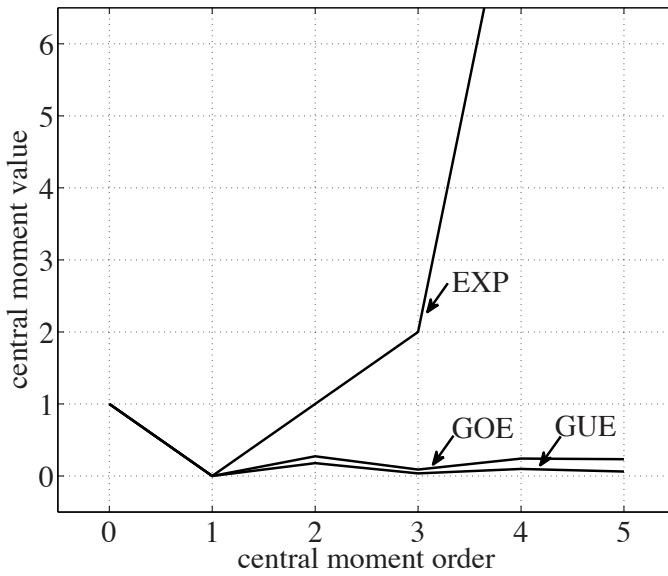


Fig. A.2: Curves marked as 'EXP' 'GOE' and 'GUE' show central moments for the three models for NNSD (Exponential or Poisson, GOE and GUE respectively).

BIBLIOGRAPHY

- [1] D.E. Newland, *An introduction to: Random Vibrations, Spectra & Wavelet Analysis*, third edition, Longman Scientific & Technical, New York, 1993
- [2] <http://www.ndt.org/>
- [3] H.-J. Stöckmann, *Quantum Chaos*, Cambridge University Press, Cambridge, 1999
- [4] T. Guhr, A. Müller-Groeling, H. A. Weidenmüller, Random-matrix theories in quantum physics: common concepts, *Physics Reports* **299** (1998) pp. 189-425
- [5] <http://hypertextbook.com/chaos/>
- [6] A. Douglas Stone, Einstein's Unknown Insight and the Problem of Quantizing Chaos, *Physics Today* **58**, issue 8 (2005) pp. 37-43
- [7] M. R. Schröder, Eigenfrequenzstatistik und Anregungsstatistik in Räumen, *Acustica* **4** (1954) pp. 456-468
- [8] K. Schaadt, *Experiments on Acoustic Chaology and Statistical Elastodynamics*, Ph.D. Thesis, University of Copenhagen, 2001
- [9] A. Andersen, C. Ellegaard, A. D. Jackson, and K. Schaadt, Random matrix theory and acoustic resonances in plates with an approximate symmetry, *Physical Review E* **63** (2001) 066204
- [10] M. V. Berry, R. G. Chambers, M. D. Large, C. Upstill and J. C. Walmley, Wavefront dislocations in the Aharonov-Bohm effect and its water wave analogue, *European Journal of Physics* **1** (1980) pp. 154-162
- [11] P. Roux and M. Fink, Experimental Evidence in Acoustics of the Violation of Time-Reversal Invariance Induced by Vorticity, *Europhysics Letters* **32** (1995) pp. 25-29

-
- [12] Julien de Rosny, Arnaud Tourin, Arnaud Derode, Philippe Roux, and Mathias Fink, Weak Localization and Time Reversal of Ultrasound in a Rotational Flow, *Physical Review Letters* **95** (2005) pp. 074301-1 - 074301-4
- [13] S. Manneville, A. Maurel, P. Roux, M. Fink, Characterization of a large vortex using acoustic time reversal mirrors, *The European Physics Journal B* **9** (1999) pp. 545-549
- [14] Mathias Fink, Time Reversed Acoustics, *Physics Today* **50** (1997) pp. 34-40
- [15] Carsten Draeger and Mathias Fink, One-Channel Time Reversal of Elastic Waves in a Chaotic 2D-Silicon Cavity, *Physical Review Letters* **79** (1997) pp. 407-410
- [16] Vincent Bertaix, Julien Garson, Nicolas Queieffin, Stefan Catheline, Julien Derosny and Mathias Fink, Time-reversal breaking of acoustic waves in a cavity, *American Journal of Physics* **72** (2004) pp. 1308-1311
- [17] M. V. Berry, The Bakerian Lecture, 1987: Quantum Chaology, *Proceedings of the Royal Society of London. Series A, Mathematical and Physical Sciences* **413** (1987) 183-198
- [18] M. V. Berry, Semiclassical Theory of Spectral Rigidity, *Proceedings of the Royal Society of London. Series A, Mathematical and Physical Sciences* **400** (1985) 229-251
- [19] F. Haake, *Quantum Signatures of Chaos, 2-nd edition*, pp. 58-60 (Springer Series in Synergetics, 2001)
- [20] N. Rosenzweig, C. E. Porter, "Repulsion of Energy Levels" in Complex Atomic Spectra, *Physical Review* **120** (1960) pp. 1698-1714
- [21] M. V. Berry and M. Robnik, Semiclassical level spacings when regular and chaotic orbits coexist, *Journal of Physics A: Mathematical and General* **17** (1984) pp. 2413-2421
- [22] K. K. Lehmann, S. L. Coy, The Gaussian orthogonal ensemble with missing and spurious levels: A model for experimental level-spacing distributions, *The Journal of Chemical Physics* **87** (1987) pp. 5415-5418

-
- [23] J. Enders, T. Guhr, N. Huxel, P. von Neumann-Cosel, C. Rangacharyulu, A. Richter, Level spacing distribution of scissors mode states in heavy deformed nuclei, *Physics Letters B* **486** (2000) pp. 273-278
- [24] T. N. Nogueira, J. C. Sartorelli, M. P. Pato and C. Ellegaard, Missing levels in acoustic resonators, *Physical Review E* **78** (2008) pp. 055201-1 - 055201-4
- [25] R. L. Weaver, Spectral statistics in elastodynamics, *The Journal of the Acoustical Society of America* **85** (1989) pp. 1005-1013
- [26] D. Delande, D. Sornette, R. Weaver, A reanalysis of experimental high-frequency spectra using periodic orbit theory, *The Journal of the Acoustical Society of America* **96** (1994) pp. 1873-1880
- [27] C. Ellegaard, T. Guhr, K. Lindemann, H. Q. Lorensen, J. Nygård, and M. Oxborrow, Spectral Statistics of Acoustic Resonances in Aluminum Blocks, *Physical Review Letters* **75** (1995) pp. 1546-1549
- [28] C. Ellegaard, T. Guhr, K. Lindemann, J. Nygård, and M. Oxborrow, Symmetry Breaking and Spectral Statistics of Acoustic Resonances in Quartz Blocks, *Physical Review Letters* **77** (1996) pp. 4918-4921
- [29] M. V. Berry and M. Robnik, Statistics of energy levels without time-reversal symmetry: Aharonov-Bohm chaotic billiards, *Journal of Physics A: Mathematical and General* **19** (1986) pp. 649-668
- [30] Mathias Fink, Time-Reversed Acoustics, *Scientific American* (November 1999) pp. 91-97
- [31] Mathias Fink, D. Cassereau, A. Derode, Claire Prada, P. Roux, M. Tanter, J-L. Thomas and F. Wu, Time-reversed acoustics, *Reports on Progress in Physics* **63** (2000) pp. 1933-1995
- [32] Claire Prada, F. Wu and Mathias Fink, The iterative time reversal mirror: A solution to self-focusing in the pulse echo mode, *The Journal of the Acoustical Society of America* **90** No. 2 (1991) pp. 1119-1129
- [33] Claire Prada, Estelle Kerbrat, Didier Cassereau and Mathias Fink, Time reversal techniques in ultrasonic nondestructive testing of scattering media, *Inverse problems* **18** (2002) pp. 1761-1773

-
- [34] Carene Larmat, Jean-Paul Montagner, Mathias Fink, Yann Capdeville, Arnaud Tourin and Eric Clévéde, Time-reversal imaging of seismic sources and application to the great Sumatra earthquake, *Geophysical Research Letters* **33** (2006) p. L19312
- [35] M. G. Heinemann, A. Larraza and K. B. Smith, Acoustic communications in an enclosure using single-channel time-reversal acoustics, *Applied Physics Letters* **80** (2002) pp. 694-696
- [36] Arnaud Derode, Arnaud Tourin, Julien de Rosny, Mickaël Tanter, Sylvain Yon and Mathias Fink, Taking Advantage of Multiple Scattering to Communicate with Time-Reversal Antennas, *Physical Review Letters* **90** (2003) pp. 014301-1 - 014301-4
- [37] Rudolf Sprik and Arnaud Tourin, Time reversed wave propagation experiments in chaotic micro-structured cavities, *Ultrasonics* **42** (2004) pp. 775-779
- [38] Gregor Tanner and Niels Søndergaard, Wave chaos in acoustics and elasticity, *Journal of Physics A* **40** (2007) pp. R443-R509
- [39] <http://www.webmd.com/kidney-stones/extracorporeal-shock-wave-lithotripsy-eswl-for-kidney-stones>
- [40] Mathias Fink, Ultrasound Puts Materials to the Test *Physics World* **11** No. 2 (February 1998) pp. 41-45
- [41] Arnaud Tourin, Geoffroy Lerosey, Julien de Rosny, Arnaud Derode, Mathias Fink, Time reversal telecommunications in complex environments, *Comptes Rendus Physique* **7** (2006) pp. 816-822
- [42] Carsten Draeger and Mathias Fink, One-channel time-reversal in chaotic cavities: Theoretical limits, *The Journal of the Acoustical Society of America* **105** (1999) pp. 611-617
- [43] Arnaud Derode, Arnaud Tourin, and Mathias Fink, Random multiple scattering of ultrasound. II. Is time reversal a self-averaging process? *Physical Review E* **64** (2001) pp. 036606-1 - 036606-13
- [44] T. Strohmer, M. Emami, J. Hansen, G. Papanicolaou and A. J. Paulraj, Application of time-reversal with MMSE equalizer to UWB communications *Proceedings of the Global Telecommunications Conference (GLOBECOM04) at Piscataway, NJ (USA)* **5** (2004) pp. 31237

-
- [45] K. Popovski, B. J. Wysocki and T. A. Wysocki, EURASIP article ID: 71610 (2007)
- [46] H. H. Demarest, Cube-Resonance Method to Determine the Elastic Constants of Solids, *The Journal of the Acoustical Society of America* **49** (1971) pp. 768-775
- [47] Richard L. Weaver, On diffuse waves in solid media, *The Journal of the Acoustical Society of America* **71** (1982) pp. 1608-1609
- [48] Software (Wave3000 program) used for simulation of acoustic responses, <http://www.cyberlogic.org/index.html>
- [49] U. Stoffregen, J. Stein, H.-J. Stöckmann, M. Kuś and F. Haake, Microwave Billiards with broken Time Reversal Symmetry, *Physical Review Letters* **74** (1995) pp. 2666-2669
- [50] Richard L. Weaver, Oleg I. Lobkis and Alexey Yamilov, Entrainment and stimulated emission of ultrasonic piezoelectric auto-oscillators, *The Journal of the Acoustical Society of America* **122** (2007) pp. 3409-3418
- [51] Rudolf Sprik, Influence of feedback in wave based chaotic networks, International Conference on Computational Science, ICCS 2010, *Procedia Computer Science* **1** (2010) pp. 1625-1633
- [52] G. Grossia, L. Peroncelli, N. Rahman, Statistics of energy levels in the quantum treatment of an elementary reaction, *Chemical Physics Letters* **313** (1999) pp. 639-646

SUMMARY

The statistical properties of wave propagation in classical chaotic systems are of fundamental interest in physics. They can be used as the basis for diagnostic tools in materials science [1, 2]. One successful statistical approach originating from quantum mechanics [3, 4] is to describe properties of eigenvalues (i.e. resonant frequencies or energy levels) and eigenfunctions of a complex chaotic system by modelling the Hamiltonian of the system with an ensemble of random matrices with certain properties. The statistical properties of the eigenvalues of this ensemble of random matrices give the statistical properties of the considered resonant frequencies or energy levels. The method can be applied to interpret the properties of acoustic waves in complex mechanical systems.

The statistical properties of the resonance frequencies depend also on the presence of time reversal invariance in the system. The role of time reversal invariance can be verified independently by time reversal experiments. In time reversal experiments part of the recorded (elastic) response is played backwards in time in order to refocus the strongly scattered signal back into a short pulse by back-propagation of the waves in the system.

As a model system to test the statistical properties of resonances with the ability to perform time reversal reconstruction, we investigated chaotic systems with time reversal invariance using ultrasonic waves in aluminum blocks (cavities). After excitation of the samples with a short acoustic pulse the reverberation responses were recorded and analyzed.

The statistical properties of resonance frequencies of the cavities were obtained from the spectral density of the reverberant responses. The distribution of the transmitted intensities displays a random division of intensity between cavity waves in narrow frequency bands. The distribution of frequency spacing between neighboring cavity resonances and the Spectral Rigidity agree with the predictions for a Gaussian Orthogonal Ensemble of random matrices. In the analysis of the spectral density of the recorded responses we explicitly included the fact that not all resonances are detected. The agreement with predictions for the Gaussian Orthogonal Ensemble is achieved if we assume that a fraction of typically 25 percent of the resonances is not detected in the experiment. We also found that moments and

central moments of different order, skewness and kurtosis for nearest neighbor resonance spacing distributions determined from experimental data fall close to the values corresponding to the Gaussian Orthogonal Ensemble. These values actually fall in between the values for the Gaussian Orthogonal Ensemble and the values corresponding to a random arrangement of resonance frequencies, the Poisson model. This may be considered a consequence of the lost resonances.

Reversibility of the excited wave dynamics in the cavity after a given time delay was studied by reconstruction of the excitation pulse in time reversal experiments. The normalized amplitude of the reconstructed pulse decays exponentially with the time delay between the original excitation pulse and the end of the reversed oscillation track. The exponential behavior exists for time delays longer than the inverse of the nearest neighbor resonance spacing.

The statistical properties of the chaotic cavity were determined both from the experimental cavity responses as well as from simulations of the elastic cavity responses (using Wave3000 simulation program [48]). In this thesis it was confirmed that the simulation correctly predicts the spectral density of the elastic responses of an aluminum cube in the low frequency limit [46].

The distribution of frequency spacing between neighboring cavity resonances and the Spectral Rigidity calculated from the responses simulated with Wave3000 program do not show behavior predicted for the fraction of the lost resonances in the Gaussian Orthogonal Ensemble. However, small peaks, being the artifact of the simulation, may be present in the higher frequency band used to study statistics. Such spurious peaks that appear around real cavity resonances may influence the statistics and cause the deviation from the prediction for Gaussian Orthogonal Ensemble.

The time reversal invariance of waves in the chaotic cavity was broken experimentally by connecting an amplified feedback loop between the two additional transducers on the surface of the aluminum block (cavity). We repeated the time reversal experiments and the statistical analysis of the spectral density of the cavity responses. Thus we did prove that the feedback loop inhibits time reversal reconstruction of the excitation pulse in time reversal experiment. The effect of the feedback loop on the nearest neighbor resonance spacing statistics has been observed. The experimental results show that the skewness and kurtosis of the distribution of the spacing between the neighboring resonances approach the values due to the Poisson model (exponential distribution) when the influence of the feedback loop is increased. This implies that the distribution approaches the case of randomly chosen resonant frequencies with increasing influence of the feedback loop in the experiment.

A random matrix model was constructed within this thesis to describe

the statistical properties of the resonance frequencies of the aluminum block (chaotic cavity) influenced by the feedback loop. Predictions for the nearest neighbor resonance spacing distribution due to this random matrix model have been made. It can be seen from these predictions that the number of small eigenvalue (resonance) spacings increases and the number of average resonance spacings decreases with increasing influence of the feedback loop. This makes the distribution closer to exponential (earlier referred as Poisson model). The calculations confirm the trend of the experimental data.

It makes sense to further investigate similar systems with (and without) the feedback loop using chaotic and regular resonators of different shapes made out of different materials. Such results would help to assess how random matrix statistics can be used in nondestructive testing techniques in material science. A good improvement would also be to improve resonance detection in case of spurious peaks in the spectral density. An important improvement to the random matrix model for the elastic chaotic cavity influenced by feedback can be made by including the linewidth (quality factors) of the individual resonances and distributions of these values.

A short overview of the content of chapters of the present thesis is given below.

Chapter 1 gives an overview of the statistics of Random Matrix Theory and Time Reversal Experiments. The Gaussian Orthogonal Ensemble, Nearest Neighbor eigenvalue Spacing Distribution and Spectral Rigidity are introduced. Distributions resulting from the coexistence of independent resonance sequences and from incomplete sequences of resonances are treated as well. The general scheme of the time-reversal experiments is also described in Chapter 1.

Experiments on and statistical properties of the elastic chaotic cavity without breaking the time reversal invariance are discussed in detail in Chapter 2. The efficiency of the time reversal experiments using this cavity is discussed as well.

In chapter 3 the statistical properties of the chaotic cavity are calculated from simulations using Wave3000 software [48].

Experimental investigation of the statistical properties and efficiency of the time reversal experiment when the time reversal invariance in a chaotic cavity is broken by a feedback loop is discussed in Chapter 4.

Chapter 5 describes a novel random matrix model for the description of a chaotic cavity influenced by a feedback loop. It discusses the corresponding Nearest Neighbor eigenvalue Spacing Distribution obtained with this model.

The following new results are claimed to be obtained within the scope of the present thesis:

- Calculation of the Nearest Neighbor eigenvalue Spacing Distributions,

its moments and spectral rigidity from experiments on a chaotic elastic volume resonator (Chapter 2). Correspondence of the found Nearest Neighbor eigenvalue Spacing Distribution and Spectral Rigidity to those of a Gaussian Orthogonal Ensemble with a fraction of lost resonances.

- Determination of the Nearest Neighbor eigenvalue Spacing Distribution and Spectral Rigidity from simulations of the acoustic wave propagation in an elastic chaotic resonator (Chapter 3).

- Measurements of the acoustic responses of the cavity influenced by the feedback loop. Calculation of the Nearest Neighbor eigenvalue Spacing Distribution, its moments and the Spectral Rigidity from these measured responses. Time reversal experiments performed on such a system (Chapter 4).

- Construction of the random matrix model of an elastic chaotic cavity influenced by a feedback loop and prediction of the behavior of the Nearest Neighbor eigenvalue Spacing Distribution behavior within this model (Chapter 5).

SAMENVATTING

De statistische eigenschappen van golfvoortplanting in klassieke chaotische systemen zijn van fundamenteel belang in de natuurkunde. Zij kunnen de basis zijn voor niet destructief testen en diagnostiek in de materiaalkunde en techniek [1, 2]. Wij gebruiken een succesvolle statistische methode afkomstig uit de kwantummechanica [3, 4] om de eigenschappen van eigenwaarden (resonantiefrequenties of energie niveaus) en eigenfuncties van een complex chaotisch systeem te beschrijven door de Hamiltoniaan van het systeem met een ensemble van toevallige matrices met bepaalde eigenschappen te modelleren. De statistische eigenschappen van de eigenwaarden van een dergelijk ensemble van toevallige matrices geven de statistische eigenschappen van de beschouwde resonantiefrequenties of energie niveaus. Dit kan ook toegepast worden om de eigenschappen van akoestische golven in complexe mechanische systemen te interpreteren.

De statistische eigenschappen van de resonantiefrequenties zijn ook afhankelijk van de aan- of afwezigheid van tijdinversie-invariantie in het systeem. Tijdinversie-invariantie kan onafhankelijk geverifieerd worden door tijdinversie experimenten. In een tijdinversie experiment wordt een deel van het opgenomen (elastische) signaal teruggespeeld zodat het sterk verspreide signaal wordt gefocuseerd in een korte puls door de voortplanting van de golven in het systeem om te keren. Als model systeem voor het testen van de statistische eigenschappen van resonanties met de mogelijkheid om een tijdinversie experiment toe te passen, hebben we chaotische systemen onderzocht. Hierbij is gebruik gemaakt van ultrasone golven in aluminium blokken. Na excitatie van de monsters met een korte akoestische puls werd het complexe responssignaal geregistreerd en geanalyseerd.

De statistische eigenschappen van resonantie frequenties zijn verkregen uit de spectrale dichtheid van de opgenomen responssignalen. De verdeling van de transmissie-intensiteit vertoont een toevalige verdeling van de intensiteit in smalle frequentiebanden. De verdeling van de frequentie-afstanden tussen naaste buur resonanties en de Spectrale Rigiditeit komen overeen met de voorspellingen voor een Gaussiaans Orthogonaal Ensemble. Bij de analyse van de spectrale dichtheid van de opgenomen responssignalen hebben wij uitdrukkelijk meegenomen dat niet alle resonanties kunnen worden gede-

tecteerd. De overeenkomst met de voorspellingen voor het Gaussiaans Orthogonaal Ensemble wordt bereikt als we veronderstellen dat een fractie van 25 procent van de resonanties niet gedetecteerd wordt in het experiment. We vonden ook dat de momenten, de centrale momenten van verschillende orde, de scheefheid en de kurtosis voor de Naaste Buur resonantie Afstand Verdelingen, bepaald op basis van de experimentele gegevens, dichtbij de waarden liggen die overeenkomen met het Gaussiaans Orthogonaal Ensemble. Deze waarden liggen tussen de waarden voor het Gaussiaans Orthogonaal Ensemble en de waarden die overeenkomen met een toevallige rangschikking van resonantiefrequenties, de Poisson verdeling. Dit kan worden beschouwd als een gevolg van de niet gedetecteerde resonanties.

De omkeerbaarheid van de golfdynamica in de resonator werd onderzocht door reconstructie van de excitatiepuls in tijdinversie experimenten. De genormaliseerde amplitude van de gereconstrueerde puls in het tijdinversie experiment vervalt exponentieel met het tijdsverschil tussen de originele excitatiepuls en de eindtijd van het deel van het responssignaal dat omgekeerd wordt. Het exponentiele gedrag wordt zichtbaar bij vertragingen langer dan de inverse van de naaste buur resonantie afstand.

De statistische eigenschappen van de chaotische resonator konden bepaald worden zowel van de experimentele resonator respons als van de gesimuleerde response van een elastische resonator met behulp van simulatie-programma's (als Wave3000 programma's [48]). In dit proefschrift werd bevestigd dat de simulaties een correcte voorspelling gaven van de spectrale dichtheid van de elastische respons van een aluminium kubus in lage frequentie limiet [46].

De verdeling van de frequentie afstand tussen naaste buur resonanties en de Spectrale Rigiditeit berekend op basis van de resonator responsen gesimuleerd met het Wave3000 programma kwam niet overeen met de voorspelling voor de fractie van de verloren resonanties in het Gaussiaans Orthogonaal Ensemble. Er kunnen echter enkele kleine pieken aanwezig zijn in de hogere frequentie band gebruikt om de statistieken te bestuderen, die een gevolg zijn van artefacten in de simulatie. Deze valse pieken rond de echte resonator resonanties kunnen invloed hebben op de statistiek en zijn de oorzaak van de afwijking van het Gaussiaans Orthogonaal Ensemble.

De tijdinversie-invariantie van golven in de chaotische resonator werd experimenteel gebroken door het aansluiten van een versterkte terugkoppeling tussen de twee extra transducers op het oppervlak van het aluminium blok. De tijdinversie experimenten en de statistische analyse van de spectrale dichtheid van de resonator responsen werden herhaald in dit proefschrift voor de actieve terugkoppeling. Wij hebben vastgesteld dat de terugkoppeling de reconstructie van de excitatie puls in het tijdinversie experiment vermindert. Het effect van de terugkoppeling op de naaste buur afstand res-

onantie statistieken is gemeten. Uit de experimentele resultaten blijkt dat de Scheefheid en Kurtosis van de Naaste Buur resonantie Afstand Verdelingen dichter bij de waarden van het Poisson-model (exponentiele verdeling) liggen naarmate de invloed van de terugkoppeling toeneemt. Dit houdt in dat de verdeling de toestand van toevallig gekozen resonantiefrequenties benaderd, als de invloed van de terugkoppeling in het experiment toeneemt.

Een toevallig matrix model werd geconstrueerd als onderdeel van dit proefschrift om de statistische eigenschappen van de resonantie frequenties van het aluminium blok (chaotische resonator) te beschrijven wanneer deze wordt beïnvloed door de terugkoppeling. Er zijn voorspellingen gedaan voor de Naaste Buur resonantie Afstand Verdelingen als gevolg van dit toevallige matrix model. Hieruit blijkt dat het aantal kleine eigenwaardenafstanden of resonantieafstanden toeneemt en het aantal gemiddelde resonantieafstanden afneemt met toenemende invloed van de terugkoppeling. Hierdoor krijgt de verdeling een exponentieel karakter en komt dichter bij het Poisson model. De berkeningen bevestigen de trend gevonden in de experimentele data.

Het is zinvol vergelijkbare systemen te onderzoeken met (en zonder) een terugkoppeling door gebruik te maken van chaotische en regelmatige resonatoren van verschillende vormen gemaakt uit verschillende materialen. Dergelijke resultaten kunnen helpen om te beoordelen hoe random matrix statistieken gebruikt kunnen worden in niet-destructieve testen in de materiaalkunde. Een goede verbetering zou ook zijn om de resonantiedetectie te verbeteren en zo de detectie van valse pieken in de spectrale dichtheid te verminderen. Het toevallige matrix model voor de elastische chaotische resonator onder invloed van een terugkoppeling kan verbeterd worden door de lijnbreedte (kwaliteitsfactoren) van de individuele resonanties en de verdeling van deze waarden in het model op te nemen.

Een kort overzicht van de inhoud van de hoofdstukken van dit proefschrift wordt hieronder gegeven.

Hoofdstuk 1 geeft een overzicht van de belangrijkste elementen van de toevallige matrix theorie en de tijdinversie experimenten. Het Gaussiaans Orthogonaal Ensemble, de Naaste Buur resonantie Afstand Verdelingen en Spectrale Rigiditeit worden geïntroduceerd. Verdelingen, die het resultaat zijn van co-existentie van onafhankelijke resonantie sequenties en verdelingen van onvolledige sequenties van resonanties worden ook bediscussieerd. De algemene opzet van het tijdinversie experiment wordt ook beschreven in Hoofdstuk 1.

Experimenten aan en statistische eigenschappen van de elastische chaotische resonator zonder verbreking van de tijdinversie-invariantie worden behandeld in detail in Hoofdstuk 2. Ook de efficiëntie van het tijdinversie experiment met deze resonator wordt beschouwd in Hoofdstuk 2.

In hoofdstuk 3 worden de statistische eigenschappen van de chaotische resonator berekend uit simulaties met behulp van Wave3000 software [48].

Experimenteel onderzoek van de statistische eigenschappen en de efficiëntie van het tijdinversie experiment in het geval van gebroken tijdinversie-invariantie in een chaotische resonator waarin de tijdinversie gebroken is door een terugkoppelingscircuit wordt behandeld in Hoofdstuk 4.

Hoofdstuk 5 beschrijft een mogelijk toevallige matrix model voor de beschrijving van de elastische chaotische resonator beïnvloed door een terugkoppelingscircuit. Hierin wordt de simulatie en de hieruit volgende NBAV bediscussieerd.

In dit proefschrift zijn de volgende nieuwe resultaten verkregen:

- Berekening van de Naaste Buur resonantie Afstand Verdelingen, zijn momenten en Spectrale Rigiditeit uit experimenten aan een chaotische elastische volume resonator (Hoofdstuk 2). Overeenkomst van deze Naaste Buur resonantie Afstand Verdelingen en Spectrale Rigiditeit met die van een Gaussiaans Orthogonaal Ensemble met een fractie van verloren resonanties.

- Bepaling van de Naaste Buur resonantie Afstand Verdelingen en de Spectrale Rigiditeit uit simulaties van akoestische golven in een chaotische resonator (Hoofdstuk 3).

- Metingen van de akoestische respons van de resonator beïnvloed door een terugkoppelingscircuit. Berekening van de Naaste Buur resonantie Afstand Verdelingen, zijn momenten en Spectrale Rigiditeit van de gemeten respons. Tijdinversie experimenten uitgevoerd op dit systeem (Hoofdstuk 4).

- Constructie van het toevallige matrix model van de elastische chaotische resonator beïnvloed door de terugkoppeling en voorspelling van de Naaste Buur resonantie Afstand Verdelingen door dit model (Hoofdstuk 5).

CURRICULUM VITAE

Name: Oleg Antoniuk
Date and place of birth: 9-th of April 1981, Kyiv, Ukraine.
Nationality: Ukrainian



Education:

-
- 2005-2010 PhD student at the *van der Waals - Zeeman Instituut of Universiteit van Amsterdam*.
-
- 2002-2005 Master studies at *Radiophysics Department of Taras Shevchenko National University*, Kyiv, Ukraine. Obtained Master Degree in Applied Physics, specialization in Radiophysics and Electronics. Major: Quantum Electronics.
- 1998-2002 Undergraduate studies at *Radiophysics Department of Taras Shevchenko National University*, Kyiv, Ukraine. Obtained Bachelor Degree in Applied Physics, specialization in Radiophysics and Electronics (*cum laude*).
- 1995-1998 Studies at *Ukrainian Physics and Mathematics Lyceum*, attached to *National University of Kyiv*, Ukraine.
- 1988-1995 Studies at school № 251 in Kyiv, Ukraine.
-

Employment history:

-
- 2011 Employment as junior researcher by *Universiteit van Amsterdam*: participation in analysis of the data from ISS (International Space Station) in the project for studies of Colloidal Phase Transitions induced by the Critical Casimir Effect.
-
- 2005-2010 Employment as junior researcher (OIO) by *Stichting voor Fundamenteel Onderzoek der Materie*, The Netherlands, <http://www.fom.nl> (Doing PhD research).
- 2004-2005 Employment as student-assistant by *Institute of Layers and Interfaces at Forschungszentrum Jülich*, Germany (related to Master diploma project).
-

PUBLICATION LIST

1. O. A. Antoniuk, V. F. Kovalenko, O. V. Tychko, Domain Wall In Cubic Magnetic Crystal with Photoinduced Magnetic Anisotropy, *Proceedings of the Third International Young Scientists Conference on Applied Physics*, pp. 98-99, June, 18-20, 2003, Kyiv, Ukraine.
2. I. O. Anisimov, O. A. Antoniuk, To the Study of Cycles of the Quadratic Mapping, *Proceedings of the Third International Young Scientists Conference on Applied Physics*, pp. 17-18, June, 18-20, 2003, Kyiv, Ukraine.
3. O. A. Antoniuk, V. F. Kovalenko, O. V. Tychko, 71°- domain wall in cubic crystal with photoinduced magnetic anisotropy, *Functional Materials*, vol. **11**, No 3, pp. 528-532 (2004)
Available online: <http://www.isc.kharkov.com/journal/contents/11-3/18.pdf> .
4. S.A. Vitusevich, S.V. Danylyuk, M.V. Petrychuk, O.A Antoniuk, N. Klein, A.E. Belyaev, Equilibrium and non-equilibrium 1/f noise in AlGaIn/GaN TLM structures, *Applied Surface Science*, vol. **238**, pp. 143–146 (2004), <http://dx.doi.org/10.1016/j.apsusc.2004.05.205> .
5. Oleg Antonyuk, Valeriy F. Kovalenko, Olexandr V. Tychko, The structure of Bloch domain wall with equilibrium orientation, *Journal of Alloys and Compounds*, vol. **369**, pp. 112-116 (2004), <http://dx.doi.org/10.1016/j.jallcom.2003.09.054> .
6. M. Schuster, O. Antoniuk, P. Lahl, N. Klein, Resonant and waveguiding defect modes in a 2D electromagnetic bandgap slab structure for millimeter wave frequencies, *Journal of Applied Physics*, vol. **97**, 044912 (2005), <http://dx.doi.org/10.1063/1.1851600> .
7. O. A. Antonyuk, V. F. Kovalenko, B. N. Moldovan and M. V. Petrichuk, Periodic Structure of Acicular Magnetic Clusters in a Magnetic Liquid, *Technical Physics*, vol. **50**, No. 6, pp. 766–770 (2005), <http://dx.doi.org/10.1134/1.1947355> , translated from *Zhurnal Tekhnicheskoi Fiziki*, vol. **75**, No. 6, pp. 93–97 (2005).
8. B. N. Moldovan, O.A. Antonyuk, M.V. Petrychuk and V.F. Kovalenko, Periodic structure of spicular magnetic clusters in a magnetic liquid, *Journal of Colloid and Interface Science*, vol. **296**, pp. 577-580 (2006), <http://dx.doi.org/10.1016/j.jcis.2005.09.026> .
9. Oleg Antoniuk and Rudolf Sprik, Measurement and Simulation of Random Matrix Statistics in Aluminum Mesoscopic Cavities, *WSPC proceedings book of the International Conference "Chaos2008"*, 03 June 2008 – 06 June 2008, Chania (Χανιά), Crete (Κρήτη), Greece, <http://www.chaos2008.net/> . This article is related to my PhD thesis.
10. O. Antoniuk and R. Sprik, Measurement and Simulation of Random Matrix Statistics in Aluminum Mesoscopic Cavities, in “*Topics on Chaotic Systems (Selected Papers from CHAOS 2008 International Conference)*”, pp. 14-21 (2009), World Scientific Publishing Co. Pte. Ltd., ISBN-13: 978-981-4271-33-2, ISBN-10: 981-4271-33-0. This article is related to my PhD thesis.
11. Oleg Antoniuk and Rudolf Sprik, Statistics of resonances and time reversal reconstruction in aluminum acoustic chaotic cavities, *Journal of Sound and Vibration*, vol. **329**, issue 26, pp. 5489-5500 (2010), <http://dx.doi.org/10.1016/j.jsv.2010.07.010> . This article is related to my PhD thesis.

12. René Delfos, Carole Leguy, Norbert Warncke, Damien George, Oleg Antoniuk, Mariya Medvedyeva, Hans Meerman, Tjerk Oosterkamp and Jerry Westerweel, The homogeneity of yarn in the heat treatment section of the production process of Twaron®, *Proceedings Physics with Industry 2010*, Lorentz Center, Leiden, The Netherlands, 11-15 October 2010, pp. 46-65.

ACKNOWLEDGEMENTS

Firstly I would like to say sincere thanks to people and institutions that made my work on this thesis possible. First of all I must acknowledge the contribution of my supervisor Dr. Rudolf Sprik. He was always there with good advice when needed and his suggestions were always useful. My promotor Prof. Dr. Gerard Wegdam had also contributed a lot to arranging formalities related to my PhD position and did a lot of proofreading of this thesis. Prof. Dr. Mark Golden, the director of the *Van der Waals-Zeeman Institute (WZI)* was very supportive and helpful. Then, of course, I have to thank *University of Amsterdam* for providing me with laboratories, computers and lab equipment. Great thanks to the workshop of the WZI for manufacturing the samples and transducer holders. *Stichting voor Fundamenteel Onderzoek der Materie* deserves a separate acknowledgement for employing me during the time I was working on my thesis and also for organizing numerous special courses, events and master classes from which I learned a lot about the Netherlands, about science, about presenting science and so on, as well as had an unique opportunity to talk to many PhD students from the other institutes and universities.

It also appropriate to thank Prof. Dr. Thomas Guhr from University of Duisburg-Essen and members of his group, Dr. Boris Gutkin, Dr. Rudi Schäfer and Dr. Vladimir Osipov. Participation in discussions with them at their group seminar in Duisburg and at the conferences significantly improved my understanding of the concept of the application of random matrices in physics.

I have to acknowledge comfortable and very friendly working environment created by my past and present colleagues at *Soft Matter Group* of the WZI: Vijayakumar Chikkadi, Antina Ghosh, Luong Duy Thanh, Abdoulaye Fall, Asmae Khaldoun, Chantal Carpentier, Chiraz Ennaceur, Javier Loaiza, Salima Rafai, Hua Guo (Tracy), Jakub Otwinowski, Yves Hennequin, Janaina de Castro, Duc van Nguyen, Rojman Zargar, Sandra Veen, Noushine Shahidzadeh, Nazly Sedghinejad, Daniel Bonn, Peter Schall, Julie Desarnaud, Mounir Aytouna, Sara Jabbari, Kinga Lörincz, Jose Paredes, Yaser Rahmani, Dang Triet, Hugo Doleman, Marthe Schut, Sareh Nakhaee, Dominik Michler, Marius Mermet-Guyennet, Henri De Cagny and Dmitry Denisov.

Great thanks to the members of the *WZI/ITF Social club*, who contributed to many wonderful free-time events: Oleksandr Zozulya, Alessia Gasparini, Fendy de Nijs, Dolf Timmerman, Gianni Galistu, Richard Newell, Rob Hagemans, Ignacio Izeddin, Freek Masee, Salvatore Minissale, Antje Ludewig, Pasquale Calabrese, Wieteke de Boer, Bahar Mehmani, Liza Huijse, Tobias Tiecke, Luuk Lusink, Rita Vinig, Ineke Baas, Tom Hijmans. Parties on various occasions and other Social club organized events made my life in Amsterdam extra nice. Thank you guys; I had a good time with you.

I had some wonderful time also together with the *volleyball group* at *UvA sport centre*: Taco Ketting, Alexandra Babich, Joël Scapin, Blazej Slezak, Martin van Steeg, Maaïke Deur, Jan Wijzman, Wander Sprenger, Jesse Vanderlee and others whose names I do not recall now.

I appreciate very much also that some of my old friends, who I knew well earlier, were here in the Netherlands during my being a PhD student: Dima Makogon, Igor Shokaryev, Maksim Sladkov and Oleksii Rudenko.

I would like to acknowledge also friends outside the above mentioned communities: Alexandra Babenko, Nancy Djadda, Oleg Karpenkov, Alina Veligura, Bruno Pisani, Guy Edmonds, Maxim Filatov, Mathias Spichtig, Blaz Zlicar, Jun Wu, Tobias Kalenscher, Alexander Issaev, Mayank Bora, Katsuhiko Sano, Ruslan Sepkhanov, Alexander Mikhnenko, Sergey Anisov, Zdenko

van Kesteren, Carole Leguy, Norbert Warncke, Damien George, Mariya Medvedyeva, Rimke van der Geest, Debby Kamstra, Arjen Sutterland, Alida Banel, Hiske Becker, Monique Bolten, Wouter van de Berg, Martyn van Poecke and Joeri Otten.

Once again my best acknowledgements to Russian speaking community of my friends in Netherlands: Oleksandr Zozulya, Dmytro Makogon, Alexandra Babich, Igor Shokaryev, Maksim Sladkov, Alina Veligura, Oleksii Rudenko, Alexandra Babenko, Oleg Karpenkov, Maxim Filatov, Ruslan Sepkhanov, Alexander Mikhnenko, Sergey Anisov, Dmitry Denisov.

It is a little sad to finish eventually this thesis. It was nice to do research for it. Hopefully it will be of certain interest for future readers.

And thank you for your attention while reading the manuscript.

July 20, 2011

Oleg Antoniuk

